# Neutralino decays in the complex MSSM at one loop:
# A comparison of on-shell renormalization schemes

A. Bharucha,[1,*] S. Heinemeyer,[2,†] F. von der Pahlen,[2,‡] and C. Schappacher[3,§]

[1]*II. Institut für Theoretische Physik, Universität Hamburg, Lupurer Chaussee 149, D22761 Hamburg, Germany*
[2]*Instituto de Física de Cantabria (CSIC-UC), E-39005 Santander, Spain*
[3]*Institut für Theoretische Physik, Karlsruhe Institute of Technology, D76128 Karlsruhe, Germany*

We evaluate two-body decay modes of neutralinos in the minimal supersymmetric Standard Model with complex parameters. Assuming heavy scalar quarks, we take into account all two-body decay channels involving charginos, neutralinos, (scalar) leptons, Higgs bosons and Standard Model gauge bosons. The evaluation of the decay widths is based on a full one-loop calculation including hard and soft QED radiation. Of particular phenomenological interest are decays involving the lightest supersymmetric particle (LSP), i.e., the lightest neutralino, or a neutral or charged Higgs boson. For the chargino/neutralino sector we employ two different renormalization schemes, which differ in the treatment of the complex phases. In the numerical analysis, we concentrate on the decay of the heaviest neutralino and show the results in the two different schemes. The higher-order corrections of the heaviest neutralino decay widths involving the LSP can easily reach a level of about 10–15%, while the corrections to the decays to Higgs bosons can be up to 20–30%, translating into corrections of similar size in the respective branching ratios. The difference between the two schemes, indicating the size of unknown two-loop corrections, is less than $\mathcal{O}(0.1\%)$. These corrections are important for the correct interpretation of LSP and Higgs production at the LHC and at a future linear $e^+e^-$ collider. The results will be implemented into the Fortran code FeynHiggs.

## I. INTRODUCTION

One of the important tasks at the LHC is to search for physics beyond the Standard Model (SM), where the minimal supersymmetric Standard Model (MSSM) [1] is one of the leading candidates.

Two related important tasks are investigating the mechanism of electroweak symmetry breaking, as well as the production and measurement of the properties of cold dark matter (CDM). The Higgs searches currently ongoing at the LHC (and previously carried out at the Tevatron [2] and LEP [3]) address both those goals. The spectacular discovery of a Higgs-like particle with a mass around $M_H \simeq 125$ GeV, which has just been announced by ATLAS and CMS [4], marks a milestone of an effort that has been ongoing for almost half a century and opens a new era of particle physics. Both ATLAS and CMS reported a clear excess around $\sim 125$ GeV in the two-photon channel, as well as in the $ZZ^{(*)}$ channel, whereas the analyses in other channels have a lower mass resolution and at present are largely less mature. The combined sensitivity in each of the experiments reaches about $\sim 5\sigma$. The discovery is consistent with the predictions for the Higgs boson in the SM [5], as well as with the predictions for the lightest Higgs boson in the MSSM [5,6]. The latter model also offers a natural candidate for CDM, the lightest supersymmetric particle (LSP), i.e., the lightest neutralino, $\tilde{\chi}_1^0$ [7]. Supersymmetry (SUSY) predicts two scalar partners for all SM fermions as well as fermionic partners to all SM bosons. Contrary to the case of the SM, in the MSSM two Higgs doublets are required. This results in five physical Higgs bosons instead of the single Higgs boson in the SM. These are the light and heavy $\mathcal{CP}$-even Higgs bosons, $h$ and $H$, the $\mathcal{CP}$-odd Higgs boson, $A$, and the charged Higgs bosons, $H^\pm$. In the MSSM with complex parameters (cMSSM), the three neutral Higgs bosons mix [8–11], giving rise to the $\mathcal{CP}$-mixed states $h_1$, $h_2$, $h_3$.

If SUSY is realized in nature and the scalar quarks and/or the gluino are in the kinematic reach of the LHC, it is expected that these strongly interacting particles are copiously produced. The primarily produced strongly interacting particles subsequently decay via cascades to SM particles and (if $R$-parity conservation is assumed, as we do) the LSP. One step in these decay chains is often the decay of a neutralino, $\tilde{\chi}_{2,3,4}^0$, to a SM particle and the LSP, or as a competing process, the neutralino decay to another SUSY particle accompanied by a SM particle. Also, neutral and charged Higgs bosons are expected to be produced this way. Via these decays, some characteristics of the LSP and/or Higgs bosons can be measured; see e.g., Refs. [12,13] and references therein. At any future $e^+e^-$ collider (such as ILC or CLIC), a precision determination of the properties of the observed particles is expected

*Aoife.Bharucha@desy.de
†Sven.Heinemeyer@cern.ch
‡pahlen@ifca.unican.es
§cs@particle.uni-karlsruhe.de

[14,15]. (For combined LHC/ILC analyses and further prospects, see Ref. [16]) Thus, if kinematically accessible, the pair production of neutralinos with a subsequent decay to the LSP and/or Higgs bosons can yield important information about the lightest neutralino and the Higgs sector of the model.

In order to yield a sufficient level of accuracy, at least one-loop corrections to the various neutralino decay modes have to be considered. In this paper we evaluate full one-loop corrections to neutralino decays in the cMSSM. If scalar quarks are sufficiently heavy (as in many GUT-based models such as CMSSM, GMSB or AMSB; see, for instance, Ref. [17]), a neutralino decay to a quark and a scalar quark is kinematically forbidden. Assuming heavy squarks, we calculate the full one-loop correction to all two-body decay modes (which are nonzero at the tree-level):

$$\Gamma(\tilde{\chi}_i^0 \to \tilde{\chi}_j^\mp H^\pm) \qquad (i = 2, 3, 4; j = 1, 2), \qquad (1)$$

$$\Gamma(\tilde{\chi}_i^0 \to \tilde{\chi}_j^\mp W^\pm) \qquad (i = 2, 3, 4; j = 1, 2), \qquad (2)$$

$$\Gamma(\tilde{\chi}_i^0 \to \tilde{\chi}_j^0 h_k) \qquad (i = 2, 3, 4; j < i; k = 1, 2, 3), \qquad (3)$$

$$\Gamma(\tilde{\chi}_i^0 \to \tilde{\chi}_j^0 Z) \qquad (i = 2, 3, 4; j < i), \qquad (4)$$

$$\Gamma(\tilde{\chi}_i^0 \to \ell^\mp \tilde{\ell}_k^\pm) \quad (i = 2, 3, 4; \ell = e, \mu, \tau; k = 1, 2), \qquad (5)$$

$$\Gamma(\tilde{\chi}_i^0 \to \bar{\nu}_\ell \tilde{\nu}_\ell / \nu_\ell \tilde{\nu}_\ell^\dagger) \qquad (i = 2, 3, 4; \ell = e, \mu, \tau). \qquad (6)$$

The total width is defined as the sum of the channels in Eqs. (1)–(6), where we neglect the decays to colored particles, as these will not be kinematically allowed for the scenarios considered in the numerical analysis. It should be noted that several modes are closed for nearly the whole MSSM parameter space due to the structure of the chargino and neutralino mass matrices (see below). Therefore, while we have evaluated analytically *all* neutralino decays, in our numerical analysis we will concentrate on the decays of the heaviest neutralino, $\tilde{\chi}_4^0$.

As explained above, we are especially interested in the branching ratios (BRs) of the decays involving a Higgs boson [Eqs. (1) and (3)] as part of an evaluation of a Higgs production cross section, and/or involving the LSP [Eqs. (3) and (4)] as part of the measurement of CDM properties at the LHC, the ILC or CLIC. Consequently, it is not necessary to investigate three- or four-body decay modes. These only play a significant role once the two-body modes are kinematically forbidden, and thus the relevant BRs are zero. The same applies to two-body decay modes that exist only at the one-loop level, such as $\tilde{\chi}_i^0 \to \tilde{\chi}_j^0 \gamma$ (see, for instance, Ref. [18]). While this channel is of $\mathcal{O}(\alpha^2)$, the size of the one-loop corrections to Eqs. (1) to (6) is of $\mathcal{O}(\alpha)$. We have numerically verified that the contribution of $\Gamma(\tilde{\chi}_i^0 \to \tilde{\chi}_j^0 \gamma)$ to the total width is completely negligible.

Tree-level results for the neutralino decays in the MSSM were presented in Refs. [18–20]. The code SDECAY [21]

includes all two-body decays of neutralinos at tree level. Tree-level studies of neutralino decays have shown that they could be invaluable in distinguishing between different patterns of supersymmetry breaking [22], as well as in detecting $\mathcal{CP}$-violating effects at a linear collider [23–28] or a muon collider [29]. Higher-order corrections to neutralino decays have been evaluated in various analyses over the last decade in the real MSSM, for which the on-shell renormalization of the chargino/neutralino sector was developed in Refs. [30–39]. In Ref. [40], three-body decays into the LSP and quarks were calculated, including corrections to the masses of third-generation fermions and SUSY particles. In Ref. [36], decays of the next-to-lightest neutralino to the lightest neutralino and two leptons were calculated at one loop. The one-loop electroweak corrections to all two-body decay channels of neutralinos, evaluated in an on-shell renormalization scheme, have been implemented in the code SloopS [41]. Radiative corrections to a number of neutralino decay channels were also recently studied in Ref. [42] for the case of real parameters. A full one-loop calculation of the electroweak corrections to the partial width of the decay of a neutralino into a chargino and a $W$ boson in the MSSM and NMSSM is presented in Ref. [43], and made available with the code CNNDecays. In the cMSSM, the on-shell renormalization of the chargino/neutralino sector was first studied in Ref. [37] and subsequently in Ref. [44], and decays of type $\Gamma(\tilde{\chi}_i^0 \to \tilde{\chi}_j^\mp H^\pm)$ were studied in Refs. [37,38]. The approach to the renormalization of the complex parameters differs slightly from that used in Refs. [45,46], where chargino decays in the cMSSM at the one-loop level were analyzed. One important part of this work consists of a comparison of these two schemes.

In this paper, we present for the first time a full one-loop calculation for all nonhadronic two-body decay channels of a neutralino, taking into account soft and hard QED radiation, simultaneously and consistently evaluated in the cMSSM. The calculation is based on two independent setups that differ slightly in the inclusion of higher-order corrections to quantities used in one-loop corrections, i.e., in effects beyond the one-loop level. The two setups furthermore employ renormalization schemes in the chargino/neutralino sector that differ in their treatment of complex phases [37,38,45,46]. The numerical results are shown for both setups, and the (small) differences indicate the size of theoretical uncertainties beyond the one-loop level.

The paper is organized as follows: In Sec. II, we review the relevant sectors of the cMSSM and give all the details about the two different renormalization schemes in the chargino/neutralino sector. Details about the calculation can be found in Sec. III. The numerical results for all decay channels are presented in Sec. IV. The conclusions can be found in Sec. V. The evaluation of the branching ratios of the neutralinos will be implemented into the Fortran code FeynHiggs [47–50].

## II. THE RELEVANT SECTORS OF THE COMPLEX MSSM

All channels [Eqs. (1)–(6)] are calculated at the one-loop level, including real QED radiation. This requires the simultaneous renormalization of several sectors of the cMSSM. In the following subsections we introduce our notation for these sectors. Details about the two renormalization schemes used in the chargino/neutralino sector are given. The renormalization of the other sectors can be found in Refs. [45,46,51].

### A. The chargino/neutralino sector of the cMSSM

While many details about the renormalization of the cMSSM can already be found in Refs. [37,38,45,46], we repeat here the most relevant aspects in order to give a complete picture and to facilitate the comparison between the two employed renormalization schemes. The chargino/neutralino sector contains two soft SUSY-breaking gaugino mass parameters $M_1$ and $M_2$ corresponding to the bino and the wino fields, respectively, as well as the Higgs superfield mixing parameter $\mu$, which, in general, can be complex. Since not all the possible phases of the cMSSM Lagrangian are physical, it is possible (without loss of generality) to choose some parameters to be real. This applies in particular to one out of the three parameters $M_1$, $M_2$, and $M_3$, the gluino mass parameter. For the numerical analysis in Sec. IV, we choose $M_2$ to be real; however, for the renormalization scheme I introduced below [45,46], we do not make such an assumption, and the analytical derivation of the renormalization constants is performed for a complex $M_2$, discussed further in Sec. IV.

The starting point for the renormalization procedure of the chargino/neutralino sector is the part of the Fourier transformed MSSM Lagrangian which is bilinear in the chargino and neutralino fields:

$$
\begin{aligned}
\mathcal{L}^{\mathrm{bil}}_{\tilde{\chi}^-,\tilde{\chi}^0} = &\, \bar{\tilde{\chi}}^-_i \slashed{p}\omega_- \tilde{\chi}^-_i + \bar{\tilde{\chi}}^-_i \slashed{p}\omega_+ \tilde{\chi}^-_i \\
&- \bar{\tilde{\chi}}^-_i [\mathbf{V}^*\mathbf{X}^\top\mathbf{U}^\dagger]_{ij}\omega_- \tilde{\chi}^-_j - \bar{\tilde{\chi}}^-_i [\mathbf{U}\mathbf{X}^*\mathbf{V}^\top]_{ij}\omega_+ \tilde{\chi}^-_j \\
&+ \frac{1}{2}(\bar{\tilde{\chi}}^0_k \slashed{p}\omega_- \tilde{\chi}^0_k + \bar{\tilde{\chi}}^0_k \slashed{p}\omega_+ \tilde{\chi}^0_k - \bar{\tilde{\chi}}^0_k [\mathbf{N}^*\mathbf{Y}\mathbf{N}^\dagger]_{kl}\omega_- \tilde{\chi}^0_l \\
&- \bar{\tilde{\chi}}^0_k [\mathbf{N}\mathbf{Y}^*\mathbf{N}^\top]_{kl}\omega_+ \tilde{\chi}^0_l),
\end{aligned}
\tag{7}
$$

already expressed in terms of the chargino and neutralino mass eigenstates $\tilde{\chi}^-_i$ and $\tilde{\chi}^0_k$, respectively, and $i, j = 1, 2$ and $k, l = 1, 2, 3, 4$. The mass eigenstates can be determined via unitary transformations where the corresponding matrices diagonalize the chargino and neutralino mass matrix, $\mathbf{X}$ and $\mathbf{Y}$, respectively.

In the chargino case, two $2 \times 2$ matrices $\mathbf{U}$ and $\mathbf{V}$ are necessary for the diagonalization of the chargino mass matrix $\mathbf{X}$:

$$
\mathbf{M}_{\tilde{\chi}^-} = \mathbf{V}^*\mathbf{X}^\top\mathbf{U}^\dagger = \begin{pmatrix} m_{\tilde{\chi}^\pm_1} & 0 \\ 0 & m_{\tilde{\chi}^\pm_2} \end{pmatrix} \quad \text{with}
$$

$$
\mathbf{X} = \begin{pmatrix} M_2 & \sqrt{2}\sin\beta M_W \\ \sqrt{2}\cos\beta M_W & \mu \end{pmatrix},
\tag{8}
$$

where $\mathbf{M}_{\tilde{\chi}^-}$ is the diagonal mass matrix with the chargino masses $m_{\tilde{\chi}^\pm_1}$, $m_{\tilde{\chi}^\pm_2}$ as entries, which are determined as the (real and positive) singular values of $\mathbf{X}$. The singular-value decomposition of $\mathbf{X}$ also yields results for $\mathbf{U}$ and $\mathbf{V}$. Using the transformation matrices $\mathbf{U}$ and $\mathbf{V}$, the interaction Higgsino and wino spinors $\tilde{H}^-_1$, $\tilde{H}^+_2$ and $\tilde{W}^\pm$, which are two component Weyl spinors, can be transformed into the mass eigenstates

$$
\tilde{\chi}^-_i = \begin{pmatrix} \psi^L_i \\ \overline{\psi^R_i} \end{pmatrix} \quad \text{with} \quad \psi^L_i = U_{ij}\begin{pmatrix} \tilde{W}^- \\ \tilde{H}^-_1 \end{pmatrix}_j \quad \text{and}
$$

$$
\psi^R_i = V_{ij}\begin{pmatrix} \tilde{W}^+ \\ \tilde{H}^+_2 \end{pmatrix}_j,
\tag{9}
$$

where the $i$th mass eigenstate can be expressed in terms of either the Weyl spinors $\psi^L_i$ and $\psi^R_i$ or the Dirac spinor $\tilde{\chi}^-_i$.

In the neutralino case, as the neutralino mass matrix $\mathbf{Y}$ is symmetric, one $4 \times 4$ matrix is sufficient for the diagonalization

$$
\mathbf{M}_{\tilde{\chi}^0} = \mathbf{N}^*\mathbf{Y}\mathbf{N}^\dagger = \mathbf{diag}(m_{\tilde{\chi}^0_1}, m_{\tilde{\chi}^0_2}, m_{\tilde{\chi}^0_3}, m_{\tilde{\chi}^0_4})
\tag{10}
$$

with

$$
\mathbf{Y} = \begin{pmatrix} M_1 & 0 & -M_Z s_{\mathrm{w}}\cos\beta & M_Z s_{\mathrm{w}}\sin\beta \\ 0 & M_2 & M_Z c_{\mathrm{w}}\cos\beta & -M_Z c_{\mathrm{w}}\sin\beta \\ -M_Z s_{\mathrm{w}}\cos\beta & M_Z c_{\mathrm{w}}\cos\beta & 0 & -\mu \\ M_Z s_{\mathrm{w}}\sin\beta & -M_Z c_{\mathrm{w}}\sin\beta & -\mu & 0 \end{pmatrix}.
\tag{11}
$$

$M_Z$ and $M_W$ are the masses of the $Z$ and $W$ boson, $c_{\mathrm{w}} = M_W/M_Z$ and $s_{\mathrm{w}} = \sqrt{1 - c^2_{\mathrm{w}}}$. The unitary $4 \times 4$ matrix $\mathbf{N}$ and the physical neutralino (tree-level) masses $m_{\tilde{\chi}^0_k}$ ($k = 1, 2, 3, 4$) result from a numerical Takagi factorization [52] of $\mathbf{Y}$. Starting from the original bino/wino/higgsino basis, the

mass eigenstates can be determined with the help of the transformation matrix $\mathbf{N}$,

$$
\tilde{\chi}^0_k = \begin{pmatrix} \psi^0_k \\ \overline{\psi^0_k} \end{pmatrix} \quad \text{with} \quad \psi^0_k = N_{kl}(\tilde{B}^0, \tilde{W}^0, \tilde{H}^0_1, \tilde{H}^0_2)^\top_l,
\tag{12}
$$

where $\psi_k^0$ denotes the two-component Weyl spinor and $\tilde{\chi}_k^0$ the four-component Majorana spinor of the $k$th neutralino field.

Concerning the renormalization of this sector, we implement two prescriptions that differ in the treatment of the complex phases. The first prescription is based on Refs. [46,53], while the second one is based on Refs. [37,38,44,54]. We will emphasize the points where the two schemes deviate from each other.

The following replacements of the parameters and the fields are performed according to the multiplicative renormalization procedure, which is formally identical for the two setups:

$$M_1 \to M_1 + \delta M_1, \tag{13}$$

$$M_2 \to M_2 + \delta M_2, \tag{14}$$

$$\mu \to \mu + \delta\mu, \tag{15}$$

$$\omega_-\tilde{\chi}_i^- \to \left[\mathbb{1} + \frac{1}{2}\delta\mathbf{Z}_{\tilde{\chi}^-}^L\right]_{ij}\omega_-\tilde{\chi}_j^- \quad (i,j=1,2), \tag{16}$$

$$\omega_+\tilde{\chi}_i^- \to \left[\mathbb{1} + \frac{1}{2}\delta\mathbf{Z}_{\tilde{\chi}^-}^R\right]_{ij}\omega_+\tilde{\chi}_j^- \quad (i,j=1,2), \tag{17}$$

$$\omega_-\tilde{\chi}_k^0 \to \left[\mathbb{1} + \frac{1}{2}\delta\mathbf{Z}_{\tilde{\chi}^0}\right]_{kl}\omega_-\tilde{\chi}_l^0 \quad (k,l=1,2,3,4), \tag{18}$$

$$\omega_+\tilde{\chi}_k^0 \to \left[\mathbb{1} + \frac{1}{2}\delta\mathbf{Z}_{\tilde{\chi}^0}^*\right]_{kl}\omega_+\tilde{\chi}_l^0 \quad (k,l=1,2,3,4). \tag{19}$$

It should be noted that the parameter counterterms are complex counterterms which each need two renormalization conditions to be fixed (except for $\delta M_2$, which in scheme II is real). The transformation matrices are not renormalized, so that, using the notation of replacing a matrix with its renormalized matrix and a counterterm matrix,

$$\mathbf{X} \to \mathbf{X} + \delta\mathbf{X}, \tag{20}$$

$$\mathbf{Y} \to \mathbf{Y} + \delta\mathbf{Y}, \tag{21}$$

with

$$\delta\mathbf{X} = \begin{pmatrix} \delta M_2 & \sqrt{2}\delta(M_W\sin\beta) \\ \sqrt{2}\delta(M_W\cos\beta) & \delta\mu \end{pmatrix}, \tag{22}$$

$$\delta\mathbf{Y} = \begin{pmatrix} \delta M_1 & 0 & -\delta(M_Z s_w\cos\beta) & \delta(M_Z s_w\sin\beta) \\ 0 & \delta M_2 & \delta(M_Z c_w\cos\beta) & -\delta(M_Z c_w\sin\beta) \\ -\delta(M_Z s_w\cos\beta) & \delta(M_Z c_w\cos\beta) & 0 & -\delta\mu \\ \delta(M_Z s_w\sin\beta) & -\delta(M_Z c_w\sin\beta) & -\delta\mu & 0 \end{pmatrix}, \tag{23}$$

the replacements of the matrices $\mathbf{M}_{\tilde{\chi}^-}$ and $\mathbf{M}_{\tilde{\chi}^0}$ can be expressed as

$$\mathbf{M}_{\tilde{\chi}^-} \to \mathbf{M}_{\tilde{\chi}^-} + \delta\mathbf{M}_{\tilde{\chi}^-} = \mathbf{M}_{\tilde{\chi}^-} + \mathbf{V}^*\delta\mathbf{X}^\top\mathbf{U}^\dagger, \tag{24}$$

$$\mathbf{M}_{\tilde{\chi}^0} \to \mathbf{M}_{\tilde{\chi}^0} + \delta\mathbf{M}_{\tilde{\chi}^0} = \mathbf{M}_{\tilde{\chi}^0} + \mathbf{N}^*\delta\mathbf{Y}\mathbf{N}^\dagger. \tag{25}$$

For convenience, we decompose the self-energies into left- and right-handed vector and scalar coefficients via

$$[\Sigma_{\tilde{\chi}}(p^2)]_{nm} = \not{p}\,\omega_-[\Sigma_{\tilde{\chi}}^L(p^2)]_{nm} + \not{p}\,\omega_+[\Sigma_{\tilde{\chi}}^R(p^2)]_{nm} + \omega_-[\Sigma_{\tilde{\chi}}^{SL}(p^2)]_{nm} + \omega_+[\Sigma_{\tilde{\chi}}^{SR}(p^2)]_{nm}. \tag{26}$$

Now the coefficients of the renormalized self-energies are given by ($i,j=1,2$; $k,l=1,2,3,4$)

$$\left[\hat{\Sigma}_{\tilde{\chi}^-}^L(p^2)\right]_{ij} = [\Sigma_{\tilde{\chi}^-}^L(p^2)]_{ij} + \frac{1}{2}[\delta\mathbf{Z}_{\tilde{\chi}^-}^L + \delta\mathbf{Z}_{\tilde{\chi}^-}^{L\dagger}]_{ij}, \tag{27}$$

$$\left[\hat{\Sigma}_{\tilde{\chi}^-}^R(p^2)\right]_{ij} = [\Sigma_{\tilde{\chi}^-}^R(p^2)]_{ij} + \frac{1}{2}[\delta\mathbf{Z}_{\tilde{\chi}^-}^R + \delta\mathbf{Z}_{\tilde{\chi}^-}^{R\dagger}]_{ij}, \tag{28}$$

$$\left[\hat{\Sigma}_{\tilde{\chi}^-}^{SL}(p^2)\right]_{ij} = [\Sigma_{\tilde{\chi}^-}^{SL}(p^2)]_{ij} - \left[\frac{1}{2}\delta\mathbf{Z}_{\tilde{\chi}^-}^{R\dagger}\mathbf{M}_{\tilde{\chi}^-} + \frac{1}{2}\mathbf{M}_{\tilde{\chi}^-}\delta\mathbf{Z}_{\tilde{\chi}^-}^L + \delta\mathbf{M}_{\tilde{\chi}^-}\right]_{ij}, \tag{29}$$

$$\left[\hat{\Sigma}_{\tilde{\chi}^-}^{SR}(p^2)\right]_{ij} = [\Sigma_{\tilde{\chi}^-}^{SR}(p^2)]_{ij} - \left[\frac{1}{2}\delta\mathbf{Z}_{\tilde{\chi}^-}^{L\dagger}\mathbf{M}_{\tilde{\chi}^-}^\dagger + \frac{1}{2}\mathbf{M}_{\tilde{\chi}^-}^\dagger\delta\mathbf{Z}_{\tilde{\chi}^-}^R + \delta\mathbf{M}_{\tilde{\chi}^-}^\dagger\right]_{ij}, \tag{30}$$

$$\left[\hat{\Sigma}_{\tilde{\chi}^0}^L(p^2)\right]_{kl} = [\Sigma_{\tilde{\chi}^0}^L(p^2)]_{kl} + \frac{1}{2}[\delta\mathbf{Z}_{\tilde{\chi}^0} + \delta\mathbf{Z}_{\tilde{\chi}^0}^\dagger]_{kl}, \tag{31}$$

$$\left[\hat{\Sigma}_{\tilde{\chi}^0}^R(p^2)\right]_{kl} = [\Sigma_{\tilde{\chi}^0}^R(p^2)]_{kl} + \frac{1}{2}[\delta\mathbf{Z}_{\tilde{\chi}^0}^* + \delta\mathbf{Z}_{\tilde{\chi}^0}^\top]_{kl}, \tag{32}$$

$$\left[\hat{\Sigma}_{\tilde{\chi}^0}^{SL}(p^2)\right]_{kl} = [\Sigma_{\tilde{\chi}^0}^{SL}(p^2)]_{kl} - \left[\frac{1}{2}\delta\mathbf{Z}_{\tilde{\chi}^0}^\top\mathbf{M}_{\tilde{\chi}^0} + \frac{1}{2}\mathbf{M}_{\tilde{\chi}^0}\delta\mathbf{Z}_{\tilde{\chi}^0} + \delta\mathbf{M}_{\tilde{\chi}^0}\right]_{kl}, \tag{33}$$

$$\left[\hat{\Sigma}_{\tilde{\chi}^0}^{SR}(p^2)\right]_{kl} = [\Sigma_{\tilde{\chi}^0}^{SR}(p^2)]_{kl} - \left[\frac{1}{2}\delta\mathbf{Z}_{\tilde{\chi}^0}^{\dagger}\mathbf{M}_{\tilde{\chi}^0}^{\dagger}\right.$$
$$\left.+ \frac{1}{2}\mathbf{M}_{\tilde{\chi}^0}^{\dagger}\delta\mathbf{Z}_{\tilde{\chi}^0}^{*} + \delta\mathbf{M}_{\tilde{\chi}^0}^{\dagger}\right]_{kl}. \quad (34)$$

Instead of choosing the three complex parameters $M_1$, $M_2$ and $\mu$ to be independent parameters, we impose on-shell conditions for the two chargino masses and the mass of the lightest neutralino (however, we do this slightly differently in the two schemes; see below) and extract the expressions for the counterterms of $M_1$, $M_2$ and $\mu$, accordingly. It was shown in Refs. [37,44,54] that for numerically stable results, one bino-, wino-, or Higgsino-like particle should be chosen on shell. Further, in a recent analysis [39] it was emphasized that in the case that two chargino masses and one neutralino mass are on-shell, the mass of the most bino-like neutralino should be chosen in order to ensure numerical stability. In Ref. [41], the problem of large unphysical contributions due to a nonbino-like lightest neutralino is also discussed. In our numerical setup (see Sec. IV), the lightest neutralino is always rather bino-like. On the other hand, it would be trivial to change our prescription from the lightest neutralino being on shell to any other neutralino, ensuring that a neutralino with a large bino component is renormalized on shell. In Ref. [39], it was also suggested that the numerically most stable result is obtained via the renormalization of one chargino and two neutralinos. However, in our approach, this choice would lead to IR divergences, since the chargino mass changes (from the tree-level mass to the one-loop pole mass) by a finite shift due to the renormalization procedure. Using the shifted mass for the external particles and the tree-level mass for internal particles results in IR divergences. On the other hand, in general, inserting the shifted chargino mass internally yields UV divergences. Consequently, we stick to our choice of imposing on-shell conditions for the two charginos and one neutralino.

As stated before, the numerical analysis is carried out using two different renormalization schemes. It should be noted that the differences arise in the renormalization of the parameters, but the expressions for the field renormalization constants are identical. This means that only the renormalization of the phases of the complex parameters differs. Therefore, the schemes are identical in the real MSSM. We will briefly describe the two schemes in the following subsections, making an attempt to highlight the differences.

*Scheme I* [45,46]: The on-shell conditions in this scheme read

$$\left(\left[\widetilde{\mathrm{Re}}\hat{\Sigma}_{\tilde{\chi}^-}(p)\right]_{ii}\tilde{\chi}_i^-(p)\right)\big|_{p^2=m_{\tilde{\chi}_i^\pm}^2} = 0 \qquad (i=1,2), \quad (35)$$

$$\left(\left[\widetilde{\mathrm{Re}}\hat{\Sigma}_{\tilde{\chi}^0}(p)\right]_{11}\tilde{\chi}_1^0(p)\right)\big|_{p^2=m_{\tilde{\chi}_1^0}^2} = 0. \quad (36)$$

These conditions can be rewritten in terms of six equations defining six real parameters or three complex ones:

$$\widetilde{\mathrm{Re}}\Big[m_{\tilde{\chi}_i^\pm}\Big(\hat{\Sigma}_{\tilde{\chi}^-}^L\Big(m_{\tilde{\chi}_i^\pm}^2\Big) + \hat{\Sigma}_{\tilde{\chi}^-}^R\Big(m_{\tilde{\chi}_i^\pm}^2\Big)\Big) + \hat{\Sigma}_{\tilde{\chi}^-}^{SL}\Big(m_{\tilde{\chi}_i^\pm}^2\Big)$$
$$+ \hat{\Sigma}_{\tilde{\chi}^-}^{SR}\Big(m_{\tilde{\chi}_i^\pm}^2\Big)\Big]_{ii} = 0, \quad (37)$$

$$\widetilde{\mathrm{Re}}\Big[m_{\tilde{\chi}_i^\pm}\Big(\hat{\Sigma}_{\tilde{\chi}^-}^L\Big(m_{\tilde{\chi}_i^\pm}^2\Big) - \hat{\Sigma}_{\tilde{\chi}^-}^R\Big(m_{\tilde{\chi}_i^\pm}^2\Big)\Big) - \hat{\Sigma}_{\tilde{\chi}^-}^{SL}\Big(m_{\tilde{\chi}_i^\pm}^2\Big)$$
$$+ \hat{\Sigma}_{\tilde{\chi}^-}^{SR}\Big(m_{\tilde{\chi}_i^\pm}^2\Big)\Big]_{ii} = 0, \quad (38)$$

$$\widetilde{\mathrm{Re}}\Big[m_{\tilde{\chi}^0}\Big(\hat{\Sigma}_{\tilde{\chi}^0}^L\Big(m_{\tilde{\chi}_1^0}^2\Big) + \hat{\Sigma}_{\tilde{\chi}^0}^R\Big(m_{\tilde{\chi}_1^0}^2\Big)\Big) + \hat{\Sigma}_{\tilde{\chi}^0}^{SL}\Big(m_{\tilde{\chi}_1^0}^2\Big)$$
$$+ \hat{\Sigma}_{\tilde{\chi}^0}^{SR}\Big(m_{\tilde{\chi}_1^0}^2\Big)\Big]_{11} = 0, \quad (39)$$

$$\widetilde{\mathrm{Re}}[m_{\tilde{\chi}_1^0}(\hat{\Sigma}_{\tilde{\chi}^0}^L(m_{\tilde{\chi}_1^0}^2) - \hat{\Sigma}_{\tilde{\chi}^0}^R(m_{\tilde{\chi}_1^0}^2)) - \hat{\Sigma}_{\tilde{\chi}^0}^{SL}(m_{\tilde{\chi}_1^0}^2)$$
$$+ \hat{\Sigma}_{\tilde{\chi}^0}^{SR}(m_{\tilde{\chi}_1^0}^2)]_{11} = 0. \quad (40)$$

Equations (38) and (40) are related to the axial and axial-vector components of the renormalized self energy, and therefore the lhs vanishes in the case of real couplings. Therefore, in the real MSSM only Eqs. (37) and (39) remain. It should be noted that since the lightest neutralino is stable, there are no absorptive contributions from its self-energy, and $\widetilde{\mathrm{Re}}$ can be dropped from Eqs. (36), (39), and (40). We retain it here in order to allow for these on-shell conditions to be generalized to other neutralinos.

For the further determination of the field renormalization constants, applicable to both schemes, we also impose

$$\lim_{p^2\to m_{\tilde{\chi}_i^\pm}^2}\left(\frac{(\not{p} + m_{\tilde{\chi}_i^\pm})\Big[\widetilde{\mathrm{Re}}\hat{\Sigma}_{\tilde{\chi}^-}(p)\Big]_{ii}}{p^2 - m_{\tilde{\chi}_i^\pm}^2}\tilde{\chi}_i^-(p)\right) = 0$$
$$(i=1,2), \quad (41)$$

$$\lim_{p^2\to m_{\tilde{\chi}_k^0}^2}\left(\frac{(\not{p} + m_{\tilde{\chi}_k^0})\Big[\widetilde{\mathrm{Re}}\hat{\Sigma}_{\tilde{\chi}^0}(p)\Big]_{kk}}{p^2 - m_{\tilde{\chi}_k^0}^2}\tilde{\chi}_k^0(p)\right) = 0$$
$$(k=1,2,3,4), \quad (42)$$

which, together with Eqs. (38) and (40), lead to the following set of equations (for $i=1,2$; $k=1$):

$$\widetilde{\mathrm{Re}}\Big[\frac{1}{2}(\hat{\Sigma}_{\tilde{\chi}^-}^L(m_{\tilde{\chi}_i^\pm}^2) + \hat{\Sigma}_{\tilde{\chi}^-}^R(m_{\tilde{\chi}_i^\pm}^2)) + m_{\tilde{\chi}_i^\pm}^2(\hat{\Sigma}_{\tilde{\chi}^-}^{L'}(m_{\tilde{\chi}_i^\pm}^2)$$
$$+ \hat{\Sigma}_{\tilde{\chi}^-}^{R'}(m_{\tilde{\chi}_i^\pm}^2)) + m_{\tilde{\chi}_i^\pm}(\hat{\Sigma}_{\tilde{\chi}^-}^{SL'}(m_{\tilde{\chi}_i^\pm}^2) + \hat{\Sigma}_{\tilde{\chi}^-}^{SR'}(m_{\tilde{\chi}_i^\pm}^2))\Big]_{ii} = 0, \quad (43)$$

$$\widetilde{\mathrm{Re}}[\hat{\Sigma}_{\tilde{\chi}^-}^L(m_{\tilde{\chi}_i^\pm}^2) - \hat{\Sigma}_{\tilde{\chi}^-}^R(m_{\tilde{\chi}_i^\pm}^2)]_{ii} = 0, \quad (44)$$

$$\widetilde{\mathrm{Re}}\Big[\frac{1}{2}(\hat{\Sigma}^L_{\tilde{\chi}^0}(m^2_{\tilde{\chi}^0_1}) + \hat{\Sigma}^R_{\tilde{\chi}^0}(m^2_{\tilde{\chi}^0_1})) + m^2_{\tilde{\chi}^0_1}(\hat{\Sigma}^{L'}_{\tilde{\chi}^0}(m^2_{\tilde{\chi}^0_1})$$
$$+ \hat{\Sigma}^{R'}_{\tilde{\chi}^0}(m^2_{\tilde{\chi}^0_1})) + m_{\tilde{\chi}^0_1}(\hat{\Sigma}^{SL'}_{\tilde{\chi}^0}(m^2_{\tilde{\chi}^0_1}) + \hat{\Sigma}^{SR'}_{\tilde{\chi}^0}(m^2_{\tilde{\chi}^0_1}))\Big]_{11} = 0,$$

$$(45)$$

$$\widetilde{\mathrm{Re}}[\hat{\Sigma}^L_{\tilde{\chi}^0}(m^2_{\tilde{\chi}^0_1}) - \hat{\Sigma}^R_{\tilde{\chi}^0}(m^2_{\tilde{\chi}^0_1})]_{11} = 0, \quad (46)$$

where we have used the shorthand $\Sigma'(m^2) \equiv (\partial\Sigma/\partial p^2)|_{p^2=m^2}$. It should be noted that Eq. (46) is already fulfilled due to the Majorana nature of the neutralinos.

Inserting Eqs. (27)–(34) for the renormalized self-energies in Eqs. (37)–(40) and solving for $[\delta\mathbf{M}_{\tilde{\chi}^-}]_{ii}$ and $[\delta\mathbf{M}_{\tilde{\chi}^0}]_{11}$ results in

$$\mathrm{Re}[\delta\mathbf{M}_{\tilde{\chi}^-}]_{ii} = \frac{1}{2}\widetilde{\mathrm{Re}}\Big[m_{\tilde{\chi}^\pm_i}\Big(\Sigma^L_{\tilde{\chi}^-}\big(m^2_{\tilde{\chi}^\pm_i}\big) + \Sigma^R_{\tilde{\chi}^-}\big(m^2_{\tilde{\chi}^\pm_i}\big)\Big)$$
$$+ \Sigma^{SL}_{\tilde{\chi}^-}\big(m^2_{\tilde{\chi}^\pm_i}\big) + \Sigma^{SR}_{\tilde{\chi}^-}\big(m^2_{\tilde{\chi}^\pm_i}\big)\Big]_{ii}, \quad (47)$$

$$\mathrm{Im}[\delta\mathbf{M}_{\tilde{\chi}^-}]_{ii} = \frac{i}{2}\widetilde{\mathrm{Re}}\Big[\Sigma^{SR}_{\tilde{\chi}^-}\big(m^2_{\tilde{\chi}^\pm_i}\big) - \Sigma^{SL}_{\tilde{\chi}^-}\big(m^2_{\tilde{\chi}^\pm_i}\big)\Big]_{ii}$$
$$- \frac{1}{2}m_{\tilde{\chi}^\pm_i}\mathrm{Im}\Big[\delta\mathbf{Z}^L_{\tilde{\chi}^-} - \delta\mathbf{Z}^R_{\tilde{\chi}^-}\Big]_{ii}, \quad (48)$$

$$\mathrm{Re}[\delta\mathbf{M}_{\tilde{\chi}^0}]_{11} = \frac{1}{2}\widetilde{\mathrm{Re}}\Big[m_{\tilde{\chi}^0_1}\Big(\Sigma^L_{\tilde{\chi}^0}\big(m^2_{\tilde{\chi}^0_1}\big) + \Sigma^R_{\tilde{\chi}^0}\big(m^2_{\tilde{\chi}^0_1}\big)\Big)$$
$$+ \Sigma^{SL}_{\tilde{\chi}^0}\big(m^2_{\tilde{\chi}^0_1}\big) + \Sigma^{SR}_{\tilde{\chi}^0}\big(m^2_{\tilde{\chi}^0_1}\big)\Big]_{11}, \quad (49)$$

$$\mathrm{Im}[\delta\mathbf{M}_{\tilde{\chi}^0}]_{11} = \frac{i}{2}\widetilde{\mathrm{Re}}\Big[\Sigma^{SR}_{\tilde{\chi}^0}\big(m^2_{\tilde{\chi}^0_1}\big) - \Sigma^{SL}_{\tilde{\chi}^0}\big(m^2_{\tilde{\chi}^0_1}\big)\Big]_{11}$$
$$- m_{\tilde{\chi}^0_1}\mathrm{Im}\Big[\delta\mathbf{Z}_{\tilde{\chi}^0}\Big]_{11}, \quad (50)$$

where we have used the relations in Eqs. (44) and (46). Using Eqs. (22)–(25), these conditions lead to [53,55]

$$\delta M_1 = \frac{1}{(N^*_{11})^2}(\delta\tilde{m}_{\tilde{\chi}^0_1} - N^{*2}_{12}\delta M_2 + 2N^*_{13}N^*_{14}\delta\mu$$
$$+ 2N^*_{11}[N^*_{13}\delta(M_Z s_{\mathrm{w}}\cos\beta) - N^*_{14}\delta(M_Z s_{\mathrm{w}}\sin\beta)]$$
$$- 2N^*_{12}[N^*_{13}\delta(M_Z c_{\mathrm{w}}\cos\beta) - N^*_{14}\delta(M_Z c_{\mathrm{w}}\sin\beta)]),$$

$$(51)$$

$$\delta M_2 = \frac{1}{2(U^*_{11}U^*_{22}V^*_{11}V^*_{22} - U^*_{12}U^*_{21}V^*_{12}V^*_{21})}$$
$$\times (2U^*_{22}V^*_{22}\delta\tilde{m}_{\tilde{\chi}^\pm_1} - 2U^*_{12}V^*_{12}\delta\tilde{m}_{\tilde{\chi}^\pm_2}$$
$$+ (U^*_{12}U^*_{21} - U^*_{11}U^*_{22})V^*_{12}V^*_{22}\delta(\sqrt{2}M_W\sin\beta)$$
$$+ U^*_{12}U^*_{22}(V^*_{12}V^*_{21} - V^*_{11}V^*_{22})\delta(\sqrt{2}M_W\cos\beta)), \quad (52)$$

$$\delta\mu = \frac{1}{2(U^*_{11}U^*_{22}V^*_{11}V^*_{22} - U^*_{12}U^*_{21}V^*_{12}V^*_{21})}$$
$$\times (2U^*_{11}V^*_{11}\delta\tilde{m}_{\tilde{\chi}^\pm_2} - 2U^*_{21}V^*_{21}\delta\tilde{m}_{\tilde{\chi}^\pm_1}$$
$$+ (U^*_{12}U^*_{21} - U^*_{11}U^*_{22})V^*_{11}V^*_{21}\delta(\sqrt{2}M_W\cos\beta)$$
$$+ U^*_{11}U^*_{21}(V^*_{12}V^*_{21} - V^*_{11}V^*_{22})\delta(\sqrt{2}M_W\sin\beta)), \quad (53)$$

where, combining Eqs. (47)–(50), we introduce the shorthand notation

$$\delta\tilde{m}_{\tilde{\chi}^0_1} = \frac{1}{2}\widetilde{\mathrm{Re}}\Big[m_{\tilde{\chi}^0_1}\Big(\Sigma^L_{\tilde{\chi}^0}\big(m^2_{\tilde{\chi}^0_1}\big) + \Sigma^R_{\tilde{\chi}^0}\big(m^2_{\tilde{\chi}^0_1}\big)\Big)$$
$$+ 2\Sigma^{SL}_{\tilde{\chi}^0}\big(m^2_{\tilde{\chi}^0_1}\big)\Big]_{11}, \quad (54)$$

$$\delta\tilde{m}_{\tilde{\chi}^\pm_i} = \frac{1}{2}\widetilde{\mathrm{Re}}\Big[m_{\tilde{\chi}^\pm_i}\Big(\Sigma^L_{\tilde{\chi}^\pm}\big(m^2_{\tilde{\chi}^\pm_i}\big) + \Sigma^R_{\tilde{\chi}^\pm}\big(m^2_{\tilde{\chi}^\pm_i}\big)\Big)$$
$$+ 2\Sigma^{SL}_{\tilde{\chi}^\pm}\big(m^2_{\tilde{\chi}^\pm_i}\big)\Big]_{ii}. \quad (55)$$

Here we have already used Eqs. (73) and (76) (see below), which fix the expressions for the imaginary parts of the chargino and neutralino field renormalization constants $\delta\mathbf{Z}^{L/R}_{\tilde{\chi}^-}$ and $\delta\mathbf{Z}_{\tilde{\chi}^0}$, respectively.

*Scheme II* [37,38]: Here, on the other hand, it is the real part of the corrections to the self-energies of the on-shell particles that is required to vanish:

$$\Big(\big[\mathrm{Re}\hat{\Sigma}_{\tilde{\chi}^-}(p)\big]_{ii}\tilde{\chi}^-_i(p)\Big)\big|_{p^2=m^2_{\tilde{\chi}^\pm_i}} = 0 \quad (i = 1, 2), \quad (56)$$

$$\Big(\big[\mathrm{Re}\hat{\Sigma}_{\tilde{\chi}^0}(p)\big]_{11}\tilde{\chi}^0_1(p)\Big)\big|_{p^2=m^2_{\tilde{\chi}^0_1}} = 0. \quad (57)$$

It should be noted that for the derivation of the field renormalization constants, in order to ensure that the on-shell propagator has only a scalar and vector part, we impose the additional conditions

$$\Big[\hat{\Sigma}^L_{\tilde{\chi}}\big(m^2_{\tilde{\chi}_j}\big)\Big]_{jj} = \Big[\hat{\Sigma}^R_{\tilde{\chi}}\big(m^2_{\tilde{\chi}_j}\big)\Big]_{jj}, \quad (58)$$

$$\Big[\hat{\Sigma}^{SL}_{\tilde{\chi}}\big(m^2_{\tilde{\chi}_j}\big)\Big]_{jj} = \Big[\hat{\Sigma}^{SR}_{\tilde{\chi}}\big(m^2_{\tilde{\chi}_j}\big)\Big]_{jj}, \quad (59)$$

with $\tilde{\chi}_j$ denoting either a chargino (with $j = 1, 2$) or a neutralino (with $j = 1, \ldots, 4$). The first equation, relating the vector coefficients, is automatically satisfied in the cMSSM for both charginos and neutralinos. This means that the conditions of Eqs. (44) and (46) that applied in scheme I, describing the axial and axial-vector components of the renormalized self-energy, are also satisfied in scheme II. It should be noted that here, however, we have dropped the $\widetilde{\mathrm{Re}}$.[1] On expanding Eqs. (56) and (57), in analogy to Eqs. (37) and (39), we find

_____

[1]See the discussion on absorptive contributions at the end of this subsection.

$$\mathrm{Re}[m_{\tilde{\chi}_i^\pm}(\hat{\Sigma}_{\tilde{\chi}^-}^L(m_{\tilde{\chi}_i^\pm}^2) + \hat{\Sigma}_{\tilde{\chi}^-}^R(m_{\tilde{\chi}_i^\pm}^2)) + \hat{\Sigma}_{\tilde{\chi}^-}^{SL}(m_{\tilde{\chi}_i^\pm}^2)$$
$$+ \hat{\Sigma}_{\tilde{\chi}^-}^{SR}(m_{\tilde{\chi}_i^\pm}^2)]_{ii} = 0, \tag{60}$$

$$\mathrm{Re}[m_{\tilde{\chi}_1^0}(\hat{\Sigma}_{\tilde{\chi}^0}^L(m_{\tilde{\chi}_1^0}^2) + \hat{\Sigma}_{\tilde{\chi}^0}^R(m_{\tilde{\chi}_1^0}^2)) + \hat{\Sigma}_{\tilde{\chi}^0}^{SL}(m_{\tilde{\chi}_1^0}^2)$$
$$+ \hat{\Sigma}_{\tilde{\chi}^0}^{SR}(m_{\tilde{\chi}_1^0}^2)]_{11} = 0. \tag{61}$$

We are left with three on-shell conditions for scheme II, Eqs. (60) and (61). Therefore, one can only fix the renormalization constants[2] $\tilde{\delta}|M_1|$, $\tilde{\delta}M_2$ (note that $M_2$ is chosen

to be real) and $\tilde{\delta}|\mu|$, but not $\tilde{\delta}\varphi_{M_1}$ or $\tilde{\delta}\phi_\mu$, where $\tilde{\delta}M_1 = \tilde{\delta}|M_1|e^{i\varphi_{M_1}}$ and $\tilde{\delta}\mu = \tilde{\delta}|\mu|e^{i\phi_\mu}$. This, however, is not a problem, as it turns out that the phases of $M_1$ and $\mu$ are UV finite at one loop (see e.g., Ref. [37]) and need not be renormalized at all, i.e., they can be set to zero, $\tilde{\delta}\varphi_{M_1} = \tilde{\delta}\phi_\mu = 0$. It should be noted that $\tilde{\delta}|\mu|$, $\tilde{\delta}|M_1|$, $\tilde{\delta}M_2$ are related to $\tilde{\delta}\mathbf{M}_{\tilde{\chi}^-}$ and $\tilde{\delta}\mathbf{M}_{\tilde{\chi}^0}$ via Eqs. (22)–(25). Expressions for these renormalization constants can then easily be obtained by inserting Eqs. (27)–(34) for the renormalized self-energies in Eqs. (60) and (61), resulting in (for details see Refs. [37,38,44,54])

$$\tilde{\delta}|M_1| = -\frac{1}{\mathrm{Re}(e^{-i\varphi_{M_1}}N_{11}^2)S} \times ([\mathrm{Re}(U_{11}V_{11})\mathrm{Re}(e^{-i\phi_\mu}U_{22}V_{22}) - \mathrm{Re}(e^{-i\phi_\mu}U_{12}V_{12})\mathrm{Re}(U_{21}V_{21})]N_1$$
$$+ [2\mathrm{Re}(e^{-i\phi_\mu}N_{13}N_{14})\mathrm{Re}(U_{11}V_{11}) + \mathrm{Re}(N_{12}^2)\mathrm{Re}(e^{-i\phi_\mu}U_{12}V_{12})]C_2$$
$$- [\mathrm{Re}(N_{12}^2)\mathrm{Re}(e^{-i\phi_\mu}U_{22}V_{22}) + 2\,\mathrm{Re}(e^{-i\phi_\mu}N_{13}N_{14})\mathrm{Re}(U_{21}V_{21})]C_1), \tag{62}$$

$$\tilde{\delta}M_2 = \frac{1}{S}[\mathrm{Re}(e^{-i\phi_\mu}U_{12}V_{12})C_2 - \mathrm{Re}(e^{-i\phi_\mu}U_{22}V_{22})C_1], \tag{63}$$

$$\tilde{\delta}|\mu| = -\frac{1}{S}[\mathrm{Re}(U_{11}V_{11})C_2 - \mathrm{Re}(U_{21}V_{21})C_1], \tag{64}$$

where we use the abbreviations

$$C_i \equiv \mathrm{Re}[m_{\tilde{\chi}_i^\pm}[\Sigma_{\tilde{\chi}^-}^L(m_{\tilde{\chi}_i^\pm}^2) + \Sigma_{\tilde{\chi}^-}^R(m_{\tilde{\chi}_i^\pm}^2)] + \Sigma_{\tilde{\chi}^-}^{SL}(m_{\tilde{\chi}_i^\pm}^2)$$
$$+ \Sigma_{\tilde{\chi}^-}^{SR}(m_{\tilde{\chi}_i^\pm}^2)]_{ii} - 2\delta(M_W\sin\beta)\mathrm{Re}(U_{i2}V_{i1})$$
$$- 2\delta(M_W\sin\beta)\mathrm{Re}(U_{i1}V_{i2}), \tag{65}$$

$$N_i \equiv \mathrm{Re}[m_{\tilde{\chi}_i^0}[\Sigma_{\tilde{\chi}^0}^L(m_{\tilde{\chi}_i^0}^2) + \Sigma_{\tilde{\chi}^0}^R(m_{\tilde{\chi}_i^0}^2)] + \Sigma_{\tilde{\chi}^0}^{SL}(m_{\tilde{\chi}_i^0}^2)$$
$$+ \Sigma_{\tilde{\chi}^0}^{SR}(m_{\tilde{\chi}_i^0}^2)]_{ii} + 4\delta(M_Z s_\mathrm{w}\cos\beta)\mathrm{Re}(N_{i1}N_{i3})$$
$$- 4\delta(M_Z c_\mathrm{w}\cos\beta)\mathrm{Re}(N_{i2}N_{i3})$$
$$- 4\delta(M_Z s_\mathrm{w}\sin\beta)\mathrm{Re}(N_{i1}N_{i4})$$
$$+ 4\delta(M_Z c_\mathrm{w}\sin\beta)\mathrm{Re}(N_{i2}N_{i4}), \tag{66}$$

$$S \equiv 2[\mathrm{Re}(U_{21}V_{21})\mathrm{Re}(e^{-i\phi_\mu}U_{12}V_{12})$$
$$- \mathrm{Re}(U_{11}V_{11})\mathrm{Re}(e^{-i\phi_\mu}U_{22}V_{22})]. \tag{67}$$

$\tilde{\delta}\mathbf{M}_{\tilde{\chi}^-}$ and $\tilde{\delta}\mathbf{M}_{\tilde{\chi}^0}$ are simply obtained by the replacements $\delta M_1$, $\delta M_2$, and $\delta\mu$ by, respectively, $\tilde{\delta}M_1$, $\tilde{\delta}M_2$, and $\tilde{\delta}\mu$ in Eqs. (20)–(25).

The following discussion of the neutralino mass shifts and the field renormalization is applicable to both schemes.

Since the chargino masses $m_{\tilde{\chi}_1^\pm}$, $m_{\tilde{\chi}_2^\pm}$ and the lightest neutralino mass $m_{\tilde{\chi}_1^0}$ have been chosen as independent parameters, the one-loop masses of the heavier neutralinos $\tilde{\chi}_i^0$ ($i = 2, 3, 4$) are obtained from the tree-level ones via the shifts

$$\Delta m_{\tilde{\chi}_i^0} = -\frac{1}{2}\,\mathrm{Re}\{m_{\tilde{\chi}_i^0}(\hat{\Sigma}_{\tilde{\chi}^0}^L(m_{\tilde{\chi}_i^0}^2) + \hat{\Sigma}_{\tilde{\chi}^0}^R(m_{\tilde{\chi}_i^0}^2))$$
$$+ \hat{\Sigma}_{\tilde{\chi}^0}^{SL}(m_{\tilde{\chi}_i^0}^2) + \hat{\Sigma}_{\tilde{\chi}^0}^{SR}(m_{\tilde{\chi}_i^0}^2)\}. \tag{68}$$

Where necessary, we distinguish the tree-level mass $m_{\tilde{\chi}_i^0}$ from the on-shell mass,

$$\hat{m}_{\tilde{\chi}_i^0} = m_{\tilde{\chi}_i^0} + \Delta m_{\tilde{\chi}_i^0}. \tag{69}$$

We use $\hat{m}_{\tilde{\chi}_i^0}$ for all externally appearing neutralino masses, which includes the (on-shell) momentum in the employed neutralino self-energies. In order to yield UV-finite results, we use the tree-level values $m_{\tilde{\chi}_i^0}$ for all internally appearing neutralino masses in loop calculations.

Equations (43) and (45) define the real part of the diagonal field renormalization constants of the chargino fields and of the lightest neutralino field. By extending Eq. (45) to apply also for $k = 2, 3, 4$, we can generalize the result for the diagonal field renormalization constants of the lightest neutralino to the other neutralino fields.

The imaginary parts of the diagonal field renormalization constants are still undefined. However, these can be obtained using Eqs. (48) and (50), where the latter is generalized to include $k = 2, 3, 4$. Now in scheme I (or scheme II), for the charginos and the lightest neutralino, Eqs. (48) and (50) define the imaginary parts of $[\delta\mathbf{M}_{\tilde{\chi}^\pm}]_{ii}$ (or $[\tilde{\delta}\mathbf{M}_{\tilde{\chi}^\pm}]_{ii}$) ($i = 1, 2$) and $[\delta\mathbf{M}_{\tilde{\chi}^0}]_{11}$ (or $[\tilde{\delta}\mathbf{M}_{\tilde{\chi}^0}]_{11}$) in terms of the imaginary part of the field renormalization constants. Therefore, these are simply set to zero [see below Eqs. (73) and (76)], which is possible as all divergences are absorbed by other counterterms.

---

[2]Here we adopt the notation $\tilde{\delta}$ for scheme II to distinguish the renormalization constants from those in scheme I.

The off-diagonal field renormalization constants are fixed by the condition that

$$([\widetilde{\text{Re}}\hat{\Sigma}_{\tilde{\chi}^-}(p)]_{ij}\tilde{\chi}_j^-(p))|_{p^2=m^2_{\tilde{\chi}_j^\pm}} = 0 \qquad (i,j=1,2), \quad (70)$$

$$([\widetilde{\text{Re}}\hat{\Sigma}_{\tilde{\chi}^0}(p)]_{kl}\tilde{\chi}_l^0(p))|_{p^2=m^2_{\tilde{\chi}_l^0}} = 0 \quad (k,l=1,2,3,4). \quad (71)$$

Finally, this yields for the field renormalization constants [53] (where we now make the correct dependence on tree-level and on-shell masses explicit)

$$\begin{aligned}\text{Re}[\delta\mathbf{Z}_{\tilde{\chi}^-}^{L/R}]_{ii} = -\widetilde{\text{Re}}[&\Sigma_{\tilde{\chi}^-}^{L/R}(m^2_{\tilde{\chi}_i^\pm}) + m^2_{\tilde{\chi}_i^\pm}(\Sigma_{\tilde{\chi}^-}^{L'}(m^2_{\tilde{\chi}_i^\pm})\\ &+ \Sigma_{\tilde{\chi}^-}^{R'}(m^2_{\tilde{\chi}_i^\pm})) + m_{\tilde{\chi}_i^\pm}(\Sigma_{\tilde{\chi}^-}^{SL'}(m^2_{\tilde{\chi}_i^\pm})\\ &+ \Sigma_{\tilde{\chi}^-}^{SR'}(m^2_{\tilde{\chi}_i^\pm}))]_{ii},\end{aligned} \quad (72)$$

$$\begin{aligned}\text{Im}[\delta\mathbf{Z}_{\tilde{\chi}^-}^{L/R}]_{ii} = \pm\frac{1}{m_{\tilde{\chi}_i^\pm}}\Big[&\frac{i}{2}\widetilde{\text{Re}}\{\Sigma_{\tilde{\chi}^-}^{SR}(m^2_{\tilde{\chi}_i^\pm}) - \Sigma_{\tilde{\chi}^-}^{SL}(m^2_{\tilde{\chi}_i^\pm})\}\\ &-\text{Im}\delta\mathbf{M}_{\tilde{\chi}^-}\Big]_{ii}\overset{\text{S}_\text{I}}{:=}0,\end{aligned} \quad (73)$$

$$\begin{aligned}[\delta\mathbf{Z}_{\tilde{\chi}^-}^{L/R}]_{ij} = \frac{2}{m^2_{\tilde{\chi}_i^\pm} - m^2_{\tilde{\chi}_j^\pm}}\widetilde{\text{Re}}[&m^2_{\tilde{\chi}_j^\pm}\Sigma_{\tilde{\chi}^-}^{L/R}(m^2_{\tilde{\chi}_j^\pm})\\ &+ m_{\tilde{\chi}_i^\pm}m_{\tilde{\chi}_j^\pm}\Sigma_{\tilde{\chi}^-}^{R/L}(m^2_{\tilde{\chi}_j^\pm}) + m_{\tilde{\chi}_i^\pm}\Sigma_{\tilde{\chi}^-}^{SL/SR}(m^2_{\tilde{\chi}_j^\pm})\\ &+ m_{\tilde{\chi}_j^\pm}\Sigma_{\tilde{\chi}^-}^{SR/SL}(m^2_{\tilde{\chi}_j^\pm}) - m_{\tilde{\chi}_{i/j}^\pm}\delta\mathbf{M}_{\tilde{\chi}^-}\\ &- m_{\tilde{\chi}_{j/i}^\pm}\delta\mathbf{M}_{\tilde{\chi}^-}^\dagger]_{ij},\end{aligned} \quad (74)$$

$$\begin{aligned}\text{Re}[\delta\mathbf{Z}_{\tilde{\chi}^0}]_{kk} = -\widetilde{\text{Re}}[&\Sigma_{\tilde{\chi}^0}^{L}(\hat{m}^2_{\tilde{\chi}_k^0}) + m^2_{\tilde{\chi}_k^0}(\Sigma_{\tilde{\chi}^0}^{L'}(\hat{m}^2_{\tilde{\chi}_k^0})\\ &+ \Sigma_{\tilde{\chi}^0}^{R'}(\hat{m}^2_{\tilde{\chi}_k^0})) + m_{\tilde{\chi}_k^0}(\Sigma_{\tilde{\chi}^0}^{SL'}(\hat{m}^2_{\tilde{\chi}_k^0})\\ &+ \Sigma_{\tilde{\chi}^0}^{SR'}(\hat{m}^2_{\tilde{\chi}_k^0}))]_{kk},\end{aligned} \quad (75)$$

$$\begin{aligned}\text{Im}[\delta\mathbf{Z}_{\tilde{\chi}^0}]_{kk} = \frac{1}{m_{\tilde{\chi}_k^0}}\Big[&\frac{i}{2}\widetilde{\text{Re}}\{\Sigma_{\tilde{\chi}^0}^{SR}(\hat{m}^2_{\tilde{\chi}_k^0}) - \Sigma_{\tilde{\chi}^0}^{SL}(\hat{m}^2_{\tilde{\chi}_k^0})\}\\ &-\text{Im}\delta\mathbf{M}_{\tilde{\chi}^0}\Big]_{kk}\overset{k=1,\text{S}_\text{I}}{:=}0,\end{aligned} \quad (76)$$

$$\begin{aligned}[\delta\mathbf{Z}_{\tilde{\chi}^0}]_{kl} = \frac{2}{m^2_{\tilde{\chi}_k^0} - m^2_{\tilde{\chi}_l^0}}\widetilde{\text{Re}}[&m^2_{\tilde{\chi}_l^0}\Sigma_{\tilde{\chi}^0}^{L}(\hat{m}^2_{\tilde{\chi}_l^0})\\ &+ m_{\tilde{\chi}_k^0}m_{\tilde{\chi}_l^0}\Sigma_{\tilde{\chi}^0}^{R}(\hat{m}^2_{\tilde{\chi}_l^0}) + m_{\tilde{\chi}_k^0}\Sigma_{\tilde{\chi}^0}^{SL}(\hat{m}^2_{\tilde{\chi}_l^0})\\ &+ m_{\tilde{\chi}_l^0}\Sigma_{\tilde{\chi}^0}^{SR}(\hat{m}^2_{\tilde{\chi}_l^0}) - m_{\tilde{\chi}_k^0}\delta\mathbf{M}_{\tilde{\chi}^0} - m_{\tilde{\chi}_l^0}\delta\mathbf{M}_{\tilde{\chi}^0}^\dagger]_{kl}\end{aligned} \quad (77)$$

within scheme I ($\text{S}_\text{I}$). Making the replacements $\delta\mathbf{M}_{\tilde{\chi}^0} \rightarrow \tilde{\delta}\mathbf{M}_{\tilde{\chi}^0}$ and $\delta\mathbf{M}_{\tilde{\chi}^-} \rightarrow \tilde{\delta}\mathbf{M}_{\tilde{\chi}^-}$ for scheme II, Eqs. (73) and (76) no longer vanish.

Contributions to the partial decay widths can arise from the product of the imaginary parts of the loop functions (absorptive contributions) of the self-energy-type contributions in the external legs and the imaginary parts of complex couplings entering the decay vertex or the self-energies. It is possible to combine these additional contributions with the field renormalization constants in a single "Z factor," $Z$; see e.g., Refs. [45,46] and references therein. In our notation (unbarred for an incoming neutralino or a negative chargino, barred for an outgoing neutralino or negative chargino, and not making the difference between scheme I and II explicit), they read

$$\begin{aligned}[\delta Z_{\tilde{\chi}^-}^{L/R}]_{ii} = -[&\Sigma_{\tilde{\chi}^-}^{L/R}(m^2_{\tilde{\chi}_i^\pm}) + m^2_{\tilde{\chi}_i^\pm}(\Sigma_{\tilde{\chi}^-}^{L'}(m^2_{\tilde{\chi}_i^\pm})\\ &+ \Sigma_{\tilde{\chi}^-}^{R'}(m^2_{\tilde{\chi}_i^\pm})) + m_{\tilde{\chi}_i^\pm}(\Sigma_{\tilde{\chi}^-}^{SL'}(m^2_{\tilde{\chi}_i^\pm})\\ &+ \Sigma_{\tilde{\chi}^-}^{SR'}(m^2_{\tilde{\chi}_i^\pm}))]_{ii} \pm \frac{1}{2m_{\tilde{\chi}_i^\pm}}[\Sigma_{\tilde{\chi}^-}^{SL}(m^2_{\tilde{\chi}_i^\pm})\\ &- \Sigma_{\tilde{\chi}^-}^{SR}(m^2_{\tilde{\chi}_i^\pm}) - \delta\mathbf{M}_{\tilde{\chi}^-} + \delta\mathbf{M}_{\tilde{\chi}^-}^*]_{ii},\end{aligned} \quad (78)$$

$$\begin{aligned}[\delta Z_{\tilde{\chi}^-}^{L/R}]_{ij} = \frac{2}{m^2_{\tilde{\chi}_i^\pm} - m^2_{\tilde{\chi}_j^\pm}}[&m^2_{\tilde{\chi}_j^\pm}\Sigma_{\tilde{\chi}^-}^{L/R}(m^2_{\tilde{\chi}_j^\pm})\\ &+ m_{\tilde{\chi}_i^\pm}m_{\tilde{\chi}_j^\pm}\Sigma_{\tilde{\chi}^-}^{R/L}(m^2_{\tilde{\chi}_j^\pm}) + m_{\tilde{\chi}_i^\pm}\Sigma_{\tilde{\chi}^-}^{SL/SR}(m^2_{\tilde{\chi}_j^\pm})\\ &+ m_{\tilde{\chi}_j^\pm}\Sigma_{\tilde{\chi}^-}^{SR/SL}(m^2_{\tilde{\chi}_j^\pm}) - m_{\tilde{\chi}_{i/j}^\pm}\delta\mathbf{M}_{\tilde{\chi}^-}\\ &- m_{\tilde{\chi}_{j/i}^\pm}\delta\mathbf{M}_{\tilde{\chi}^-}^\dagger]_{ij},\end{aligned} \quad (79)$$

$$\begin{aligned}[\delta Z_{\tilde{\chi}^0}^{L/R}]_{kk} = -[&\Sigma_{\tilde{\chi}^0}^{L/R}(\hat{m}^2_{\tilde{\chi}_k^0}) + m^2_{\tilde{\chi}_k^0}(\Sigma_{\tilde{\chi}^0}^{L'}(\hat{m}^2_{\tilde{\chi}_k^0}) + \Sigma_{\tilde{\chi}^0}^{R'}(\hat{m}^2_{\tilde{\chi}_k^0}))\\ &+ m_{\tilde{\chi}_k^0}(\Sigma_{\tilde{\chi}^0}^{SL'}(\hat{m}^2_{\tilde{\chi}_k^0}) + \Sigma_{\tilde{\chi}^0}^{SR'}(\hat{m}^2_{\tilde{\chi}_k^0}))]_{kk}\\ &\pm \frac{1}{2m_{\tilde{\chi}_k^0}}[\Sigma_{\tilde{\chi}^0}^{SL}(\hat{m}^2_{\tilde{\chi}_k^0}) - \Sigma_{\tilde{\chi}^0}^{SR}(\hat{m}^2_{\tilde{\chi}_k^0})\\ &- \delta\mathbf{M}_{\tilde{\chi}^0} + \delta\mathbf{M}_{\tilde{\chi}^0}^*]_{kk},\end{aligned} \quad (80)$$

$$\begin{aligned}[\delta Z_{\tilde{\chi}^0}^{L/R}]_{kl} = \frac{2}{m^2_{\tilde{\chi}_k^0} - m^2_{\tilde{\chi}_l^0}}[&m^2_{\tilde{\chi}_l^0}\Sigma_{\tilde{\chi}^0}^{L/R}(\hat{m}^2_{\tilde{\chi}_l^0})\\ &+ m_{\tilde{\chi}_k^0}m_{\tilde{\chi}_l^0}\Sigma_{\tilde{\chi}^0}^{R/L}(\hat{m}^2_{\tilde{\chi}_l^0}) + m_{\tilde{\chi}_k^0}\Sigma_{\tilde{\chi}^0}^{SL/SR}(\hat{m}^2_{\tilde{\chi}_l^0})\\ &+ m_{\tilde{\chi}_l^0}\Sigma_{\tilde{\chi}^0}^{SR/SL}(\hat{m}^2_{\tilde{\chi}_l^0}) - m_{\tilde{\chi}_{k/l}^0}\delta\mathbf{M}_{\tilde{\chi}^0}\\ &- m_{\tilde{\chi}_{l/k}^0}\delta\mathbf{M}_{\tilde{\chi}^0}^\dagger]_{kl},\end{aligned} \quad (81)$$

$$\begin{aligned}[\delta\bar{Z}_{\tilde{\chi}^-}^{L/R}]_{ii} = -[&\Sigma_{\tilde{\chi}^-}^{L/R}(m^2_{\tilde{\chi}_i^\pm}) + m^2_{\tilde{\chi}_i^\pm}(\Sigma_{\tilde{\chi}^-}^{L'}(m^2_{\tilde{\chi}_i^\pm})\\ &+ \Sigma_{\tilde{\chi}^-}^{R'}(m^2_{\tilde{\chi}_i^\pm})) + m_{\tilde{\chi}_i^\pm}(\Sigma_{\tilde{\chi}^-}^{SL'}(m^2_{\tilde{\chi}_i^\pm})\\ &+ \Sigma_{\tilde{\chi}^-}^{SR'}(m^2_{\tilde{\chi}_i^\pm}))]_{ii} \mp \frac{1}{2m_{\tilde{\chi}_i^\pm}}[\Sigma_{\tilde{\chi}^-}^{SL}(m^2_{\tilde{\chi}_i^\pm})\\ &- \Sigma_{\tilde{\chi}^-}^{SR}(m^2_{\tilde{\chi}_i^\pm}) - \delta\mathbf{M}_{\tilde{\chi}^-} + \delta\mathbf{M}_{\tilde{\chi}^-}^*]_{ii},\end{aligned} \quad (82)$$

$$[\delta\bar{\mathcal{Z}}^{L/R}_{\tilde{\chi}^{\pm}}]_{ij} = \frac{2}{m^2_{\tilde{\chi}^{\pm}_j} - m^2_{\tilde{\chi}^{\pm}_i}}[m^2_{\tilde{\chi}^{\pm}_i}\Sigma^{L/R}_{\tilde{\chi}^{\pm}}(m^2_{\tilde{\chi}^{\pm}_i})$$

$$+ m_{\tilde{\chi}^{\pm}_i}m_{\tilde{\chi}^{\pm}_j}\Sigma^{R/L}_{\tilde{\chi}^{\pm}}(m^2_{\tilde{\chi}^{\pm}_i}) + m_{\tilde{\chi}^{\pm}_i}\Sigma^{SL/SR}_{\tilde{\chi}^{\pm}}(m^2_{\tilde{\chi}^{\pm}_i})$$

$$+ m_{\tilde{\chi}^{\pm}_j}\Sigma^{SR/SL}_{\tilde{\chi}^{\pm}}(m^2_{\tilde{\chi}^{\pm}_i}) - m_{\tilde{\chi}^{\pm}_{i/j}}\delta\mathbf{M}_{\tilde{\chi}^-}$$

$$- m_{\tilde{\chi}^{\pm}_{j/i}}\delta\mathbf{M}^{\dagger}_{\tilde{\chi}^-}]_{ij}, \tag{83}$$

$$[\delta\bar{\mathcal{Z}}^{L/R}_{\tilde{\chi}^0}]_{kk} = [\delta\mathcal{Z}^{R/L}_{\tilde{\chi}^0}]_{kk}, \tag{84}$$

$$[\delta\bar{\mathcal{Z}}^{L/R}_{\tilde{\chi}^0}]_{kl} = [\delta\mathcal{Z}^{R/L}_{\tilde{\chi}^0}]_{lk} \tag{85}$$

within scheme I, with $\delta\mathbf{M}_{\tilde{\chi}^0} \rightarrow \tilde{\delta}\mathbf{M}_{\tilde{\chi}^0}$ and $\delta\mathbf{M}_{\tilde{\chi}^-} \rightarrow \tilde{\delta}\mathbf{M}_{\tilde{\chi}^-}$ for scheme II. The chargino/neutralino $\mathcal{Z}$ factors obey $\widetilde{\mathrm{Re}}\delta\bar{\mathcal{Z}}^{L/R}_{\tilde{\chi}} = [\widetilde{\mathrm{Re}}\delta\mathcal{Z}^{L/R}_{\tilde{\chi}}]^{\dagger} = [\delta\mathbf{Z}^{L/R}_{\tilde{\chi}}]^{\dagger}$, which is exactly the case without absorptive contributions. Equations (84) and (85) hold due to the Majorana character of the neutralinos. We will use these $\mathcal{Z}$ factors rather than the field renormalization constants defined in Eqs. (72)–(77) in the following numerical analysis.

Special care has to be taken in the regions of the cMSSM parameter space where the gaugino-Higgsino mixing in the chargino sector is maximal, i.e., where $|\mu| \approx M_2$. Here $\delta M_2$ [see Eq. (52)] and $\delta\mu$ [see Eq. (53)] diverge as $(U^*_{11}U^*_{22}V^*_{11}V^*_{22} - U^*_{12}U^*_{21}V^*_{12}V^*_{21})^{-1}$ for scheme I or $2[\mathrm{Re}(U_{21}V_{21})\mathrm{Re}(e^{-i\phi_\mu}U_{12}V_{12}) - \mathrm{Re}(U_{11}V_{11})\mathrm{Re}(e^{-i\phi_\mu}U_{22}V_{22})]$ for scheme II, and the loop calculation does not yield a reliable result.[3] It should be noted that the singularity arises in both schemes for $|\mu| = M_2$. These kinds of divergences were also discussed in Refs. [37,39,44].

Our two renormalization schemes differ in the treatment of complex contributions in the chargino/neutralino sector. The first difference is that in scheme I, in the derivation of the renormalization conditions, $\delta M_2$ is allowed to be complex. Therefore, six real conditions must be imposed in order to renormalize the mass matrices **X**

and **Y**, Eqs. (8) and (11), as opposed to the five in scheme II. In addition, in scheme I, the renormalization of the phases is obtained by imposing that the imaginary parts of the relevant diagonal renormalization constants [Eqs. (73) and (76)] vanish. In scheme II the phases are not renormalized, as they are found to be UV finite.

Scheme I is based on the idea that the absorptive contributions should not enter the renormalization procedure. Therefore, it requires that the absorptive contributions not be included in the on-shell mass renormalization conditions [Eqs. (37) and (39)]. While the phases of the complex counterterms of the mass matrix parameters are also found to be UV finite, no condition is imposed on them. Notice that it is always possible to rephase the parameters of the chagino/neutralino sector, since only the relative phases are physically relevant. Scheme II is supported by the argument that the phases are not renormalized, i.e., they are the same at tree level and loop level. Therefore, it is clear which of the fundamental parameters are chosen to be real and which are chosen to be complex; i.e., in scheme II $M_2$ is fixed to be real, while in scheme I its counterterm is allowed to be complex. As stated earlier, the results in both schemes should agree in the case of real parameters. In the complex case, we expect the differences to be very small, as they are of higher order.

### B. The lepton/slepton sector of the cMSSM

For the discussion of the one-loop contributions to the decay channels in Eqs. (5) and (6), a description of the scalar lepton ($\tilde{\ell}$) and neutrino ($\tilde{\nu}_\ell$) sector as well as their fermionic SM partners is needed (we assume no generation mixing and discuss the case for one generation only). The bilinear part of the $\tilde{\ell}$ and $\tilde{\nu}_\ell$ Lagrangian,

$$\mathcal{L}^{\mathrm{mass}}_{\tilde{\ell}/\tilde{\nu}_\ell} = -(\tilde{\ell}^{\dagger}_L, \tilde{\ell}^{\dagger}_R)\mathbf{M}_{\tilde{\ell}}\begin{pmatrix}\tilde{\ell}_L \\ \tilde{\ell}_R\end{pmatrix} - (\tilde{\nu}_\ell{}^{\dagger})\mathbf{M}_{\tilde{\nu}_\ell}(\tilde{\nu}_\ell), \tag{86}$$

contains the slepton and sneutrino mass matrices $\mathbf{M}_{\tilde{\ell}}$ and $\mathbf{M}_{\tilde{\nu}_\ell}$, given by

$$\mathbf{M}_{\tilde{\ell}} = \begin{pmatrix} M^2_{\tilde{\ell}_L} + m^2_\ell + M^2_Z c_{2\beta}(I^3_\ell - Q_\ell s^2_{\mathrm{w}}) & m_\ell X^*_\ell \\ m_\ell X_\ell & M^2_{\tilde{\ell}_R} + m^2_\ell + M^2_Z c_{2\beta}Q_\ell s^2_{\mathrm{w}} \end{pmatrix}, \tag{87}$$

$$\mathbf{M}_{\tilde{\nu}_\ell} = M^2_{\tilde{\ell}_L} + I^3_\nu c_{2\beta}M^2_Z, \tag{88}$$

with

$$X_\ell = A_\ell - \mu^* \tan\beta. \tag{89}$$

$M_{\tilde{\ell}_L}$ and $M_{\tilde{\ell}_R}$ are the soft SUSY-breaking mass parameters, where $M_{\tilde{\ell}_L}$ is equal for all members of an $SU(2)_L$ doublet. $m_\ell$ and $Q_\ell$ are, respectively, the mass and the charge of the

corresponding lepton; $I^3_{\ell/\nu}$ denotes the isospin of $\ell/\nu$; and $A_\ell$ is the trilinear soft-breaking parameter. We use the shorthand notations $c_x = \cos(x)$, $s_x = \sin(x)$. The mass matrix $\mathbf{M}_{\tilde{\ell}}$ can be diagonalized with the help of a unitary transformation $\mathbf{U}_{\tilde{\ell}}$:

$$\mathbf{D}_{\tilde{\ell}} = \mathbf{U}_{\tilde{\ell}}\mathbf{M}_{\tilde{\ell}}\mathbf{U}^{\dagger}_{\tilde{\ell}} = \begin{pmatrix} m^2_{\tilde{\ell}_1} & 0 \\ 0 & m^2_{\tilde{\ell}_2} \end{pmatrix},$$

$$\mathbf{U}_{\tilde{\ell}} = \begin{pmatrix} U_{\tilde{\ell}_{11}} & U_{\tilde{\ell}_{12}} \\ U_{\tilde{\ell}_{21}} & U_{\tilde{\ell}_{22}} \end{pmatrix}. \tag{90}$$

---

[3]Similar divergences appearing in the on-shell renormalization in the sbottom sector, occurring for "maximal sbottom mixing," have been observed and discussed in Refs. [45,46,56].

The mass eigenvalues depend only on $|X_\ell|$. The scalar lepton masses will always be mass ordered, i.e., $m_{\tilde{\ell}_1} \leq m_{\tilde{\ell}_2}$:

$$m_{\tilde{\ell}_{1,2}}^2 = \frac{1}{2}(M_{\tilde{\ell}_L}^2 + M_{\tilde{\ell}_R}^2) + m_\ell^2 + \frac{1}{2}I_\ell^3 c_{2\beta}M_Z^2 \quad (91)$$

$$m_{\tilde{\nu}_\ell}^2 = M_{\tilde{\ell}_L}^2 + I_\nu^3 c_{2\beta}M_Z^2. \quad (92)$$

A detailed description of the renormalization of this sector can be found in Refs. [45,46,51]. Here we just briefly review the restoration of the $SU(2)_L$ relation for the renormalized slepton mass parameters. Since our on-shell approach results in an independent renormalization of the charged sleptons and of the scalar neutrino, we need to restore the $SU(2)_L$ relation at one loop to avoid problems concerning UV and IR finiteness, as discussed in detail in Ref. [56]. This is achieved via a shift in the $M_{\tilde{\ell}_L}$ parameter entering the $\tilde{\ell}$ mass matrix (see also Refs. [45,46,57,58]). Requiring the $SU(2)_L$ relation to be valid at the loop level induces the following shift in $M_{\tilde{\ell}_L}^2(\tilde{\ell})$:

$$M_{\tilde{\ell}_L}^2(\tilde{\ell}) = M_{\tilde{\ell}_L}^2(\tilde{\nu}_\ell) + \delta M_{\tilde{\ell}_L}^2(\tilde{\nu}_\ell) - \delta M_{\tilde{\ell}_L}^2(\tilde{\ell}), \quad (93)$$

with

$$\delta M_{\tilde{\ell}_L}^2(\tilde{\ell}) = |U_{\tilde{\ell}_{11}}|^2 \delta m_{\tilde{\ell}_1}^2 + |U_{\tilde{\ell}_{12}}|^2 \delta m_{\tilde{\ell}_2}^2 - U_{\tilde{\ell}_{22}}U_{\tilde{\ell}_{12}}^* \delta Y_\ell$$
$$- U_{\tilde{\ell}_{12}}U_{\tilde{\ell}_{22}}^* \delta Y_\ell^* - 2m_\ell \delta m_\ell + M_Z^2 c_{2\beta}Q_\ell \delta s_w^2$$
$$- (I_\ell^3 - Q_\ell s_w^2)(c_{2\beta}\delta M_Z^2 + M_Z^2 \delta c_{2\beta}), \quad (94)$$

$$\delta M_{\tilde{\ell}_L}^2(\tilde{\nu}_\ell) = \delta m_{\tilde{\nu}_\ell}^2 - I_\nu^3(c_{2\beta}\delta M_Z^2 + M_Z^2 \delta c_{2\beta}). \quad (95)$$

Such shifts, however, mean that both slepton masses are no longer on shell. An additional shift in $M_{\tilde{\ell}_R}$ restores at least one slepton mass to be on shell:

$$M_{\tilde{\ell}_R}^2(\tilde{\ell}_i) = \frac{m_\ell^2|A_\ell^* - \mu \tan\beta|^2}{M_{\tilde{\ell}_L}^2(\tilde{\ell}) + m_\ell^2 + M_Z^2 c_{2\beta}(I_\ell^3 - Q_\ell s_w^2) - m_{\tilde{\ell}_i}^2}$$
$$- m_\ell^2 - M_Z^2 c_{2\beta}Q_\ell s_w^2 + m_{\tilde{\ell}_i}^2. \quad (96)$$

A "natural" choice is to preserve the character of the sleptons in the renormalization process, and this additional shift relates the mass of the chosen slepton to the slepton parameter $M_{\tilde{\ell}_R}$. As $m_{\tilde{\ell}_1} \leq m_{\tilde{\ell}_2}$ (see above) and $M_{\tilde{\ell}_L}^2 < M_{\tilde{\ell}_R}^2$ for both scenarios considered later (see Table I), we choose to insert $m_{\tilde{\ell}_2}$ into Eq. (96) and recover its original value from the rediagonalization after applying this shift.

The renormalization of the quark/squark sector is described in detail in Ref. [46]. As for the slepton sector, the restoration of the $SU(2)_L$ relation in the squark sector leads to shifts analogous to Eqs. (93) and (96) in the left and right squark mass parameters, respectively, $M_{\tilde{q}_L}$ and $M_{\tilde{q}_R}$. In our subsequent numerical analysis, these shifts have been included for the results calculated in scheme I, but their

effect is found to be negligible for our choice of parameters.

### C. The Higgs boson sector of the cMSSM

The two Higgs doublets of the cMSSM are decomposed in the following way:

$$\mathcal{H}_1 = \begin{pmatrix} H_{11} \\ H_{12} \end{pmatrix} = \begin{pmatrix} v_1 + \frac{1}{\sqrt{2}}(\phi_1 - i\chi_1) \\ -\phi_1^- \end{pmatrix},$$
$$\mathcal{H}_2 = \begin{pmatrix} H_{21} \\ H_{22} \end{pmatrix} = e^{i\xi}\begin{pmatrix} \phi_2^+ \\ v_2 + \frac{1}{\sqrt{2}}(\phi_2 + i\chi_2) \end{pmatrix}. \quad (97)$$

Besides the vacuum expectation values $v_1$ and $v_2$, in Eq. (97) a possible new phase $\xi$ between the two Higgs doublets is introduced. After a rotation to the physical fields, one obtains for the terms linear and bilinear in the fields

$$V_H = \dots + T_h h + T_H H + T_A A$$
$$- \frac{1}{2}(h, H, A, G)\mathbf{M}_{hHAG}^{\text{diag}}\begin{pmatrix} h \\ H \\ A \\ G \end{pmatrix}$$
$$+ (H^+, G^+)\mathbf{M}_{H^\pm G^\pm}^{\text{diag}}\begin{pmatrix} H^- \\ G^- \end{pmatrix} + \cdots, \quad (98)$$

where the tree-level masses are denoted as $m_h$, $m_H$, $m_A$, $m_G$, $M_{H^\pm}$, $m_{G^\pm}$. With the help of a Peccei-Quinn transformation [59], $\mu$ and the complex soft SUSY-breaking parameters in the Higgs sector can be redefined [60] such that the complex phases vanish at tree level.

Including higher-order corrections, the three neutral Higgs bosons can mix [8,10,11,50],

$$(h, H, A) \longrightarrow (h_1, h_2, h_3), \quad (99)$$

where we define the loop corrected masses according to

$$M_{h_1} \leq M_{h_2} \leq M_{h_3}. \quad (100)$$

Details about the renormalization and the **Z** factors, ensuring the on-shell properties of external Higgs bosons, can be found in Refs. [46,50]. For the renormalization of $\tan\beta$ and the Higgs field renormalization the $\overline{\text{DR}}$ scheme is chosen [46,50]. This leads to the introduction of the scale $\mu_R$, which will be fixed later to the mass of the decaying particle.

TABLE I. MSSM parameters for the initial numerical investigation; all mass parameters are in GeV. $M_1$, $M_2$ and $\mu$ are chosen such that the values for $m_{\tilde{\chi}_1^\pm}$ and $m_{\tilde{\chi}_2^\pm}$ and Eq. (101) are fulfilled (see text).

| $\tan\beta$ | $M_{H^\pm}$ | $m_{\tilde{\chi}_2^\pm}$ | $m_{\tilde{\chi}_1^\pm}$ | $M_{\tilde{\ell}_L}$ | $M_{\tilde{\ell}_R}$ | $A_\ell$ | $M_{\tilde{q}_L}$ | $M_{\tilde{q}_R}$ | $A_q$ |
|---|---|---|---|---|---|---|---|---|---|
| 20 | 160 | 600 | 350 | 300 | 310 | 400 | 1300 | 1100 | 2000 |

## III. CALCULATION OF LOOP DIAGRAMS

In this section, we give some details about the calculation of the higher-order corrections to the neutralino decays. Sample diagrams are shown in Figs. 1–6. Here the generic internal particles are labeled as follows: $F$ denotes a SM fermion, chargino, or neutralino, $S$ denotes a sfermion or a Higgs, and $V$ denotes a $\gamma$, $Z$, or $W^{\pm}$. Concerning the diagrams for decays into charged particles, although we only show diagrams for decays into $\tilde{\chi}_i^-$ or leptons, we also include the corresponding diagrams for the decays into $\tilde{\chi}_i^+$ or antileptons. Not shown are the diagrams for real (hard or soft) photon radiation. These are obtained from the corresponding tree-level diagrams by attaching a photon to the electrically charged external particles. It should be noted that the expressions for the tree-level diagrams are given explicitly in the Appendix. Counterterm diagrams are also not shown, but these can be obtained from the corresponding tree-level diagrams by replacing the tree-level vertex with the counterterm vertex.

Internally appearing Higgs bosons do not receive higher-order corrections in their masses or couplings, which would correspond to effects beyond one loop. Furthermore, we find that using loop-corrected Higgs boson masses and couplings for the internal Higgs bosons
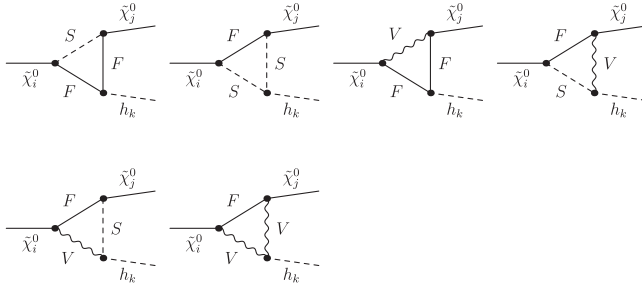
leads to a divergent result. For external Higgs bosons, as mentioned in Sec. II C, the appropriate **Z** factors are applied, following the prescription of Ref. [50]. For the numerical analysis, these factors, as well as the loop-corrected masses for external Higgs bosons, are obtained from FeynHiggs 2.9.0. Diagrams with a gauge boson/ Goldstone-Higgs self-energy contribution on the external Higgs boson leg, absent from the Higgs **Z** factors [50], are also required for the decays $\tilde{\chi}_i^0 \rightarrow \tilde{\chi}_j^0 h_k$ ($i = 2, 3, 4$; $j < i$;



FIG. 3.   Generic Feynman diagrams for the decay $\tilde{\chi}_i^0 \rightarrow \tilde{\chi}_j^- H^+$ ($i = 2, 3, 4$; $j = 1, 2$). $F$ can be a SM fermion, chargino, or neutralino; $S$ can be a sfermion or a Higgs boson; $V$ can be a $\gamma$, $Z$, or $W^{\pm}$. Not shown are the diagrams with a $W^+$-$H^+$ or $G^+$-$H^+$ transition contribution on the external Higgs boson leg.



FIG. 1.   Generic Feynman diagrams for the decay $\tilde{\chi}_i^0 \rightarrow \tilde{\chi}_j^0 h_k$ ($i = 2, 3, 4$; $j < i$; $k = 1, 2, 3$). $F$ can be a SM fermion, chargino, or neutralino; $S$ can be a sfermion or a Higgs boson; $V$ can be a $\gamma$, $Z$, or $W^{\pm}$. Not shown are the diagrams with a $Z$-$h_k$ or $G$-$h_k$ transition contribution on the external Higgs boson leg.



FIG. 4.   Generic Feynman diagrams for the decay $\tilde{\chi}_i^0 \rightarrow \tilde{\chi}_j^- W^+$ ($i = 2, 3, 4$; $j = 1, 2$). $F$ can be a SM fermion, chargino, or neutralino; $S$ can be a sfermion or a Higgs boson; $V$ can be a $\gamma$, $Z$, or $W^{\pm}$.
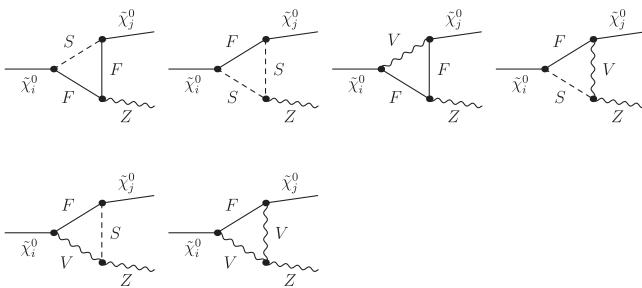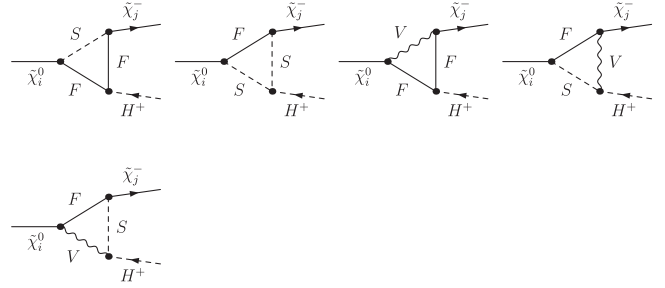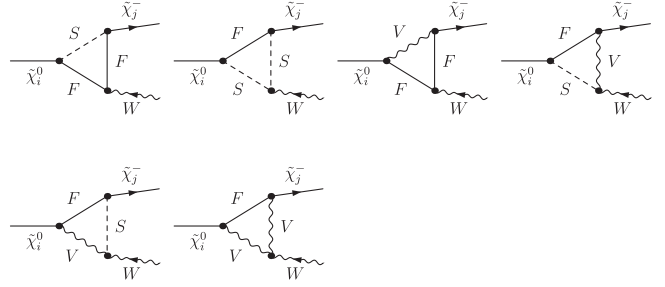


FIG. 2.   Generic Feynman diagrams for the decay $\tilde{\chi}_i^0 \rightarrow \tilde{\chi}_j^0 Z$ ($i = 2, 3, 4$; $j < i$). $F$ can be a SM fermion, chargino, or neutralino; $S$ can be a sfermion or a Higgs boson; $V$ can be a $\gamma$, $Z$, or $W^{\pm}$.
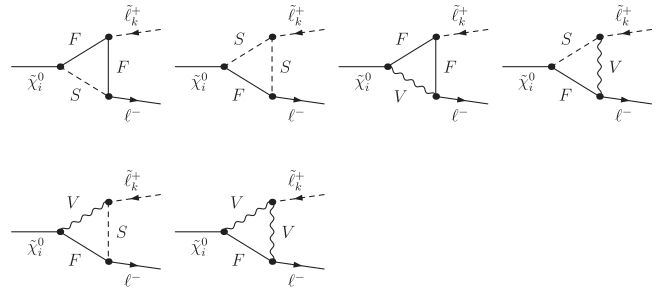


FIG. 5.   Generic Feynman diagrams for the decay $\tilde{\chi}_i^0 \rightarrow \ell^- \tilde{\ell}_k^+$ ($i = 2, 3, 4$; $\ell = e, \mu, \tau$; $k = 1, 2$). $F$ can be a SM fermion, chargino, or neutralino; $S$ can be a sfermion or a Higgs boson; $V$ can be a $\gamma$, $Z$, or $W^{\pm}$.
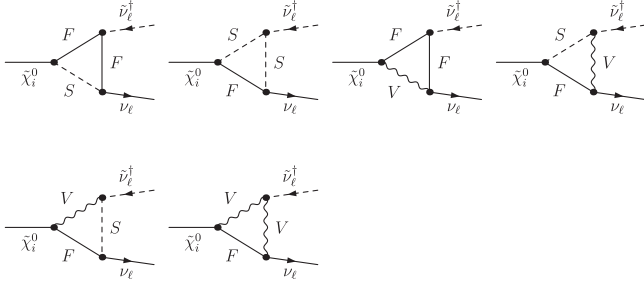
FIG. 6. Generic Feynman diagrams for the decay $\tilde{\chi}_i^0 \to \nu_\ell \tilde{\nu}_\ell^\dagger$ ($i = 2, 3, 4; \ell = e, \mu, \tau$). $F$ can be a SM fermion, chargino, or neutralino; $S$ can be a sfermion or a Higgs boson; $V$ can be a $\gamma$, $Z$, or $W^\pm$.

$k = 1, 2, 3$), (Fig. 1, with a $Z/G - h_k$ transition), and similarly for the decays $\tilde{\chi}_i^0 \to \tilde{\chi}_j^- H^+$ ($i = 2, 3, 4$; $j = 1, 2$), (Fig. 3, with a $W^+/G^+ - H^+$ transition). On the other hand, Goldstone-Higgs/gauge boson self-energy corrections for the neutralino decay to a chargino/neutralino and a gauge boson $\tilde{\chi}_i^0 \to \tilde{\chi}_j^0 Z$ ($i = 2, 3, 4$; $j < i$) or $\tilde{\chi}_i^0 \to \tilde{\chi}_j^- W^+$ ($i = 2, 3, 4$; $j = 1, 2$) can be neglected, as these vanish on mass shell; i.e., for $p^2 = M_Z^2$ ($p^2 = M_W^2$) due to $\varepsilon \cdot p = 0$, where $p$ denotes the external momentum and $\varepsilon$ the polarization vector of the gauge boson.

The diagrams and corresponding amplitudes have been obtained with FeynArts [61]. The model file for calculations in scheme I, including the MSSM counterterms, is described in more detail in Ref. [46], and the model file used for calculations in scheme II is based on that discussed in Refs. [37,44]. The further evaluation has been performed with FormCalc (and LoopTools) [62]. As a regularization scheme for the UV divergences we have used constrained differential renormalization [63], which has been shown to be equivalent to dimensional reduction [64] at the one-loop level [62]. Thus, the employed regularization preserves SUSY [65,66]. All UV divergences cancel in the final result.

The IR divergences from diagrams with an internal photon have to cancel with the ones from the corresponding real soft radiation, where we have included the soft photon contribution following the description given in Ref. [67]. The IR divergences arising from the diagrams involving a $\gamma$ are regularized by introducing a finite photon mass, $\lambda$. All IR divergences, i.e., all divergences in the limit $\lambda \to 0$, cancel to all orders once virtual and real diagrams for one decay channel are added. The only exceptions are the decays $\tilde{\chi}_{2,3,4}^0 \to \tilde{\chi}_1^\pm W^\mp$. The shift to the neutralino on-shell masses via Eq. (68) results in an IR divergence at the two-loop level, i.e., here we find a cancellation of the divergences "only" at the one-loop level, as required for our one-loop calculation. The remaining two-loop IR divergence could be eliminated by a symmetry-restoring counterterm in the $\tilde{\chi}_{2,3,4}^0 \to \tilde{\chi}_1^\pm W^-$ vertex, similar to the evaluation of the decay $\tilde{t}_2 \to \tilde{b}_{1,2} W^+$

in Ref. [46]. We have furthermore checked that our result does not depend on $\Delta E$, defining the energy cut that separates the soft from the hard radiation. Our numerical results have been obtained for $\Delta E = 10^{-5} \times m_{\tilde{\chi}_i^0}$ for all channels.[4]

## IV. NUMERICAL ANALYSIS

In this section, we will first introduce and motivate the scenarios studied, discussing the current experimental constraints considered, then introduce the observables calculated, and finally present our results for each of the decay channels of the heavier neutralino ($\tilde{\chi}_4^0 \to xy$) as a function of $\varphi_{M_1}$.

As stated earlier, we present our results in two scenarios. In both, the absolute value of $M_1$ (see above) is fixed via the GUT relation (with $|M_2| \equiv M_2$):

$$|M_1| = \frac{5}{3}\tan^2\theta_w M_2 \approx \frac{1}{2}M_2. \tag{101}$$

For the numerical analysis, we obtain $M_2$ and $\mu$ from the fixed chargino masses $m_{\tilde{\chi}_{1,2}^\pm}$, and $|M_1|$ via Eq. (101), leaving $\varphi_{M_1}$ as a free parameter. Our two scenarios arise due to the ambiguity in calculating $\mu$ and $M_2$ from $m_{\tilde{\chi}_{1,2}^\pm}$. This ambiguity can be resolved by choosing an addition condition, $\mu > M_2$ or $\mu < M_2$. The first choice, denoted by $\mathcal{S}_h$, results in a Higgsino-like $\tilde{\chi}_4^0$, while the second choice, denoted by $\mathcal{S}_g$, results in a gaugino-like $\tilde{\chi}_4^0$.

The values of the parameters for these scenarios are given in Table I, where, in analogy to the slepton parameters $M_{\tilde{\ell}_L}$, $M_{\tilde{\ell}_R}$ and $A_\ell$ defined in Sec. II B for the sleptons, $M_{\tilde{q}_L}$ and $M_{\tilde{q}_R}$ are the left- and right-handed soft SUSY-breaking mass parameters, and $A_q$ is the trilinear soft-breaking parameter for the squarks. These are chosen such that most decay modes are open simultaneously to permit an analysis of as many channels as possible. Only decays into the heavier chargino $\tilde{\chi}_2^\pm$ in general degenerate with the heavier neutralino, and the decay channels $\tilde{\chi}_4^0 \to \tilde{\chi}_3^0 h_k/Z$, ($k = 1, 2, 3$) in $\mathcal{S}_h$ are kinematically closed. We also ensure that the scenarios are consistent with the MSSM Higgs boson searches at LEP [3], Tevatron [68] and LHC [69]. The light Higgs mass scale together with the value of $\tan\beta = 20$ are in potential conflict with the recent MSSM Higgs search results, which, however, have only been obtained in the $m_h^{max}$ scenario [70]. We stick to our parameter combination to facilitate the numerical analysis with all decay channels involving Higgs bosons being open simultaneously. On the other hand, the recent discovery of the (lightest) Higgs boson at the LHC [4] allows for

---

[4]The larger cut is necessary to obtain a better convergence of the integration over the three-body phase space. The contribution from nearly collinear photons (along the direction of the electron) leads to numerical instabilities in the integration.

TABLE II.    The chargino and neutralino masses in the scenarios $\mathcal{S}_g$ and $\mathcal{S}_h$. We also show the values for the "derived" parameters $M_1$, $M_2$ and $\mu$. All mass parameters are in GeV, rounded to 0.1 GeV to show the sizes of small mass differences, which can determine whether a certain decay channel is kinematically closed or open.

| Scenario | $m_{\tilde{\chi}_2^\pm}$ | $m_{\tilde{\chi}_1^\pm}$ | $m_{\tilde{\chi}_4^0}$ | $m_{\tilde{\chi}_3^0}$ | $m_{\tilde{\chi}_2^0}$ | $m_{\tilde{\chi}_1^0}$ | $\mu$ | $M_2$ | $M_1$ |
|---|---|---|---|---|---|---|---|---|---|
| $\mathcal{S}_g$ | 600.0 | 350.0 | 600.0 | 364.2 | 359.6 | 267.2 | 362.1 | 581.8 | 277.7 |
| $\mathcal{S}_h$ | 600.0 | 350.0 | 600.1 | 586.2 | 349.9 | 171.4 | 581.8 | 362.1 | 172.8 |

TABLE III.    The slepton and Higgs masses in the scenarios $\mathcal{S}_g$ and $\mathcal{S}_h$. The selectron and electron sneutrino masses are equal to those of the corresponding smuon and muon sneutrino up to a few tenths of GeV. All masses are in GeV, rounded to 0.1 GeV.

| Scenario | $m_{\tilde{\mu}_1}$ | $m_{\tilde{\mu}_2}$ | $m_{\tilde{\tau}_1}$ | $m_{\tilde{\tau}_2}$ | $m_{\tilde{\nu}_\mu}$ | $m_{\tilde{\nu}_\tau}$ | $M_{H^\pm}$ | $m_{h_1}$ | $m_{h_2}$ | $m_{h_3}$ |
|---|---|---|---|---|---|---|---|---|---|---|
| $\mathcal{S}_g$ | 303.2 | 313.1 | 287.3 | 328.0 | 293.0 | 293.0 | 160.0 | 125.8 | 137.2 | 140.3 |
| $\mathcal{S}_h$ | 302.9 | 313.3 | 273.7 | 339.5 | 293.0 | 293.0 | 160.0 | 125.8 | 137.4 | 140.3 |

$\tan\beta \gtrsim 9$, as given in Table I.[5] Furthermore, the following exclusion limits for neutralinos [71] hold in our numerical scenarios:

$$m_{\tilde{\chi}_1^0} > 46 \text{ GeV}, \qquad m_{\tilde{\chi}_2^0} > 62 \text{ GeV},$$
$$m_{\tilde{\chi}_3^0} > 100 \text{ GeV}, \qquad m_{\tilde{\chi}_4^0} > 116 \text{ GeV}. \qquad (102)$$

It should be noted that the limit for $m_{\tilde{\chi}_1^0}$ arises solely when Eq. (101) is assumed to hold. In the absence of this condition, no limit on a light neutralino mass exists; see Ref. [72] and references therein.

The most restrictive experimental constraints on the phase of $\varphi_{M_1}$ arise due to the bounds on the electric dipole moments (EDMs) of the neutron $d_n$, mercury $d_{\text{Hg}}$, and thallium $d_{\text{Tl}}$ [73–75].[6] Using CPsuperH 2.2 [80], we have calculated these EDMs and find that in the scenarios studied, the bounds due to the thallium EDM are the most constraining: $\varphi_{M_1} \lesssim \pi/100$. This is mainly because, in order to keep all channels open, the selectrons in our scenarios are light. On increasing the masses of the lower generation of sleptons to 1.2 TeV, $\varphi_{M_1}$ is unconstrained. It should be noted that such a change would only affect our results such that the decays to the lower generation slepton channels are no longer open: the loop corrections to the other decays are largely independent of these masses.

The chargino and neutralino masses for $\varphi_{M_1} = 0$ are shown in Table II, while the Higgs and slepton masses are shown in Table III. Here $h_2$ corresponds to the pure $\mathcal{CP}$-odd Higgs boson. For $\varphi_{M_1} = 90°$ (i.e., the maximal $\mathcal{CP}$ violation possible in our numerical analysis), we find the same Higgs boson masses within the precision of

Table III. In this case, $h_2$ receives a very small $\mathcal{CP}$-even admixture of $\lesssim 0.003\%$ in both scenarios, while $h_1$ and $h_3$ remain correspondingly a nearly pure $\mathcal{CP}$-even state. The masses $m_{\tilde{\chi}_i^0}$ are chosen such that the neutralinos would be copiously produced in SUSY cascades at the LHC. Furthermore, the production of $\tilde{\chi}_i^0 \tilde{\chi}_j^0$ for $i = 1, 2$ and $j = 2, 3, 4$ at the ILC 1000, i.e., with $\sqrt{s} = 1000$ GeV via $e^+ e^- \rightarrow \tilde{\chi}_i^0 \tilde{\chi}_j^0$, will be possible, where unpolarized tree-level cross sections in the scenarios $\mathcal{S}_g$ and $\mathcal{S}_h$ are shown in Table IV. All the subsequent decay modes [Eqs. (3)–(6)] would be (in principle) open, and the clean environment would permit a detailed study of neutralino decays [15,16]. Higher-order corrections to the production cross sections would change the values in Table IV by up to $\mathcal{O}(10\%)$ [81], and choosing appropriate polarized beams could enhance the cross sections by a factor of 2 to 3. The accuracy of the relative branching ratio [Eq. (105)] at the ILC would be close to the statistical uncertainty, and from the high-luminosity running of the ILC 1000, a determination of the branching ratios at the percent level might be achievable. We have calculated the decay width at tree level ("tree") and at the one-loop level ("full"), including *all* one-loop contributions as described in Sec. III, and in addition the relative size of this one-loop correction via

$$\Gamma^{\text{tree}} \equiv \Gamma^{\text{tree}}(\tilde{\chi}_i^0 \rightarrow \text{xy}), \qquad \Gamma^{\text{full}} \equiv \Gamma^{\text{full}}(\tilde{\chi}_i^0 \rightarrow \text{xy}),$$
$$\Delta\Gamma/\Gamma \equiv \frac{\Gamma^{\text{full}} - \Gamma^{\text{tree}}}{\Gamma^{\text{tree}}}. \qquad (103)$$

In the figures below, we show the absolute value of the various decay widths, $\Gamma(\tilde{\chi}_4^0 \rightarrow \text{xy})$ on the left and the relative correction from the full one-loop contributions on the right. The total decay width is defined as the sum of all kinematically open two-body decay widths,

---

[5]The Higgs mass in the allowed range can be obtained by varying the squark trilinear coupling $A_q$.

[6]In addition, the EDMs of heavy quarks [76], the electron [77,78] and the deuteron [79] should be taken into account.

TABLE IV.   Neutralino production cross sections at the ILC 1000. Here $\sigma_{0,0}$ denotes the cross section for unpolarized beams, while $\sigma_{\rm pol}$ denotes the cross section with electron and positron polarization $-80\%$ and $+60\%$, respectively. The sums of $\tilde{\chi}_i^0 \tilde{\chi}_j^0$ for $i = 2, 3, 4$ are performed over $j \leq i$. The two rightmost columns show the statistical precision for a (hypothetical) branching ratio of 10% assuming an integrated luminosity of 1 ab$^{-1}$, rounded to 1%.

| Scenario | Process | $\sigma_{0,0}$[fb] | $\sigma_{\rm pol}$[fb] | Stat. prec.$_{0,0}$ (%) | Stat. prec.$_{\rm pol}$ (%) |
|---|---|---|---|---|---|
| $\mathcal{S}_g$ | $e^+e^- \rightarrow \tilde{\chi}_4^0 \tilde{\chi}_1^0$ | 5.2 | 15.0 | 4 | 3 |
| $\mathcal{S}_h$ | $e^+e^- \rightarrow \tilde{\chi}_4^0 \tilde{\chi}_1^0$ | 1.0 | 1.6 | 10 | 8 |
| $\mathcal{S}_g$ | $e^+e^- \rightarrow \tilde{\chi}_4^0 \tilde{\chi}_2^0$ | 1.0 | 2.9 | 10 | 6 |
| $\mathcal{S}_h$ | $e^+e^- \rightarrow \tilde{\chi}_4^0 \tilde{\chi}_2^0$ | 0.4 | 1.1 | 16 | 10 |
| $\mathcal{S}_g$ | $e^+e^- \rightarrow \tilde{\chi}_4^0 \tilde{\chi}_3^0$ | 0.5 | 0.4 | 14 | 16 |
| $\mathcal{S}_g$ | $e^+e^- \rightarrow \sum \tilde{\chi}_4^0 \tilde{\chi}_j^0$ | 6.7 | 18.3 | 4 | 2 |
| $\mathcal{S}_h$ | $e^+e^- \rightarrow \sum \tilde{\chi}_4^0 \tilde{\chi}_j^0$ | 1.4 | 2.7 | 8 | 6 |
| $\mathcal{S}_g$ | $e^+e^- \rightarrow \sum \tilde{\chi}_3^0 \tilde{\chi}_j^0$ | 39.9 | 71.8 | 2 | 1 |
| $\mathcal{S}_h$ | $e^+e^- \rightarrow \sum \tilde{\chi}_3^0 \tilde{\chi}_j^0$ | 3.2 | 6.1 | 6 | 4 |
| $\mathcal{S}_g$ | $e^+e^- \rightarrow \sum \tilde{\chi}_2^0 \tilde{\chi}_j^0$ | 13.5 | 11.0 | 3 | 3 |
| $\mathcal{S}_h$ | $e^+e^- \rightarrow \sum \tilde{\chi}_2^0 \tilde{\chi}_j^0$ | 46.2 | 132.4 | 1 | 1 |

$$\Gamma_{\rm tot}^{\rm tree} \equiv \sum_{xy} \Gamma^{\rm tree}(\tilde{\chi}_i^0 \rightarrow xy), \qquad \Gamma_{\rm tot}^{\rm full} \equiv \sum_{xy} \Gamma^{\rm full}(\tilde{\chi}_i^0 \rightarrow xy).$$

$$(104)$$

The absolute and relative changes of the branching ratios are defined as follows:

$$\mathrm{BR}^{\rm tree} \equiv \frac{\Gamma^{\rm tree}(\tilde{\chi}_i^0 \rightarrow xy)}{\Gamma_{\rm tot}^{\rm tree}}, \qquad \mathrm{BR}^{\rm full} \equiv \frac{\Gamma^{\rm full}(\tilde{\chi}_i^0 \rightarrow xy)}{\Gamma_{\rm tot}^{\rm full}},$$

$$\frac{\Delta \mathrm{BR}}{\mathrm{BR}} \equiv \frac{\mathrm{BR}^{\rm full} - \mathrm{BR}^{\rm tree}}{\mathrm{BR}^{\rm full}}. \qquad (105)$$

The last quantity is crucial in order to analyze the impact of the one-loop corrections on the phenomenology at the LHC and the ILC (see below). Since decays to a light Higgs and the LSP are of particular importance, for the decay $\tilde{\chi}_4^0 \rightarrow \tilde{\chi}_1^0 h_1$, we also show, in the lower panels, the branching ratio $\mathrm{BR}(\tilde{\chi}_4^0 \rightarrow xy)$ (left) and the relative size of the one-loop correction (right). The corresponding branching ratios for the other channels can be inferred from these plots.

In order to distinguish the results evaluated in the two schemes, we denote those of scheme II with a tilde, i.e., $\tilde{\mathcal{S}}_g$ and $\tilde{\mathcal{S}}_h$ for the scenarios $\mathcal{S}_g$ and $\mathcal{S}_h$, respectively. It should be noted that the tree-level results obtained for the two schemes fully agree, as our two renormalization schemes differ only in the treatment of complex parts. The difference of one-loop results for real parameters is negligible, and is only due to a different handling of the corrections in the squark sector, which is not highly relevant for the electroweak decays. Therefore, the results for both schemes are only shown on the right panels for the relative corrections. In Sec. IV F, we will summarize and discuss the differences between these schemes, highlighting those channels where the deviations are largest.

The numerical results we show in this section are, of course, dependent on the choice of MSSM parameters. Nevertheless, they give an idea of the relevance of the full one-loop corrections. Decay widths (and their respective one-loop corrections) that may appear to be unobservable due to the small size of their BR could become important if other channels are kinematically forbidden. Consequently, the one-loop corrections to *all* channels are evaluated analytically, but in the numerical analysis we only show the channels that are kinematically open in our numerical scenarios, except for the decays into leptons of the first two families, which are closely related to the decays into third-family leptons.

### A. Decays into charged Higgs and W bosons

We start our numerical analysis with the decays $\tilde{\chi}_4^0 \rightarrow \tilde{\chi}_1^- H^+$, presented in Fig. 7. The partial decay width for the charge conjugated process $\tilde{\chi}_4^0 \rightarrow \tilde{\chi}_1^+ H^-$ can be obtained by taking the charge conjugate of all the couplings. Since in our analysis only $M_1$ is complex, this is obtained with the transformation $\varphi_{M_1} \rightarrow 2\pi - \varphi_{M_1}$. This argument will also be valid for all the decays into $W$ bosons and lepton-slepton pairs described below. All these decays have also been computed in order to evaluate the total decay width at the one-loop level.

This channel yields decay widths of around 0.7 GeV in both scenarios, corresponding to BRs of $\sim 4.5\%$ for $\mathcal{S}_g$ and $\sim 11\%$ for $\mathcal{S}_h$. The tree-level partial widths are almost equal in both scenarios due to the symmetry of the Higgs-gaugino-Higgsino couplings under $M_2 \leftrightarrow \mu$ exchange, as well as to the similar phase space. The relative corrections, shown in the right plot, are on the order of a few percent. The mild dependence on $\varphi_{M_1}$ for this process is due to our choice of parameters, in particular the GUT relation on the gaugino parameters $M_1$ and $M_2$, which leads to a weak dependence of the heavier neutralinos on
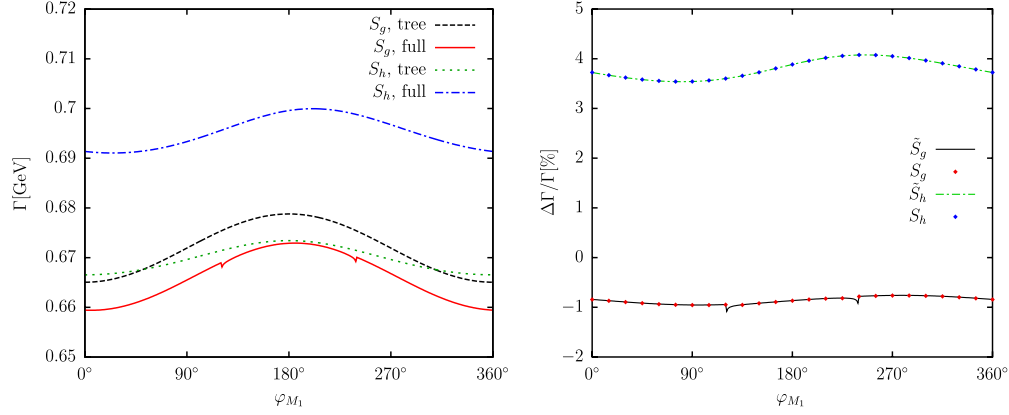
FIG. 7 (color online). $\Gamma(\tilde{\chi}_4^0 \to \tilde{\chi}_1^- H^+)$. Tree-level ("tree") and full one-loop ("full") corrected decay widths are shown with the parameters chosen according to Table I, with $\varphi_{M_1}$ varied. The left plot shows the decay width, and the right plot shows the relative size of the corrections.

$M_1$. The dips best visible in the right panel are due to the $\tilde{\chi}_1^- \to \tilde{\chi}_1^0 W^-$ threshold, at $\varphi_{M_1} \simeq 125°$ and $\varphi_{M_1} \simeq 235°$. Due to $\mathcal{CPT}$ invariance, the masses are invariant under $\varphi_{M_1} \to -\varphi_{M_1}$, resulting in mirrored threshold effects. These effects are further discussed in Sec. IV B for the decays into the second lightest neutralino.

The results for the two schemes are shown for the relative corrections in the right panel. The agreement between the relative corrections is at the level of $10^{-5}$ for both scenarios (see Table V), and therefore cannot be visibly distinguished here. It should be noted that the differences between the schemes are particularly small due to mild dependence of the tree-level decay width on

$\varphi_{M_1}$. As the schemes are identical in the real case, only decays with a stronger dependence on the phase $\varphi_{M_1}$ are sensitive to the differences between them.

Next we analyze the decays $\tilde{\chi}_4^0 \to \tilde{\chi}_1^- W^+$ shown in Fig. 8. The general behavior of the decays into $W^+$ is very similar to those into $H^+$ discussed above. This decay yields decay widths around $\sim 1$ GeV in both scenarios, corresponding to BRs of $\sim 7\%$ and $\sim 17\%$ for, respectively, $\mathcal{S}_g$ and $\mathcal{S}_h$, with a mild dependence on $\varphi_{M_1}$. The one-loop effects are found to be, respectively, of $\sim -8\%$ and $\sim -4\%$, and the same thresholds as in the previous process can be observed as dips in the right panels. The agreement between the relative corrections is at the level

TABLE V. Differences between the relative corrections to the decay width for schemes I and II, shown in both scenarios $\mathcal{S}_g$ and $\mathcal{S}_h$, i.e., $\Delta\Gamma/\Gamma(\mathcal{S}_g/\mathcal{S}_h) - \Delta\Gamma/\Gamma(\tilde{\mathcal{S}}_g/\tilde{\mathcal{S}}_h)$, at the specified values of $\varphi_{M_1}$. The missing results correspond to those channels for which the decays are below threshold $\mathcal{S}_h$.

| Channel | $\mathcal{S}_g$ | | $\mathcal{S}_h$ | |
|---|---|---|---|---|
| | 45° | 90° | 45° | 90° |
| $\tilde{\chi}_4^0 \to \tilde{\chi}_1^- H^+$ | $1.5 \times 10^{-5}$ | $2.0 \times 10^{-5}$ | $-6.9 \times 10^{-6}$ | $-4.8 \times 10^{-6}$ |
| $\tilde{\chi}_4^0 \to \tilde{\chi}_1^- W^+$ | $3.4 \times 10^{-6}$ | $6.1 \times 10^{-6}$ | $9.9 \times 10^{-5}$ | $9.7 \times 10^{-5}$ |
| $\tilde{\chi}_4^0 \to \tilde{\chi}_1^0 h_1$ | $-1.9 \times 10^{-4}$ | $-6.1 \times 10^{-4}$ | $-6.3 \times 10^{-5}$ | $-1.8 \times 10^{-4}$ |
| $\tilde{\chi}_4^0 \to \tilde{\chi}_1^0 h_2$ | $4.5 \times 10^{-4}$ | $5.2 \times 10^{-4}$ | $1.5 \times 10^{-4}$ | $1.7 \times 10^{-4}$ |
| $\tilde{\chi}_4^0 \to \tilde{\chi}_1^0 h_3$ | $-1.4 \times 10^{-4}$ | $-3.6 \times 10^{-4}$ | $-9.1 \times 10^{-5}$ | $-2.2 \times 10^{-4}$ |
| $\tilde{\chi}_4^0 \to \tilde{\chi}_2^0 h_1$ | $-1.2 \times 10^{-5}$ | $5.4 \times 10^{-5}$ | $2.7 \times 10^{-6}$ | $6.1 \times 10^{-6}$ |
| $\tilde{\chi}_4^0 \to \tilde{\chi}_2^0 h_2$ | $1.3 \times 10^{-4}$ | $-4.9 \times 10^{-4}$ | $6.0 \times 10^{-6}$ | $7.1 \times 10^{-6}$ |
| $\tilde{\chi}_4^0 \to \tilde{\chi}_2^0 h_3$ | $5.5 \times 10^{-5}$ | $1.0 \times 10^{-4}$ | $4.5 \times 10^{-6}$ | $8.6 \times 10^{-6}$ |
| $\tilde{\chi}_4^0 \to \tilde{\chi}_3^0 h_1$ | $2.4 \times 10^{-4}$ | $-7.2 \times 10^{-4}$ | $\cdots$ | $\cdots$ |
| $\tilde{\chi}_4^0 \to \tilde{\chi}_3^0 h_2$ | $-2.8 \times 10^{-5}$ | $3.2 \times 10^{-5}$ | $\cdots$ | $\cdots$ |
| $\tilde{\chi}_4^0 \to \tilde{\chi}_3^0 h_3$ | $-5.1 \times 10^{-5}$ | $-1.6 \times 10^{-4}$ | $\cdots$ | $\cdots$ |
| $\tilde{\chi}_4^0 \to \tilde{\chi}_1^0 Z$ | $1.2 \times 10^{-3}$ | $7.5 \times 10^{-4}$ | $1.2 \times 10^{-4}$ | $1.7 \times 10^{-4}$ |
| $\tilde{\chi}_4^0 \to \tilde{\chi}_2^0 Z$ | $2.2 \times 10^{-4}$ | $-3.4 \times 10^{-4}$ | $9.5 \times 10^{-6}$ | $7.3 \times 10^{-6}$ |
| $\tilde{\chi}_4^0 \to \tilde{\chi}_3^0 Z$ | $-4.5 \times 10^{-5}$ | $1.2 \times 10^{-5}$ | $\cdots$ | $\cdots$ |
| $\tilde{\chi}_4^0 \to \tau^- \tilde{\tau}_1^+$ | $-1.3 \times 10^{-6}$ | $3.7 \times 10^{-6}$ | $-3.5 \times 10^{-5}$ | $-1.1 \times 10^{-5}$ |
| $\tilde{\chi}_4^0 \to \tau^- \tilde{\tau}_2^+$ | $-6.5 \times 10^{-5}$ | $-6.2 \times 10^{-5}$ | $-1.1 \times 10^{-4}$ | $-1.1 \times 10^{-4}$ |
| $\tilde{\chi}_4^0 \to \nu_\tau \tilde{\nu}_\tau^\dagger$ | $-3.5 \times 10^{-6}$ | $-7.0 \times 10^{-6}$ | $-8.9 \times 10^{-6}$ | $-1.9 \times 10^{-5}$ |
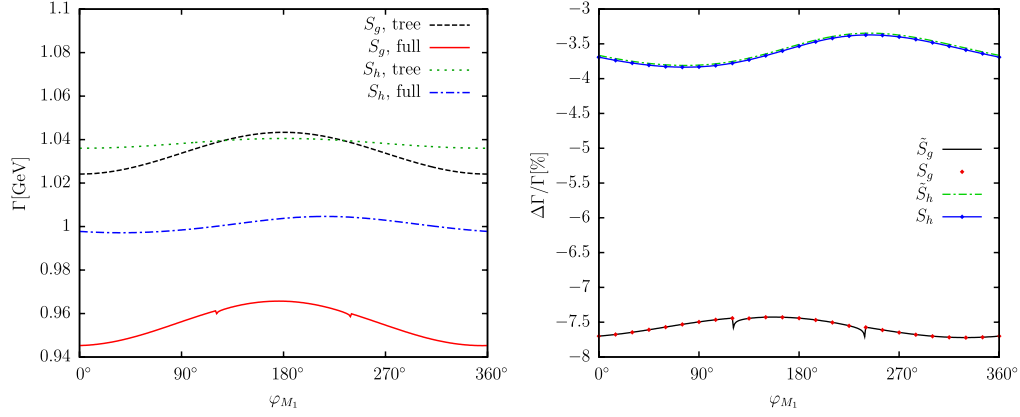
FIG. 8 (color online).   $\Gamma(\tilde{\chi}_4^0 \rightarrow \tilde{\chi}_1^- W^+)$. Tree-level ("tree") and full one-loop ("full") corrected decay widths are shown with the parameters chosen according to Table I, with $\varphi_{M_1}$ varied. The left plot shows the decay width, the right plot shows the relative size of the corrections.

of $10^{-5}$ for $\mathcal{S}_g$ and $10^{-4}$ for $\mathcal{S}_h$ (see Table V), and therefore is again too high to be observed.

## B. Decays into neutral Higgs bosons

Now we turn to the decays involving neutral Higgs bosons. The channels $\tilde{\chi}_4^0 \rightarrow \tilde{\chi}_j^0 h_k$ ($j = 1, 2, 3$; $k = 1, 2, 3$)

can serve as sources for Higgs production from SUSY cascades at the LHC, and are therefore of particular interest.

The decay $\tilde{\chi}_4^0 \rightarrow \tilde{\chi}_1^0 h_1$ is shown in Fig. 9. Contrary to what we observed for the decays into charginos, the two scenarios result in very different decay widths, and both show a strong dependence on $\varphi_{M_1}$, with partial widths
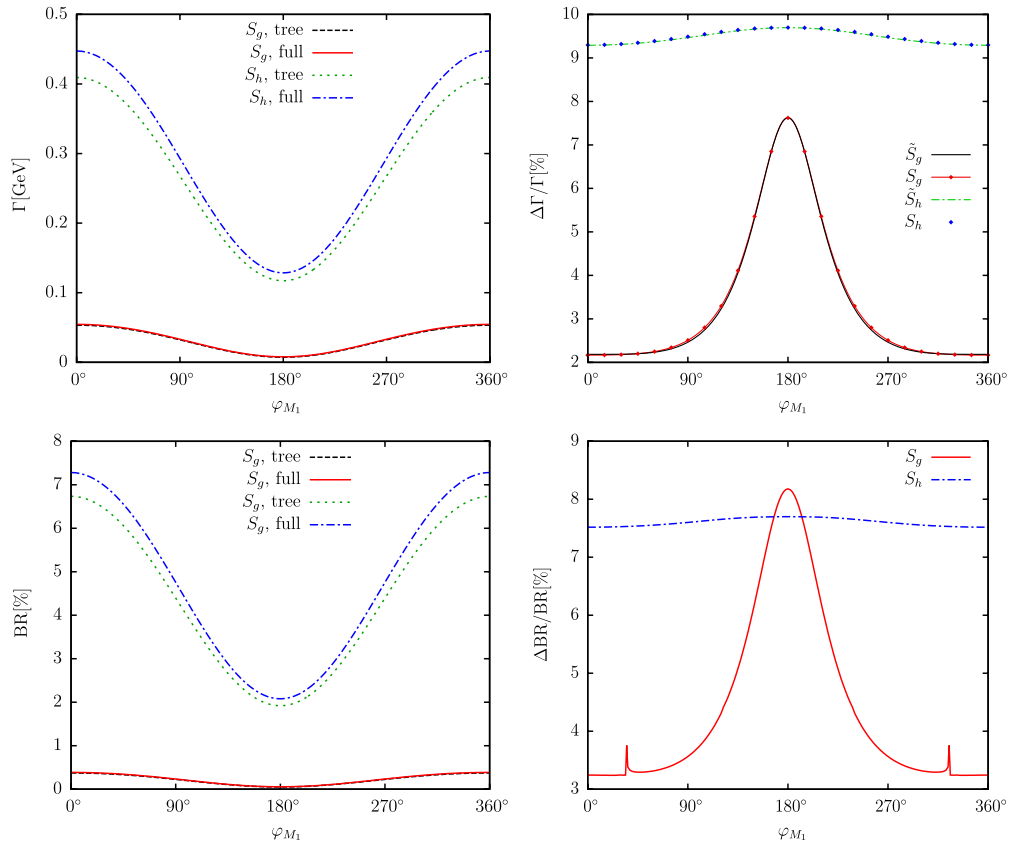


FIG. 9 (color online).   $\Gamma(\tilde{\chi}_4^0 \rightarrow \tilde{\chi}_1^0 h_1)$. Tree-level ("tree") and full one-loop ("full") corrected decay widths are shown with the parameters chosen according to Table I, with $\varphi_{M_1}$ varied. The upper-left plot shows the decay width, and the upper-right plot shows the relative size of the corrections. The lower-left plot shows the BR, and the lower-right plot shows the relative size of the BR.

varying between 0.45 and 0.13 GeV for $\mathcal{S}_h$ and between 0.06 and 0.01 GeV for $\mathcal{S}_g$. The strong dependence on the phase $\varphi_{M_1}$ is a consequence of the change in the relative $\mathcal{CP}$ phase of $\tilde{\chi}_4^0$ and $\tilde{\chi}_1^0$, while the corresponding $\mathcal{CP}$ parity of the light Higgs, which here is $\mathcal{CP}$ even, is not strongly affected. For $\varphi_{M_1} = 0$, $\tilde{\chi}_4^0$ and $\tilde{\chi}_1^0$ have the same relative $\mathcal{CP}$ parity, while for $\varphi_{M_1} = \pi$ they have the opposite one. Therefore, at $\phi_{M_1} = \pi$ the decay is $p$-wave suppressed, while at $\phi_{M_1} = 0$ the $s$-wave mode is allowed. In $\mathcal{S}_h$ the partial decay widths are only partially suppressed, due to the relatively large phase space. In $\mathcal{S}_g$ the suppression is stronger for the tree-level amplitude, leading to larger relative corrections. The relative corrections, shown in the upper-right panel, are $\sim 10\%$ for $\mathcal{S}_h$ and are between 2% and 8% for $\mathcal{S}_g$. For $\mathcal{S}_g$ we observe a small difference between the two schemes at $\varphi_{M_1} \approx \pm 90°$ on the order of 0.1% (see also Table V). It should be noted that here, as opposed to the case of the previous decays, the fact that the tree-level decay width depends strongly on $\varphi_{M_1}$ leads to a noticeable difference between the two schemes. This difference has been highlighted in Fig. 27. In the lower-left panel we show the branching ratios, and in the lower-right panel its relative corrections. Since the difference between the schemes is here very small, we only show these results in scheme I. The peaks at $\varphi_{M_1} = 35°$ and $325°$ are due to the threshold for the decay $\tilde{\chi}_2^0 \to \tilde{\chi}_1^0 h_1$, which leads to a singularity which affects the total width (see the discussion below on these threshold effects). It should be noted that the decay widths and the corresponding branching ratios, as well as their relative corrections, are roughly proportional here because the total width of $\tilde{\chi}_4^0$, shown in Fig. 24 below, is almost independent of $\varphi_{M_1}$ in both scenarios (see the discussion in Sec. IV F).

The results for the decay $\tilde{\chi}_4^0 \to \tilde{\chi}_1^0 h_2$ are shown in Fig. 10. Since in both scenarios $h_2$ tends to the $\mathcal{CP}$-odd Higgs boson for real couplings, the dependence on $\varphi_{M_1}$ is

opposite to that for the decay $\tilde{\chi}_4^0 \to \tilde{\chi}_1^0 h_1$ discussed above, with a $p$-wave suppression at $\varphi_{M_1} = 0$ and with the $s$-wave mode being allowed at $\phi_{M_1} = \pi$. The decay widths are a factor of 2 smaller than those for the decay into the lightest Higgs for $\mathcal{S}_h$, and of the same order for $\mathcal{S}_g$. The relative corrections are also similar, of order $\sim 10\%$ in $\mathcal{S}_h$ and between 2% and 10% for $\mathcal{S}_g$. We can also observe a small difference at large $\varphi_{M_1}$ between the two schemes in $\mathcal{S}_g$, on the order of 0.05% (see Table V).

The decay $\tilde{\chi}_4^0 \to \tilde{\chi}_1^0 h_3$ is shown in Fig. 11. The $\varphi_{M_1}$ dependence of the partial width and its relative correction for this process is qualitatively similar to that of $\tilde{\chi}_4^0 \to \tilde{\chi}_1^0 h_1$. However, for $\mathcal{S}_h$ the partial width is much smaller, between 0.01 and 0.04 GeV. As the difference between the two schemes is on the order of 0.01% (see Table V), they cannot be visibly distinguished here.

The decays $\tilde{\chi}_4^0 \to \tilde{\chi}_2^0 h_1$, $\tilde{\chi}_4^0 \to \tilde{\chi}_2^0 h_2$, and $\tilde{\chi}_4^0 \to \tilde{\chi}_2^0 h_3$ are shown in Figs. 12–14, respectively. In scenario $\mathcal{S}_h$, the second-lightest neutralino is mainly wino-like, with a small mixing with the bino component, leading to a weak dependence on $\varphi_{M_1}$. For $\mathcal{S}_g$, the dependence on $\varphi_{M_1}$ is much larger, since the second-lightest neutralino's Higgsino and bino components are both large.

For $\tilde{\chi}_4^0 \to \tilde{\chi}_2^0 h_1$ in $\mathcal{S}_g$, as shown in Fig. 12, the decay width oscillates from $\sim 1.05$ to 1.2 GeV, and for $\mathcal{S}_h$ the decay width is $\sim 1.2$ GeV. It should be noted that this decay is $s$-wave mode allowed, and therefore the decay widths are 2.5 to 9 times larger than the decay into the lightest Higgs and neutralino. This turns out to be the dominating process, with branching ratios of up to $\sim 8\%$ and $\sim 19\%$ for, respectively, $\mathcal{S}_g$ and $\mathcal{S}_h$. The larger $\varphi_{M_1}$ dependence in $\mathcal{S}_g$ is due to the strong bino-Higgsino mixing of $\tilde{\chi}_2^0$ in this scenario. This feature will be equally relevant for the remaining decays into either $\tilde{\chi}_2^0$ or $\tilde{\chi}_3^0$ discussed below. For $\mathcal{S}_g$, we observe the effect of the threshold for $\tilde{\chi}_2^0 \to \tilde{\chi}_1^0 h_1$ at $\varphi_{M_1} = 35°$ and $325°$. The
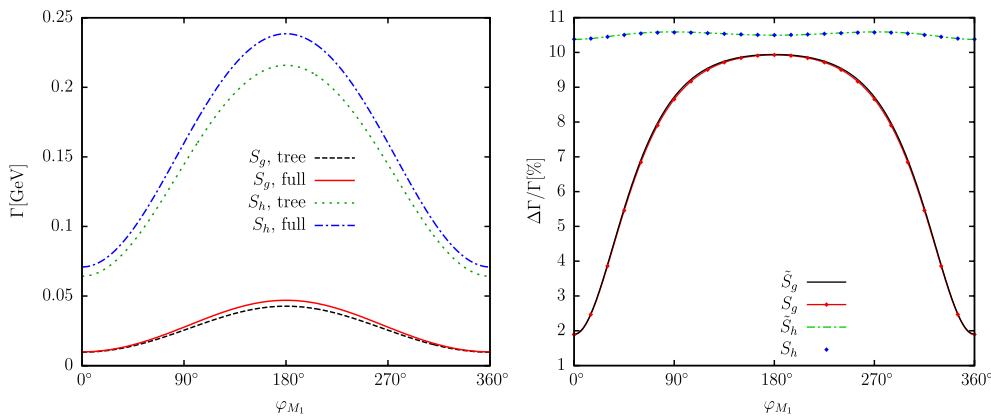


FIG. 10 (color online).　$\Gamma(\tilde{\chi}_4^0 \to \tilde{\chi}_1^0 h_2)$. Tree-level ("tree") and full one-loop ("full") corrected decay widths are shown with the parameters chosen according to Table I, with $\varphi_{M_1}$ varied. The left plot shows the decay width, and the right plot shows the relative size of the corrections.
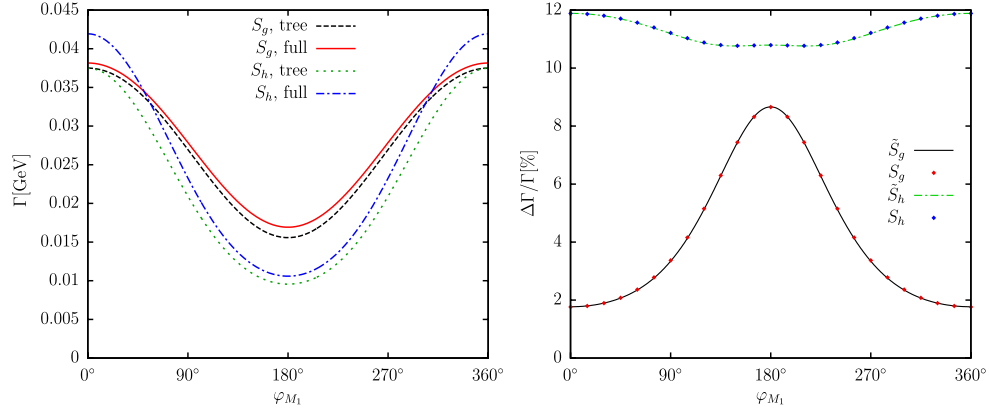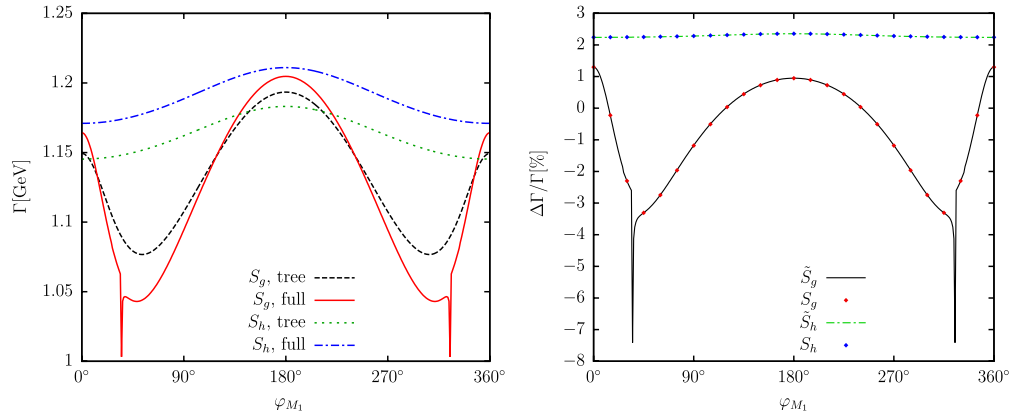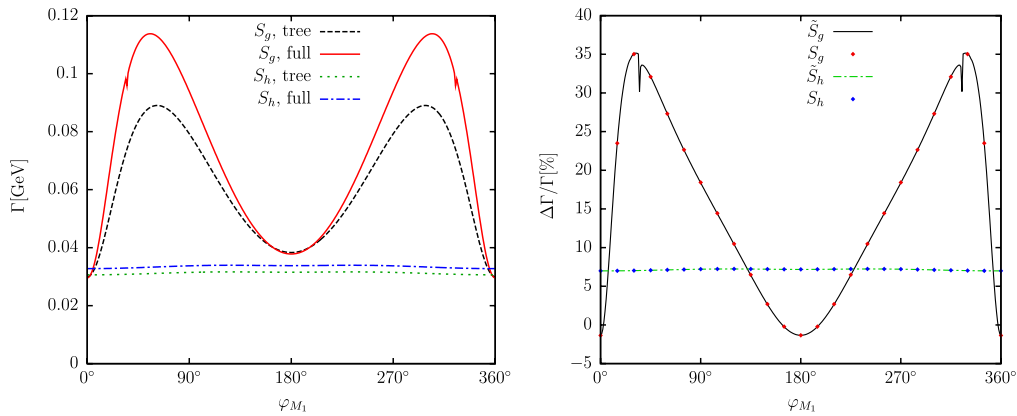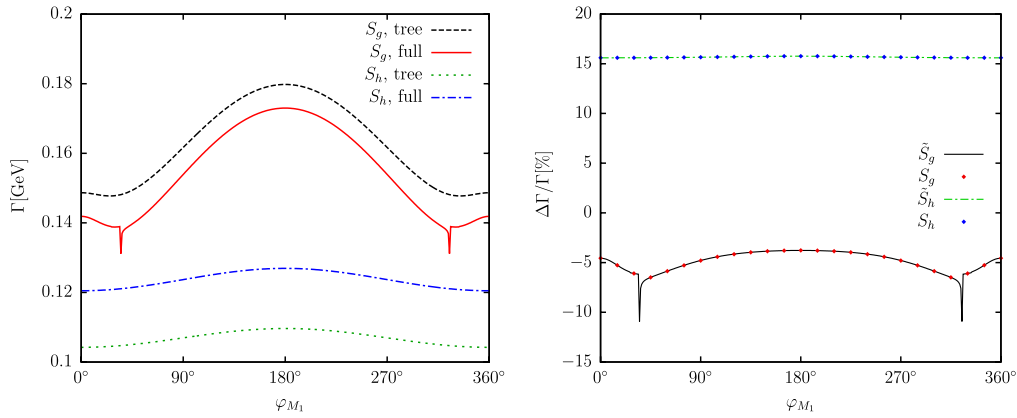
FIG. 11 (color online).  $\Gamma(\tilde{\chi}_4^0 \to \tilde{\chi}_1^0 h_3)$. Tree-level ("tree") and full one-loop ("full") corrected decay widths are shown with the parameters chosen according to Table I, with $\varphi_{M_1}$ varied. The left plot shows the decay width, and the right plot shows the relative size of the corrections.



FIG. 12 (color online).  $\Gamma(\tilde{\chi}_4^0 \to \tilde{\chi}_2^0 h_1)$. Tree-level ("tree") and full one-loop ("full") corrected decay widths are shown with the parameters chosen according to Table I, with $\varphi_{M_1}$ varied. The left plot shows the decay width, and the right plot shows the relative size of the corrections.



FIG. 13 (color online).  $\Gamma(\tilde{\chi}_4^0 \to \tilde{\chi}_2^0 h_2)$. Tree-level ("tree") and full one-loop ("full") corrected decay widths are shown with the parameters chosen according to Table I, with $\varphi_{M_1}$ varied. The left plot shows the decay width, and the right plot shows the relative size of the corrections.

FIG. 14 (color online).   $\Gamma(\tilde{\chi}_4^0 \to \tilde{\chi}_2^0 h_3)$. Tree-level ("tree") and full one-loop ("full") corrected decay widths are shown with the parameters chosen according to Table I, with $\varphi_{M_1}$ varied. The left plot shows the decay width, and the right plot shows the relative size of the corrections.

dips are due to the resulting singular behavior of the derivatives of the self-energies entering the field renormalization constants. This effect will also be observed in the other decays to a $\tilde{\chi}_2^0$ (see Figs. 13, 14, and 19) in the total width of $\tilde{\chi}_4^0$, in Fig. 24, and in the branching ratios (see e.g., Fig. 9). It should be noted that both schemes have the same dips at $\varphi_{M_1} = 35°$ and $325°$. This will be true as well for the other decays to $\tilde{\chi}_2^0$ described below. The corrections are relatively small, $\sim 1\%$ to $-3\%$ for $\mathcal{S}_h$ and $\sim 2\%$ for $\mathcal{S}_h$. In Fig. 12, the renormalization schemes cannot be visibly distinguished from each other. The difference is below 0.01% for $\mathcal{S}_g$, and below $10^{-5}$ for $\mathcal{S}_h$ (see Table V for details).

For $\tilde{\chi}_4^0 \to \tilde{\chi}_2^0 h_2$ in $\mathcal{S}_g$, as shown in Fig. 13, the decay width oscillates from $\sim 0.03$ to 0.11 GeV, while for $\mathcal{S}_h$ it is $\sim 0.03$ GeV. The corresponding branching ratios in $\mathcal{S}_g$ and $\mathcal{S}_h$ are, respectively, $\sim 0.2$–0.8% and $\sim 0.5\%$. It should be noted that this decay is $s$-wave mode suppressed, and the decay width is therefore smaller than that for the decays into $h_1$ and $h_3$. Again, for $\mathcal{S}_g$, the effect of the threshold for

$\tilde{\chi}_2^0 \to \tilde{\chi}_1^0 h_1$ at $\varphi_{M_1} = 35°$ and $325°$ is visible. The corrections are comparatively large for $\mathcal{S}_g$, $\sim 0$ to 35%, and for $\mathcal{S}_h$ are $\sim 6\%$. Despite a relatively significant difference between the schemes of 0.05% for $\mathcal{S}_g$, in Fig. 13 this remains invisible. The large relative corrections in $\mathcal{S}_g$ are a consequence of the suppressed tree-level result, as well as the strong effect of the corrections on the mixing of the second-lightest neutralino.

The decay $\tilde{\chi}_4^0 \to \tilde{\chi}_2^0 h_3$, shown in Fig. 14, is $s$-wave mode allowed, and qualitatively similar to $\tilde{\chi}_4^0 \to \tilde{\chi}_2^0 h_1$. However, its decay width is smaller due to phase space suppression, oscillating from 0.14 to 0.18 GeV for $\mathcal{S}_g$ and 0.12 GeV for $\mathcal{S}_h$, and corrections are sizeable: $\sim -5\%$ and 15% for $\mathcal{S}_g$ and $\mathcal{S}_h$, respectively. The two schemes cannot be visibly distinguished here. The difference between the schemes reaches 0.01% for $\mathcal{S}_g$, and again this remains invisible (see Table V).

The decays $\tilde{\chi}_4^0 \to \tilde{\chi}_3^0 h_1$, $\tilde{\chi}_4^0 \to \tilde{\chi}_3^0 h_2$, and $\tilde{\chi}_4^0 \to \tilde{\chi}_3^0 h_3$, shown in Figs. 15–17, respectively, are kinematically



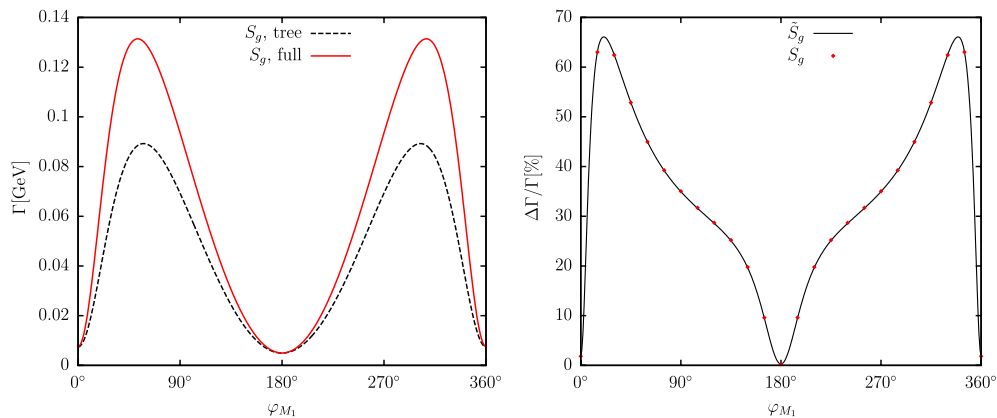FIG. 15 (color online).   $\Gamma(\tilde{\chi}_4^0 \to \tilde{\chi}_3^0 h_1)$. Tree-level ("tree") and full one-loop ("full") corrected decay widths are shown with the parameters chosen according to Table I, with $\varphi_{M_1}$ varied. The left plot shows the decay width, and the right plot shows the relative size of the corrections.
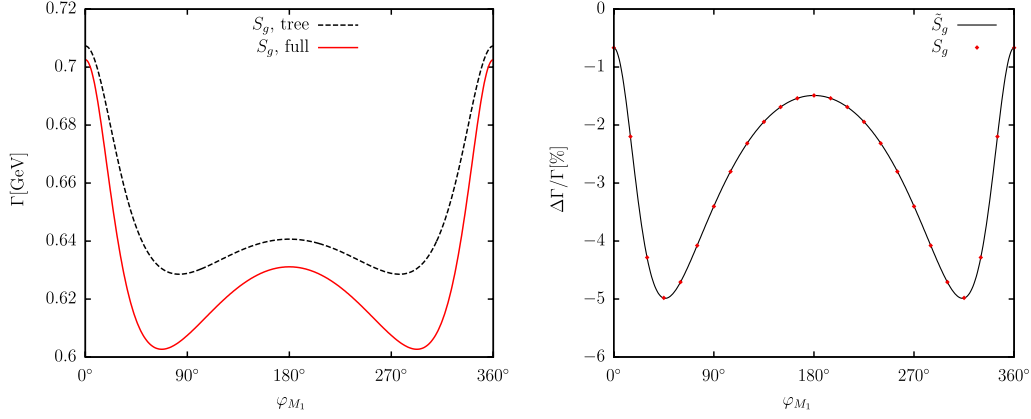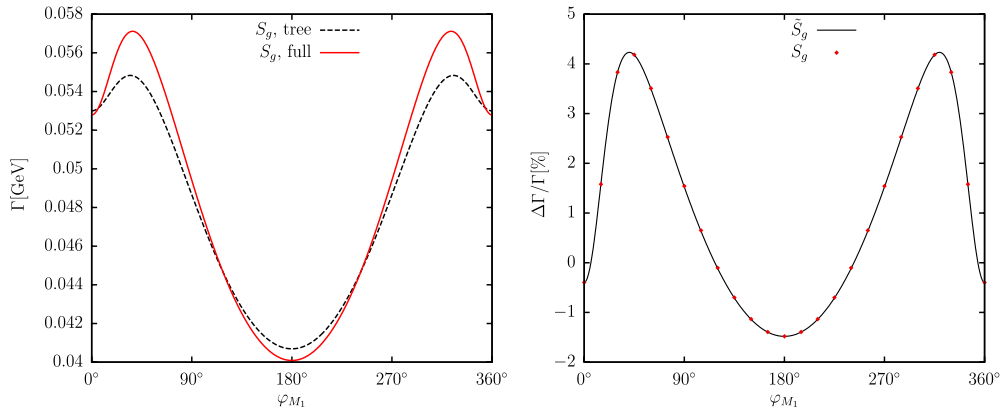
FIG. 16 (color online).   $\Gamma(\tilde{\chi}_4^0 \to \tilde{\chi}_3^0 h_2)$. Tree-level ("tree") and full one-loop ("full") corrected decay widths are shown with the parameters chosen according to Table I, with $\varphi_{M_1}$ varied. The left plot shows the decay width, and the right plot shows the relative size of the corrections.



FIG. 17 (color online).   $\Gamma(\tilde{\chi}_4^0 \to \tilde{\chi}_3^0 h_3)$. Tree-level ("tree") and full one-loop ("full") corrected decay widths are shown with the parameters chosen according to Table I, with $\varphi_{M_1}$ varied. The left plot shows the decay width, and the right plot shows the relative size of the corrections.

closed in scenario $\mathcal{S}_h$. For $\mathcal{S}_g$, there is a strong dependence on $\varphi_{M_1}$ since $\tilde{\chi}_3^0$ has both large Higgsino and bino components. However, contrary to what we observed for the decays to $\tilde{\chi}_2^0$ in $\mathcal{S}_g$, the decay to $h_2$ is $s$-wave mode allowed for $\varphi_{M_1} = 0$, while the other two decays are suppressed. This is due to the opposite relative $\mathcal{CP}$-parity of the $\tilde{\chi}_3^0 - \tilde{\chi}_4^0$ pair relative to the $\tilde{\chi}_2^0 - \tilde{\chi}_4^0$ pair.

For $\tilde{\chi}_4^0 \to \tilde{\chi}_3^0 h_1$, as shown in Fig. 15, an oscillating behaviour similar to that for $\tilde{\chi}_4^0 \to \tilde{\chi}_2^0 h_2$ but even more enhanced (going from $\sim 0.01$ to 0.13 GeV) results in even larger relative corrections. In fact, the suppression of the tree level is now larger due to the smaller phase space for this decay, and mixing with the unsuppressed states of the neutralinos has a dramatic effect, with corrections approaching 70%. Notice, however, that the second and third lightest neutralinos are roughly degenerate in $\mathcal{S}_g$, see Tab. I. This leads naturally to a large mixing character for these two mass eigenstates, supported by the fact that the sum of the decay widths is much less sensitive to $\varphi_{M_1}$.

Therefore, the large corrections should not be regarded as a breakdown of the renormalization procedure but rather as an indication that one should consider all the neutralino states simultaneously. For this particular decay the branching ratio does not reach 1%. In Fig. 15, the difference between the renormalization schemes reaches $\sim 0.02\%$ and they cannot be visibly distinguished from each other, see Tab. V for details.

For the decays into the heavier Higgs bosons, the corrections are mild, at the level of a few percent. In $\tilde{\chi}_4^0 \to \tilde{\chi}_3^0 h_2$, as shown in Fig. 16, the unsuppressed decay, with widths between $\sim 0.6$ and 0.7 GeV, receives small corrections via mixing with the $p$-wave suppressed states.

In $\tilde{\chi}_4^0 \to \tilde{\chi}_3^0 h_3$, as shown in Fig. 17, the $\varphi_{M_1}$ dependence is small due to the combination of one $p$-wave suppressed amplitude with an $s$-wave allowed one for which the couplings are small, resulting in corrections of a few percent. For these decays, the small difference between the two schemes cannot be observed in the figures.

### C. Decays into Z bosons

The channels involving the $Z$ boson, $\tilde{\chi}_4^0 \to \tilde{\chi}_j^0 Z$, are presented in Figs. 18–20. The strong resemblance between the $\varphi_{M_1}$ dependence between these plots and those for the decay into $h_2$ is due to the fact that gauge bosons are $\mathcal{CP}$ odd, while in our scenarios the second Higgs boson has a very small $\mathcal{CP}$-even component and tends to the $\mathcal{CP}$-odd state for $\varphi_{M_1} = 0, \pi$. There is a strong dependence on the relative $\mathcal{CP}$ phase of the neutralinos in the initial and final states, which leads to visible differences between the re-normalization schemes, given explicitly in Table V.

In both scenarios, the lightest neutralino is mainly bino-like; therefore $\tilde{\chi}_4^0 \to \tilde{\chi}_1^0 Z$ depends strongly on $\varphi_{M_1}$, as shown in Fig. 18. The decay is both qualitatively and quantitatively similar to the case of $\tilde{\chi}_4^0 \to \tilde{\chi}_1^0 h_2$: due to the relative $\mathcal{CP}$ phase of the neutralinos and the fact that the $Z$ is $\mathcal{CP}$ odd, the decay is suppressed at $\varphi_{M_1} = 0$ and maximal at $\varphi_{M_1} = 180°$, and the decay width ranges from

0 to 0.14 GeV and from 0.08 to 0.25 GeV for $\mathcal{S}_g$ and $\mathcal{S}_h$, respectively. For $\mathcal{S}_g$, the dependence of the relative size of the corrections on $\varphi_{M_1}$ is much larger, from 1% to 15%, with visible differences between the schemes at large $\varphi_{M_1}$ of up to 0.2%, while the loop corrections for $\mathcal{S}_h$ are almost independent of $\varphi_{M_1}$, at $\sim 8\%$. The difference between the schemes in $\mathcal{S}_g$ has been highlighted in Fig. 27.

For $\tilde{\chi}_4^0 \to \tilde{\chi}_2^0 Z$, in $\mathcal{S}_g$ the decay width oscillates from $\sim 0.05$ to 0.15 GeV, and for $\mathcal{S}_h$ the decay width is $\sim 0.06$ GeV, as shown in Fig. 19. For $\mathcal{S}_g$, the effect of the threshold for $\tilde{\chi}_2^0 \to \tilde{\chi}_1^0 h_1$ at $\varphi_{M_1} = 35°$ and $325°$ is visible as a small dip in the decay width and a marked dip in the relative corrections. The corrections for $\mathcal{S}_g$ are comparatively large, $\sim 0$ to 25%, and for $\mathcal{S}_h$ they are $\sim 3\%$. The two schemes are not visibly distinguished from each other, with the largest differences in $\mathcal{S}_g$ of $\sim 4 \times 10^{-4}$. Although in $\mathcal{S}_h$ it is below threshold, in $\mathcal{S}_g$ the decay $\tilde{\chi}_4^0 \to \tilde{\chi}_3^0 Z$, shown in Fig. 20, is $s$-wave mode allowed, resulting in the largest
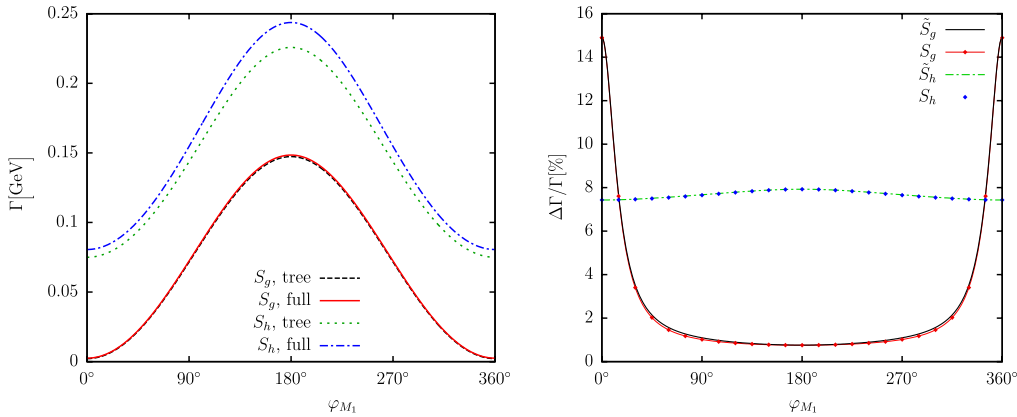


FIG. 18 (color online). $\Gamma(\tilde{\chi}_4^0 \to \tilde{\chi}_1^0 Z)$. Tree-level ("tree") and full one-loop ("full") corrected decay widths are shown with the parameters chosen according to Table I, with $\varphi_{M_1}$ varied. The left plot shows the decay width, and the right plot shows the relative size of the corrections.
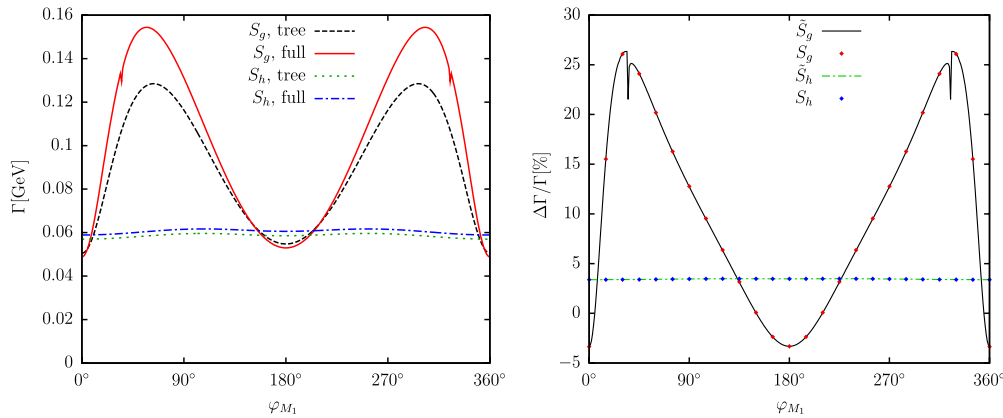


FIG. 19 (color online). $\Gamma(\tilde{\chi}_4^0 \to \tilde{\chi}_2^0 Z)$. Tree-level ("tree") and full one-loop ("full") corrected decay widths are shown with the parameters chosen according to Table I, with $\varphi_{M_1}$ varied. The left plot shows the decay width, and the right plot shows the relative size of the corrections.
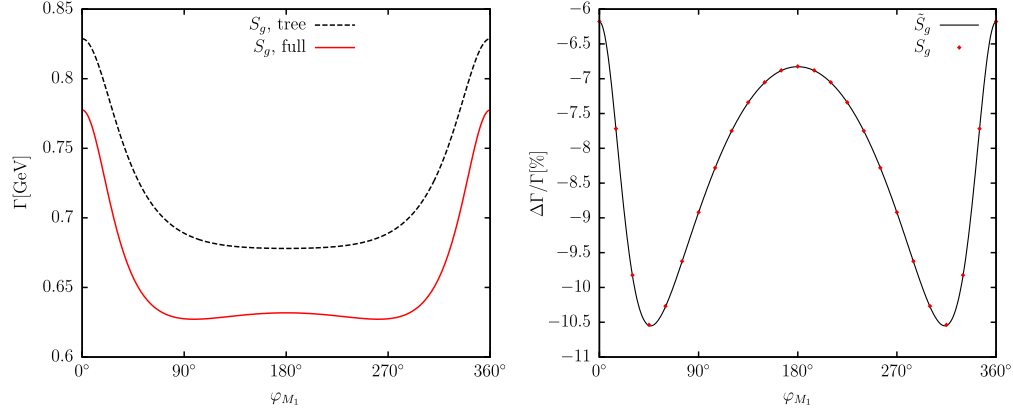
FIG. 20 (color online).   $\Gamma(\tilde{\chi}_4^0 \rightarrow \tilde{\chi}_3^0 Z)$. Tree-level ("tree") and full one-loop ("full") corrected decay widths are shown with the parameters chosen according to Table I, with $\varphi_{M_1}$ varied. The left plot shows the decay width, and the right plot shows the relative size of the corrections.

branching ratio into $Z$. The decay width goes from 0.78 GeV at $\varphi_{M_1} \approx 0$ to 0.62 GeV, with the corrections between $\sim 6.2$ and 10.5%. The two schemes differ by up to $\sim 5 \times 10^{-5}$ and cannot be visibly distinguished.

### D. Decays into (s)leptons

Now we turn to the decays involving (scalar) leptons. The expressions for all these decay widths follow the same pattern (see the expressions for the tree-level widths in the Appendix). The dependence on $\varphi_{M_1}$ is small, although the results for $\mathcal{S}_h$ do show some dependence due to the small bino-like component of the decaying neutralino. We have chosen $M_{\tilde{\ell}_L} < M_{\tilde{\ell}_R}$, leading to lighter left-handed and heavier right-handed sleptons, and significant mixing in the scalar tau sector.

In Fig. 21, we show the results for the decay $\tilde{\chi}_4^0 \rightarrow \tau^- \tilde{\tau}_1^+$. The decay widths are found to be an order of magnitude larger in $\mathcal{S}_g$ ($\sim 0.37$ GeV) than in $\mathcal{S}_h$

($\sim 0.03$ GeV), since the gaugino-like neutralino has an unsuppressed coupling to the large left component of the stau, while the Higgsino-like neutralino couples to the suppressed Yukawa coupling. This pattern is even more significant for the decays into the lower-generation sleptons not shown here. In the right panel, we observe that the one-loop corrections are very small in $\mathcal{S}_g$, while they are around $\sim 20\%$ in $\mathcal{S}_h$, due to the larger dependence on the stau mixing.

The results for the decay into the heavier scalar tau are shown in Fig. 22. The pattern is similar to the preceding decay, the difference being that here the right-handed component of the heavier stau is larger, resulting in a decay width which is four times larger for $\mathcal{S}_h$ and 30% smaller for $\mathcal{S}_g$. The corrections in $\mathcal{S}_g$ remain very small while those in $\mathcal{S}_h$ are now $\sim 7\%$. For the decay into the first two generations, where the slepton mixing is usually negligible, both scenarios have very small partial widths.
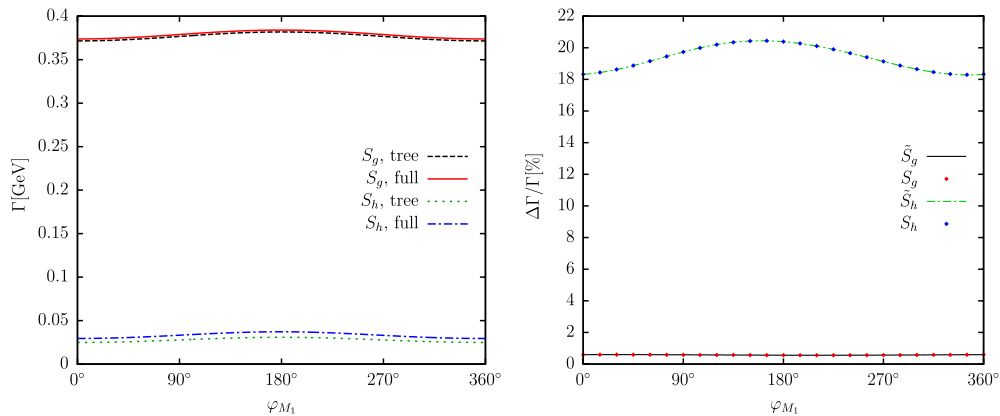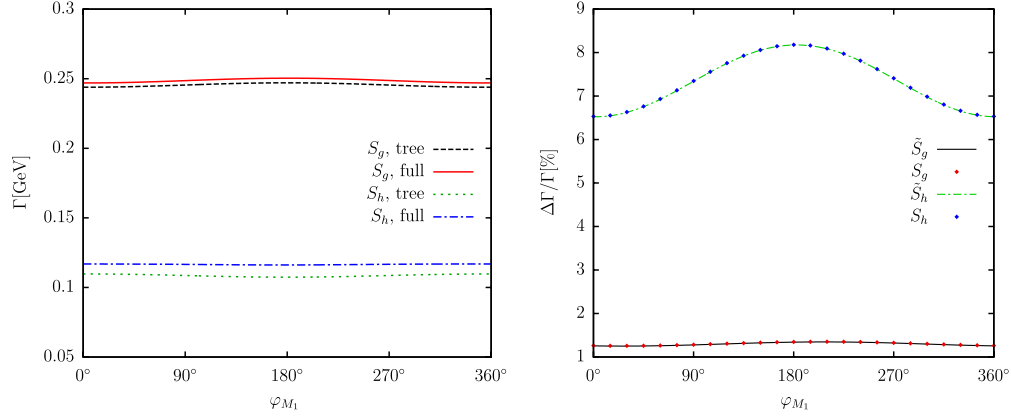


FIG. 21 (color online).   $\Gamma(\tilde{\chi}_4^0 \rightarrow \tau^+ \tilde{\tau}_1^-)$. Tree-level ("tree") and full one-loop ("full") corrected decay widths are shown with the parameters chosen according to Table I, with $\varphi_{M_1}$ varied. The left plot shows the decay width, and the right plot shows the relative size of the corrections.
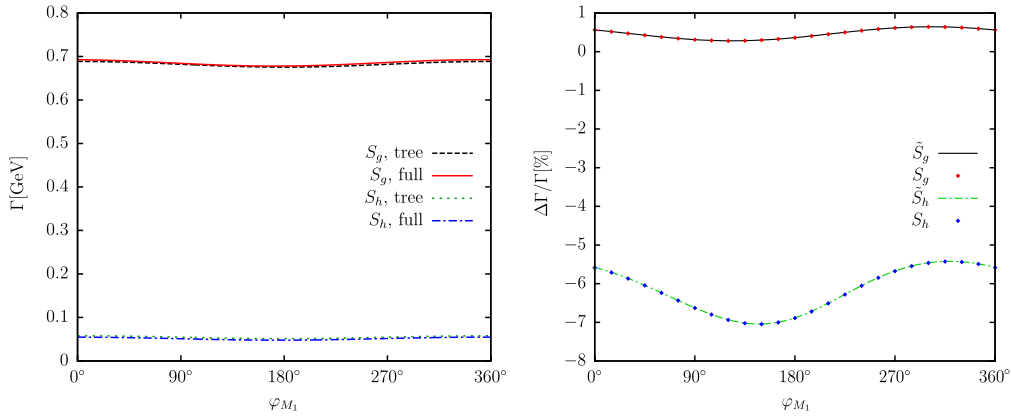
FIG. 22 (color online). $\Gamma(\tilde{\chi}_4^0 \to \tau^+ \tilde{\tau}_2^-)$. Tree-level ("tree") and full one-loop ("full") corrected decay widths are shown with the parameters chosen according to Table I, with $\varphi_{M_1}$ varied. The left plot shows the decay width, and the right plot shows the relative size of the corrections.



FIG. 23 (color online). $\Gamma(\tilde{\chi}_4^0 \to \nu_\tau \tilde{\nu}_\tau^\dagger)$. Tree-level ("tree") and full one-loop ("full") corrected decay widths are shown with the parameters chosen according to Table I, with $\varphi_{M_1}$ varied. The left plot shows the decay width, and the right plot shows the relative size of the corrections.

The results for the decay $\tilde{\chi}_4^0 \to \nu_\tau \tilde{\nu}_\tau^\dagger$ are shown in Fig. 23. Here, the gaugino-like neutralino has a decay width which is roughly the sum of decay widths for $\tilde{\chi}_4^0 \to \tau^- \tilde{\tau}_1^+$ and $\tilde{\chi}_4^0 \to \tau^- \tilde{\tau}_2^+$, i.e., $\sim 0.7$ GeV for $\mathcal{S}_g$ and $\sim 0.05$ GeV for $\mathcal{S}_h$. The radiative corrections are $\sim 0.5\%$ in $\mathcal{S}_g$ and $\sim -6\%$ in $\mathcal{S}_h$.

In $\mathcal{S}_g$, where the neutralino is gaugino-like, the branching ratios for these tree processes are, respectively, $\sim 2.5\%$, $\sim 2\%$, and $\sim 5\%$. Taking into account the charged conjugated processes, this results in a branching ratio of almost 20% for the third lepton family. For the first two generations, the branching ratios into every left-handed slepton or sneutrino are $\sim 4.5$ and 5%, respectively, while the decays into the right-handed sleptons are negligible. Therefore, in this class of scenarios, the leptonic decays could be the dominant ones. In $\mathcal{S}_h$, on the other hand, the leptonic decays are subdominant, especially for the first two generations, and mainly due to the small gaugino component of the decaying neutralino.

In all the decays to leptons, the difference between the renormalization schemes is negligible, as shown in Figs. 21–23, and summarized in Table V.

### E. Full one-loop results: total decay widths

In this subsection, we briefly show the results for the total decay widths and the relative corrections of the three heaviest neutralinos in $\mathcal{S}_g$ and $\mathcal{S}_h$. The decay width of $\tilde{\chi}_4^0$, shown in the lhs of Fig. 24, is almost independent of $\varphi_{M_1}$, as is expected from the heavier neutralino in a GUT-related scenario. Therefore, the branching ratios can be easily obtained from the partial widths. The large $\varphi_{M_1}$ dependence of the single channels is due to the strong effect on the mixing of the different neutralinos, as already argued in the preceding subsections. The corrections are also very small, $\sim \pm 1\%$, with the expected dips due to the thresholds for $\tilde{\chi}_2^0 \to \tilde{\chi}_1^0 h_1$ at $\varphi_{M_1} = 35°$ and $325°$, and for $\tilde{\chi}_1^- \to \tilde{\chi}_1^0 W^-$ at $\varphi_{M_1} = 125°$ and $235°$.
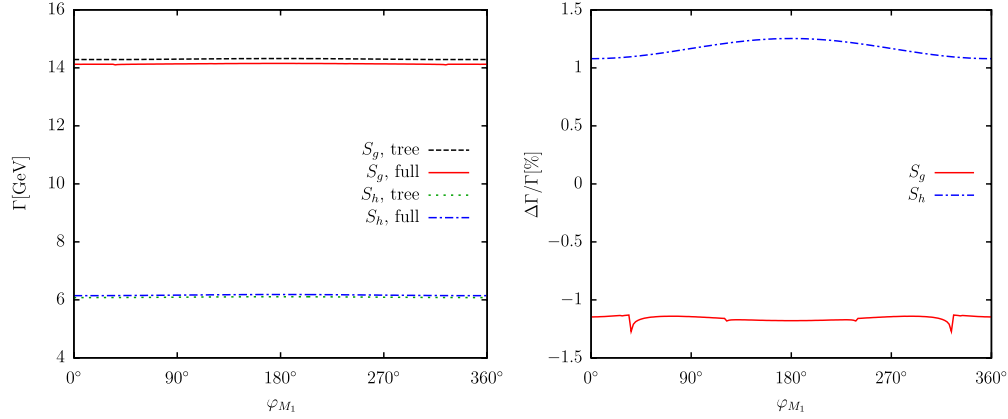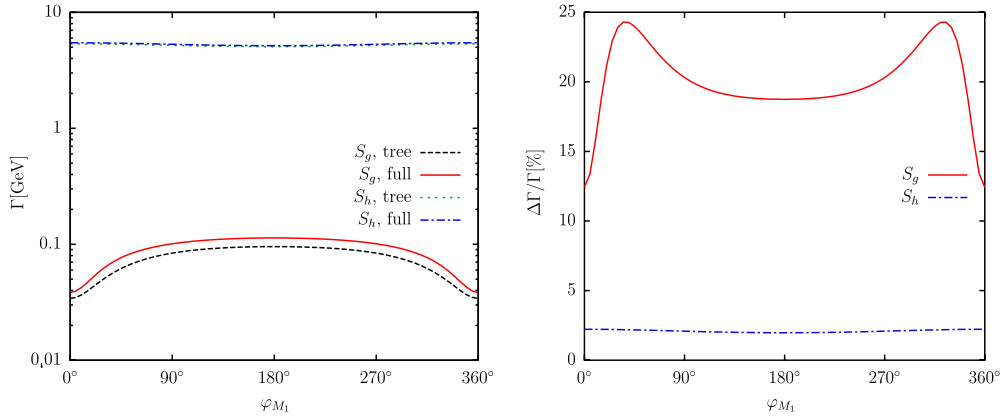
FIG. 24 (color online). $\Gamma_{\text{tot}}(\tilde{\chi}_4^0)$. Tree-level ("tree") and full one-loop ("full") corrected total decay widths are shown with the parameters chosen according to Table I, with $\varphi_{M_1}$ varied. The left panel shows the decay width, and the right panel shows the corresponding relative size of the corrections.



FIG. 25 (color online). $\Gamma_{\text{tot}}(\tilde{\chi}_3^0)$. Tree-level ("tree") and full one-loop ("full") corrected total decay widths are shown with the parameters chosen according to Table I, with $\varphi_{M_1}$ varied. The left panel shows the decay width, and the right panel shows the corresponding relative size of the corrections.

The total decay width of $\tilde{\chi}_3^0$ is shown in the lhs of Fig. 25. As already discussed, in $\mathcal{S}_g$ the second- and third-lightest neutralinos have similar masses and have a Higgsino-bino mixing character which strongly depends on $\varphi_{M_1}$. This is true at the tree level, where the total width goes from ~0.04 GeV for $\varphi_{M_1} = 0$ to almost three times as much for $\varphi_{M_1} = \pi$, as well as for the loop corrections, which are of $\mathcal{O}(20\%)$. The total width is also significantly smaller than that of $\tilde{\chi}_4^0$, largely due to the reduced phase space (see Table II). Here only the leptonic decays and those to $Z$ and the lightest neutralino are open. On the contrary, in $\mathcal{S}_h$ both $\tilde{\chi}_3^0$ and $\tilde{\chi}_4^0$ are Higgsino-dominated and nearly degenerate. Consequently, the same decay channels are open and their widths are similar, both at tree level and at one loop.

The total decay width of $\tilde{\chi}_2^0$ is shown in the lhs of Fig. 26. The strong mixing of the second- and third-lightest neutralinos in $\mathcal{S}_g$ has already been discussed. The same decay channels as for $\tilde{\chi}_3^0$ are open, except for that to $Z$ and the lightest neutralino, which is only open for $|\varphi_{M_1}| < 32°$.

However, the decay to $Z$ is subdominant with a BR smaller than 1%. The threshold effect we observe in the right panel for the relative corrections is due to the decay into the lightest Higgs boson, as already discussed in this section for those decays with final $\tilde{\chi}_2^0$.[7] The decay width and its relative correction show a complementary behavior to the corresponding ones for the third-lightest neutralino, i.e., the dependence on $\varphi_{M_1}$ of the sum of both widths is much weaker, with corrections of ~10%.

In $\mathcal{S}_h$, again, the neutralinos do not strongly mix, and $\tilde{\chi}_2^0$ is wino-dominated. Here the decays into left-handed

---

[7]It should be noted that this effect, due to the singularity of the wave function renormalization, is characteristic of on-shell renormalization schemes, which are less precise when thresholds of external particles are open. The masses entering these thresholds are the tree-level ones, which in the case of the lightest Higgs boson is close to that of the $Z$ boson. The renormalized lightest Higgs boson, on the other hand, has a mass of ~126 GeV, and the decay is closed.
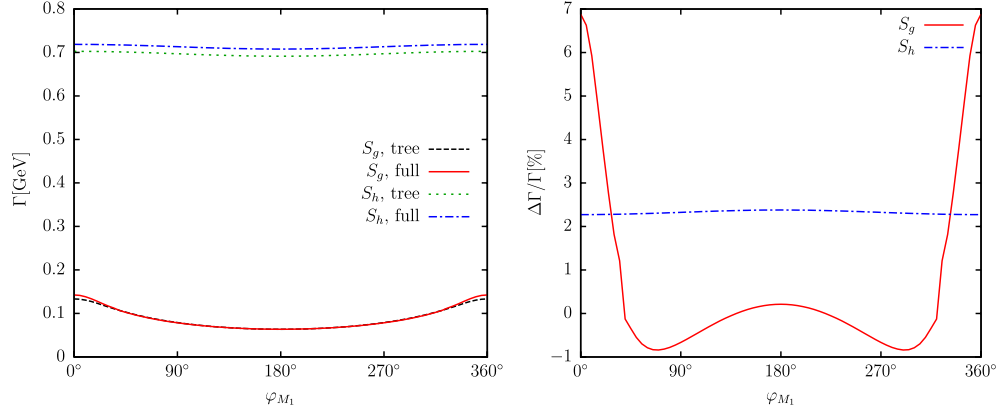
FIG. 26 (color online).   $\Gamma_{\text{tot}}(\tilde{\chi}_2^0)$. Tree-level ("tree") and full one-loop ("full") corrected total decay widths are shown with the parameters chosen according to Table I, with $\varphi_{M_1}$ varied. The left panel shows the decay width, and the right panel shows the corresponding relative size of the corrections.

sleptons or sneutrinos dominate due to the strong wino coupling. However, the subdominant decays to the lightest neutralino, and $Z$ or Higgs bosons become the only open channels if the sleptons are chosen to be heavier. These decays show a strong (and complementary) dependence on $\varphi_{M_1}$ due to the change in the relative $\mathcal{CP}$ parity of the two lightest neutralinos.

### F. Differences between the renormalization schemes

In our benchmark scenarios $\mathcal{S}_g$ and $\mathcal{S}_h$ we have found remarkably good agreement between the two schemes. For most decay channels, the difference between the relative corrections to the partial widths $\Delta\Gamma/\Gamma$ for schemes I and II is on the order of $10^{-5}$. In Table V, we show this difference for all the decay channels, in both $\mathcal{S}_g$ and $\mathcal{S}_h$, and find that the largest differences are observed in $\tilde{\chi}_4^0 \rightarrow \tilde{\chi}_1^0 h_{1,2,3}$, $\tilde{\chi}_4^0 \rightarrow \tilde{\chi}_2^0 h_2$, $\tilde{\chi}_4^0 \rightarrow \tilde{\chi}_3^0 h_1$, and $\tilde{\chi}_4^0 \rightarrow \tilde{\chi}_{1,2}^0 Z$. In Fig. 27, we highlight these differences in $\mathcal{S}_g$ for $\tilde{\chi}_4^0 \rightarrow \tilde{\chi}_1^0 Z$ and

$\tilde{\chi}_4^0 \rightarrow \tilde{\chi}_1^0 h_1$. To be precise, in this figure we compare the full one-loop correction $\Delta\Gamma$ calculated in scheme I, both with and without the squark shifts (see the end of Sec. II B), to that calculated in scheme II, where squark shifts are not included. One can see that at $\varphi_{M_1} = 0°$ and $180°$ the difference between the results without squark shifts vanishes, confirming that the schemes differ only in the treatment of the phases. One can also clearly see the impact of the squark shifts on the size of the one-loop correction. Earlier in this section, it was noted that larger differences between the schemes are observed when the tree-level decay width depends strongly on the phase $\varphi_{M_1}$. This explains why decays to the lightest neutralino are the most strongly affected ones. Also, the differences are in general much more pronounced in $\mathcal{S}_g$ than in $\mathcal{S}_h$, due to the mixing between the bino and Higgsino components, except for the decays into sleptons or a $W$ boson, where the Higgsino component has a negligible role.
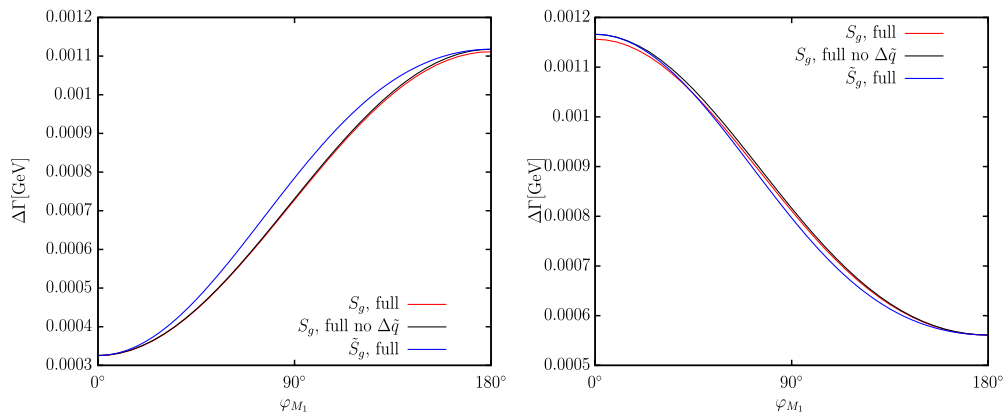


FIG. 27 (color online).   $\Gamma(\tilde{\chi}_4^0 \rightarrow \tilde{\chi}_1^0 Z)$ and $\Gamma(\tilde{\chi}_4^0 \rightarrow \tilde{\chi}_1^0 h_1)$. The one-loop ("full") correction to the partial decay widths are shown as a function of $\varphi_{M_1}$. The parameters are chosen according to Tab. I. Also shown is the correction without including the shifts in the squark sector ("full no $\Delta\tilde{q}$").

## V. CONCLUSIONS

We have evaluated all nonhadronic two-body decay widths of neutralinos in the cMSSM. Assuming heavy scalar quarks, we take into account all decay channels involving charginos, neutralinos, (scalar) leptons, Higgs bosons and SM gauge bosons. The decay modes are given in Eqs. (3)–(5). The evaluation of the decay widths is based on a full one-loop calculation including hard and soft QED radiation. Such a calculation is necessary to derive a reliable prediction of any two-body branching ratio. Three-body decay modes can become sizable only if all the two-body channels are kinematically (nearly) closed and have thus been neglected throughout the paper. The same applies to two-body decay modes that appear only at the one-loop level.

We first reviewed the one-loop renormalization of the cMSSM, concentrating on the most relevant aspects for our calculation, except for the details for the Higgs boson sector, which can be found in Ref. [46]. More importantly, we have given details for the chargino/neutralino sector in the two on-shell renormalization schemes which we have compared in this work. The two schemes differ in the treatment of complex contributions in the chargino/neutralino sector. The different renormalization of the $CP$-violating phases leads to small differences in the cMSSM, which are, however, of higher order in the electroweak coupling and vanish in the limit of real couplings. Differences indicate the size of unknown higher-order corrections involving complex phases beyond the one-loop level. We have also discussed the calculation of the one-loop diagrams, and the treatment of UV and IR divergences that are canceled by the inclusion of soft QED radiation. Our calculation setup can easily be extended to other two-body decays involving (scalar) quarks. We have taken into account all absorptive contributions, explicitly inlcuding those of self-energy type on external legs. This ensures that all $CP$-violating effects are correctly accounted for.

In the numerical analysis, we mainly concentrated on the decays of the heaviest neutralino, $\tilde{\chi}_4^0$. For this analysis we have chosen a parameter set that allows simultaneously *all* two-body decay modes under investigation, and respects the current experimental bounds on Higgs boson and SUSY searches (where the combination of low $M_{H^\pm}$ and relatively large $\tan\beta$ is in a potential conflict with the most recent LHC searches for the heavy MSSM Higgs bosons). The masses of the charginos, and thus roughly those of the second and fourth neutralino, are in this scenario, respectively, 350 and 600 GeV. This leads to two representative scenarios for the chargino/neutralino sector, for $\mu > M_2$ or $\mu < M_2$. These benchmark scenarios allow copious production of the neutralinos in SUSY cascades at the LHC. Furthermore, the production of $\tilde{\chi}_4^0 \tilde{\chi}_j^0$ at the ILC 1000, i.e., with $\sqrt{s} = 1000$ GeV, via $e^+ e^- \rightarrow \tilde{\chi}_4^0 \tilde{\chi}_j^0$ will be possible, with all the subsequent decay modes [Eqs. (3)–(6)] being

(in principle) open. The clean environment of the ILC would then permit a detailed, statistically dominated study of the neutralino decays. Depending on the channel and the polarization, a precision at the percent level seems to be achievable. Special attention is paid to neutralino decays involving the lightest supersymmetric particle (LSP), i.e., the lightest neutralino, or a neutral or charged Higgs boson.

We have shown results for varying $\varphi_{M_1}$, the phase of the soft SUSY-breaking parameter $M_1$, which leads to $CP$ violation in the chargino and neutralino sectors. We have analyzed the tree-level and full one-loop results for all kinematically open decay channels of the heaviest neutralino. For the decays of the second and third neutralinos, we have only shown the total widths.

We found sizable corrections in many of the decay channels. The higher-order corrections of the neutralino decay widths involving the LSP are generically up to a level of about 10%, and decay modes involving Higgs bosons can easily have corrections up to 20–30%. The size of the full one-loop corrections to the decay widths and the branching ratios also depends strongly on $\varphi_{M_1}$, especially for those decays in which an external neutralino is a mixed Higgsino-bino state. We conclude that the largest effect of the radiative corrections is due to its effect on the mixing of the neutralinos. All results on partial decay widths of $\tilde{\chi}_4^0$, as well as the total decay widths of all neutralinos, are given in detail in Sec. IV.

For the two on-shell renormalization schemes considered, we have found very good agreement: the difference between the relative size of the corrections is found to be $\lesssim 0.1\%$. The largest differences have been found for decays with a strong dependence on the parameter $\varphi_{M_1}$. The good agreement between the two schemes is not unexpected, as they are found to be equivalent up to a higher-order effect, as discussed in Sec. IV F.

The numerical results we have shown are, of course, dependent on the choice of MSSM parameters. Nevertheless, they give an idea of the relevance of the full one-loop corrections. For other choices of SUSY masses, the corrections to the decay widths would stay the same, but the branching ratios would look very different. Channels for which the decay width (and its respective one-loop corrections) may look unobservable due to the smallness of the BR in our numerical examples could become important if other channels are kinematically forbidden.

Following our analysis, it is evident that the full one-loop corrections are mandatory for a precise prediction of the various branching ratios. This applies to LHC analyses, but even more to analyses at the ILC or CLIC, where a precision at the percent level is anticipated for the determination of neutralino branching ratios (depending on the neutralino masses, the center-of-mass energy and the integrated luminosity). The results for the neutralino decays will be implemented into the Fortran code FeynHiggs.

## ACKNOWLEDGMENTS

## APPENDIX: TREE-LEVEL RESULTS

For completeness, we include here the expressions for the tree-level decay widths:

$$
\begin{aligned}
\Gamma^{\text{tree}}(\tilde{\chi}_i^0 \to \tilde{\chi}_j^- H^+) = &[(|C(\tilde{\chi}_i^0, \tilde{\chi}_j^+, H^-)_L|^2 + |C(\tilde{\chi}_i^0, \tilde{\chi}_j^+, H^-)_R|^2)(m_{\tilde{\chi}_i^0}^2 + m_{\tilde{\chi}_j^\pm}^2 - M_{H^\pm}^2) \\
&+ 4\,\text{Re}\{C(\tilde{\chi}_i^0, \tilde{\chi}_j^+, H^-)_L^* C(\tilde{\chi}_i^0, \tilde{\chi}_j^+, H^-)_R\} m_{\tilde{\chi}_i^0} m_{\tilde{\chi}_j^\pm}] \frac{\lambda^{1/2}(m_{\tilde{\chi}_i^0}^2, m_{\tilde{\chi}_j^\pm}^2, M_{H^\pm}^2)}{32\pi m_{\tilde{\chi}_i^0}^3} \quad (i=2,3,4, j=1,(2)),
\end{aligned}
\tag{A1}
$$

$$
\begin{aligned}
\Gamma^{\text{tree}}(\tilde{\chi}_i^0 \to \tilde{\chi}_j^- W^+) = &\left[ (|C(\tilde{\chi}_i^0, \tilde{\chi}_j^+, W^-)_L|^2 + |C(\tilde{\chi}_i^0, \tilde{\chi}_j^+, W^-)_R|^2)\left(m_{\tilde{\chi}_i^0}^2 + m_{\tilde{\chi}_j^\pm}^2 - 2M_W^2 + \frac{(m_{\tilde{\chi}_i^0}^2 - m_{\tilde{\chi}_j^\pm}^2)^2}{M_W^2}\right) \right. \\
&\left. - 12\,\text{Re}\{C(\tilde{\chi}_i^0, \tilde{\chi}_j^+, W^-)_L^* C(\tilde{\chi}_i^0, \tilde{\chi}_j^+, W^-)_R\} m_{\tilde{\chi}_i^0} m_{\tilde{\chi}_j^\pm} \right] \frac{\lambda^{1/2}(m_{\tilde{\chi}_i^0}^2, m_{\tilde{\chi}_j^\pm}^2, M_W^2)}{32\pi m_{\tilde{\chi}_i^0}^3} \quad (i=2,3,4, j=1,(2)),
\end{aligned}
\tag{A2}
$$

$$
\begin{aligned}
\Gamma^{\text{tree}}(\tilde{\chi}_i^0 \to \tilde{\chi}_j^0 h_k) = &[(|C(\tilde{\chi}_i^0, \tilde{\chi}_j^0, h_k)_L|^2 + |C(\tilde{\chi}_i^0, \tilde{\chi}_j^0, h_k)_R|^2)(m_{\tilde{\chi}_i^0}^2 + m_{\tilde{\chi}_j^0}^2 - m_{h_k}^2) \\
&+ 4\,\text{Re}\{C(\tilde{\chi}_i^0, \tilde{\chi}_j^0, h_k)_L^* C(\tilde{\chi}_i^0, \tilde{\chi}_j^0, h_k)_R\} m_{\tilde{\chi}_i^0} m_{\tilde{\chi}_j^0}] \frac{\lambda^{1/2}(m_{\tilde{\chi}_i^0}^2, m_{\tilde{\chi}_j^0}^2, m_{h_k}^2)}{32\pi m_{\tilde{\chi}_i^0}^3} \quad (i=2,3,4, j=1,(2), k=1,2,3) \\
= &[(|C(\tilde{\chi}_i^0, \tilde{\chi}_j^0, h_k)_R|^2)(m_{\tilde{\chi}_i^0}^2 + m_{\tilde{\chi}_j^0}^2 - m_{h_k}^2) + 2\,\text{Re}\{(C(\tilde{\chi}_i^0, \tilde{\chi}_j^0, h_k)_R)^2\} m_{\tilde{\chi}_i^0} m_{\tilde{\chi}_j^0}] \\
&\times \frac{\lambda^{1/2}(m_{\tilde{\chi}_i^0}^2, m_{\tilde{\chi}_j^0}^2, m_{h_k}^2)}{16\pi m_{\tilde{\chi}_i^0}^3} \quad (i=2,3,4, j=1,(2), k=1,2,3),
\end{aligned}
\tag{A3}
$$

$$
\begin{aligned}
\Gamma^{\text{tree}}(\tilde{\chi}_i^0 \to \tilde{\chi}_j^0 Z) = &\left[ (|C(\tilde{\chi}_i^0, \tilde{\chi}_j^0, Z)_L|^2 + |C(\tilde{\chi}_i^0, \tilde{\chi}_j^0, Z)_R|^2)\left(m_{\tilde{\chi}_i^0}^2 + m_{\tilde{\chi}_j^0}^2 - 2M_Z^2 + \frac{(m_{\tilde{\chi}_i^0}^2 - m_{\tilde{\chi}_j^0}^2)^2}{M_Z^2}\right) \right. \\
&\left. - 12\,\text{Re}\{C(\tilde{\chi}_i^0, \tilde{\chi}_j^0, Z)_L^* C(\tilde{\chi}_i^0, \tilde{\chi}_j^0, Z)_R\} m_{\tilde{\chi}_i^0} m_{\tilde{\chi}_j^0} \right] \frac{\lambda^{1/2}(m_{\tilde{\chi}_i^0}^2, m_{\tilde{\chi}_j^0}^2, M_Z^2)}{32\pi m_{\tilde{\chi}_i^0}^3} \\
= &\left[ |C(\tilde{\chi}_i^0, \tilde{\chi}_j^0, Z)_R|^2\left(m_{\tilde{\chi}_i^0}^2 + m_{\tilde{\chi}_j^0}^2 - 2M_Z^2 + \frac{(m_{\tilde{\chi}_i^0}^2 - m_{\tilde{\chi}_j^0}^2)^2}{M_Z^2}\right) \right. \\
&\left. + 6\,\text{Re}\{(C(\tilde{\chi}_i^0, \tilde{\chi}_j^0, Z)_R)^2\} m_{\tilde{\chi}_i^0} m_{\tilde{\chi}_j^0} \right] \frac{\lambda^{1/2}(m_{\tilde{\chi}_i^0}^2, m_{\tilde{\chi}_j^0}^2, M_Z^2)}{16\pi m_{\tilde{\chi}_i^0}^3} \quad (i=2,3,4, j<i),
\end{aligned}
\tag{A4}
$$

$$\Gamma^{\text{tree}}(\tilde{\chi}_i^0 \to \ell^- \tilde{\ell}_k^+) = [(|C(\tilde{\chi}_i^0, \bar{\ell}, \tilde{\ell}_k)_L|^2 + |C(\tilde{\chi}_i^0, \bar{\ell}, \tilde{\ell}_k)_R|^2)(m_{\tilde{\chi}_i^0}^2 + m_\ell^2 - m_{\tilde{\ell}_k}^2)$$

$$+ 4\,\text{Re}\{C(\tilde{\chi}_i^0, \bar{\ell}, \tilde{\ell}_k)_L^* C(\tilde{\chi}_i^0, \bar{\ell}, \tilde{\ell}_k)_R\} m_{\tilde{\chi}_i^0} m_\ell] \frac{\lambda^{1/2}(m_{\tilde{\chi}_i^0}^2, m_\ell^2, m_{\tilde{\ell}_k}^2)}{32\pi m_{\tilde{\chi}_i^0}^3} \qquad (i = 2, 3, 4, \ell = e, \mu, \tau, k = 1, 2),$$

$$(A5)$$

$$\Gamma^{\text{tree}}(\tilde{\chi}_i^0 \to \nu_\ell \tilde{\nu}_\ell^\dagger) = |C(\tilde{\chi}_i^0, \bar{\nu}_\ell, \tilde{\nu}_\ell)_R|^2 (m_{\tilde{\chi}_i^0}^2 - m_{\tilde{\nu}_\ell}^2) \frac{\lambda^{1/2}(m_{\tilde{\chi}_i^0}^2, 0, m_{\tilde{\nu}_\ell}^2)}{32\pi m_{\tilde{\chi}_i^0}^3} \qquad (i = 2, 3, 4, \ell = e, \mu, \tau), \qquad (A6)$$

where $\lambda(x, y, z) = (x - y - z)^2 - 4yz$, and the couplings $C(a, b, c)$ can be found in the FeynArts model files [82]. $C(a, b, c)_{L,R}$ denote the part of the coupling which is proportional to $\omega_\mp = \frac{1}{2}(\mathbb{1} \mp \gamma_5)$.

[1] H. Nilles, Phys. Rep. **110**, 1 (1984); H. Haber and G. Kane, Phys. Rep. **117**, 75 (1985); R. Barbieri, Riv. Nuovo Cimento **11N4**, 1 (1988).

[2] Tevatron New Physics Higgs Working Group, CDF, and D0 Collaborations, arXiv:1207.0449.

[3] R. Barate *et al.* (LEP Working Group for Higgs Boson Searches and ALEPH, DELPHI, L3, and OPAL Collaborations), Phys. Lett. B **565**, 61 (2003); S. Schael *et al.* (ALEPH, DELPHI, L3, OPAL Collaborations, and LEP Working Group for Higgs Boson Searches), Eur. Phys. J. C **47**, 547 (2006).

[4] G. Aad *et al.* (ATLAS Collaboration), Phys. Lett. B **716**, 1 (2012); S. Chatrchyan *et al.* (CMS Collaboration), Phys. Lett. B **716**, 30 (2012).

[5] S. Dittmaier *et al.* (LHC Higgs Cross Section Working Group), arXiv:1101.0593; arXiv:1201.3084.

[6] A. Djouadi, Phys. Rep. **459**, 1 (2008).

[7] H. Goldberg, Phys. Rev. Lett. **50**, 1419 (1983); J. Ellis, J. Hagelin, D. Nanopoulos, K. Olive, and M. Srednicki, Nucl. Phys. **B238**, 453 (1984).

[8] A. Pilaftsis, Phys. Rev. D **58**, 096010 (1998); Phys. Lett. B **435**, 88 (1998).

[9] D. A. Demir, Phys. Rev. D **60**, 055006 (1999).

[10] A. Pilaftsis and C. Wagner, Nucl. Phys. **B553**, 3 (1999).

[11] S. Heinemeyer, Eur. Phys. J. C **22**, 521 (2001).

[12] G. Aad *et al.* (ATLAS Collaboration), arXiv:0901.0512.

[13] G. Bayatian *et al.* (CMS Collaboration), J. Phys. G **34**, 995 (2007).

[14] Physics at an $e^+e^-$ Linear Collider, edited by R. D. Heuer, D. Miller, F. Richard, and P. Zerwas, *TESLA Technical Design Report*, Part 3, arXiv:hep-ph/0106315; see http://tesla.desy.de/new_pages/TDR_CD/start.html; K. Ackermann *et al.*, Report No. DESY-PROC-2004-01.

[15] J. Brau *et al.* (ILC Collaboration), arXiv:0712.1950; G. Aarons *et al.* (ILC Collaboration), arXiv:0709.1893; E. Accomando *et al.* (CLIC Physics Working Group Collaboration), arXiv:hep-ph/0412251; L. Linssen, A. Miyamoto, M. Stanitzki, and H. Weerts, arXiv:1202.5940.

[16] G. Weiglein *et al.* (LHC/ILC Study Group), Phys. Rep. **426**, 47 (2006); A. De Roeck *et al.*, Eur. Phys. J. C **66**, 525 (2010); A. De Roeck, J. Ellis, and S. Heinemeyer, CERN Courier **49N10**, 27 (2009).

[17] S. AbdusSalam *et al.*, Eur. Phys. J. C **71**, 1835 (2011).

[18] J. F. Gunion and H. E. Haber, Phys. Rev. D **37**, 2515 (1988).

[19] H. Baer, R. Barnett, M. Drees, J. Gunion, H. Haber, D. Karatas, and X. Tata, Int. J. Mod. Phys. A **02**, 1131 (1987); H. Baer, A. Bartl, D. Karatas, W. Majerotto, and X. Tata, Int. J. Mod. Phys. A **04**, 4111 (1989).

[20] J. Gunion and H. Haber, Nucl. Phys. **B307**, 445 (1988).

[21] M. Mühlleitner, A. Djouadi, and Y. Mambrini, Comput. Phys. Commun. **168**, 46 (2005).

[22] K. Huitu, J. Laamanen, P. N. Pandita, and P. Tiitola, Phys. Rev. D **82**, 115003 (2010).

[23] S. Y. Choi, M. Drees, B. Gaissmaier, and J. Song, Phys. Rev. D **69**, 035008 (2004).

[24] S. Y. Choi and Y. G. Kim, Phys. Rev. D **69**, 015011 (2004).

[25] A. Bartl, H. Fraas, S. Hesselbach, K. Hohenwarter-Sodek, and G. Moortgat-Pick, J. High Energy Phys. 08 (2004) 038.

[26] S. Choi, B. Chung, J. Kalinowski, Y. Kim, and K. Rolbiecki, Eur. Phys. J. C **46**, 511 (2006).

[27] S. Choi, M. Drees, and J. Song, J. High Energy Phys. 09 (2006) 064.

[28] A. Bartl, K. Hohenwarter-Sodek, T. Kernreiter, and O. Kittel, J. High Energy Phys. 09 (2007) 079.

[29] H. Dreiner, O. Kittel, and F. von der Pahlen, J. High Energy Phys. 01 (2008) 017.

[30] A. Lahanas, K. Tamvakis, and N. Tracas, Phys. Lett. B **324**, 387 (1994).

[31] D. Pierce and A. Papadopoulos, Phys. Rev. D **50**, 565 (1994).

[32] D. Pierce and A. Papadopoulos, Nucl. Phys. **B430**, 278 (1994).

[33] H. Eberl, M. Kincel, W. Majerotto, and Y. Yamada, Phys. Rev. D **64**, 115013 (2001).

[34] T. Fritzsche and W. Hollik, Eur. Phys. J. C **24**, 619 (2002).

[35] W. Oller, H. Eberl, W. Majerotto, and C. Weber, Eur. Phys. J. C **29**, 563 (2003).

[36] M. Drees, W. Hollik, and Q. Xu, J. High Energy Phys. 02 (2007) 032.

[37] A. Fowler, Ph.D. thesis, Durham University, 2010.

[38] A. Fowler and G. Weiglein, J. High Energy Phys. 01 (2010) 108.

[39] A. Chatterjee, M. Drees, S. Kulkarni, and Q. Xu, Phys. Rev. D **85**, 075013 (2012).

[40] A. Djouadi, Y. Mambrini, and M. Mühlleitner, Eur. Phys. J. C **20**, 563 (2001).

[41] N. Baro and F. Boudjema, Phys. Rev. D **80**, 076010 (2009).

[42] B. Schraußer, dissertation, Vienna University of Technology, 2010.

[43] S. Liebler and W. Porod, Nucl. Phys. **B849**, 213 (2011); **B856**, 125(E) (2012).

[44] A. Bharucha, A. Fowler, G. Moortgat-Pick, and G. Weiglein, Report No. DESY-12-015.

[45] S. Heinemeyer, F. von der Pahlen, and C. Schappacher, Eur. Phys. J. C **72**, 1892 (2012).

[46] T. Fritzsche, S. Heinemeyer, H. Rzehak, and C. Schappacher, Phys. Rev. D **86**, 035014 (2012).

[47] G. Degrassi, S. Heinemeyer, W. Hollik, P. Slavich, and G. Weiglein, Eur. Phys. J. C **28**, 133 (2003).

[48] S. Heinemeyer, W. Hollik, and G. Weiglein, Comput. Phys. Commun. **124**, 76 (2000); see http://www .feynhiggs.de.

[49] S. Heinemeyer, W. Hollik, and G. Weiglein, Eur. Phys. J. C **9**, 343 (1999).

[50] M. Frank, T. Hahn, S. Heinemeyer, W. Hollik, R. Rzehak, and G. Weiglein, J. High Energy Phys. 02 (2007) 047.

[51] S. Heinemeyer and C. Schappacher, arXiv:1204.4001.

[52] T. Takagi, Japanese Journal of mathematics **1**, 83 (1925).

[53] T. Fritzsche, Ph.D. thesis, Cuvillier Verlag, Göttingen, 2005.

[54] A. Bharucha, arXiv:1202.6284.

[55] T. Fritzsche and W. Hollik, Eur. Phys. J. C **24**, 619 (2002); T. Fritzsche, Diploma thesis, Institut für Theoretische Physik, Universität Karlsruhe, Germany, 2000 [see http:// www-itp.particle.uni-karlsruhe.de/diplomatheses.de.shtml].

[56] S. Heinemeyer, H. Rzehak, and C. Schappacher, Phys. Rev. D **82**, 075010 (2010); Proc. Sci., CHARGED2010 (2010) 039 [arXiv:1012.4572].

[57] A. Bartl, H. Eberl, K. Hidaka, S. Kraml, W. Majerotto, W. Porod, and Y. Yamada, Phys. Rev. D **59**, 115007 (1999).

[58] A. Djouadi, P. Gambino, S. Heinemeyer, W. Hollik, C. Jünger, and G. Weiglein, Phys. Rev. Lett. **78**, 3626 (1997); Phys. Rev. D **57**, 4179 (1998).

[59] R. D. Peccei and H. R. Quinn, Phys. Rev. Lett. **38**, 1440 (1977); Phys. Rev. D **16**, 1791 (1977).

[60] S. Dimopoulos and S. Thomas, Nucl. Phys. **B465**, 23 (1996).

[61] J. Küblbeck, M. Böhm, and A. Denner, Comput. Phys. Commun. **60**, 165 (1990); T. Hahn, Comput. Phys. Commun. **140**, 418 (2001); T. Hahn and C. Schappacher, Comput. Phys. Commun. **143**, 54 (2002). The program, the user's guide, and the MSSM model files are available via http://www.feynarts.de.

[62] T. Hahn and M. Pérez-Victoria, Comput. Phys. Commun. **118**, 153 (1999).

[63] F. del Aguila, A. Culatti, R. Munoz Tapia, and M. Perez-Victoria, Nucl. Phys. **B537**, 561 (1999).

[64] W. Siegel, Phys. Lett. **84B**, 193 (1979); D. Capper, D. Jones, and P. van Nieuwenhuizen, Nucl. Phys. **B167**, 479 (1980).

[65] D. Stöckinger, J. High Energy Phys. 03 (2005) 076.

[66] W. Hollik and D. Stöckinger, Phys. Lett. B **634**, 63 (2006).

[67] A. Denner, Fortschr. Phys. **41**, 307 (1993).

[68] S. Chakrabarti *et al.* (D0 and CDF Collaborations), arXiv:1110.2421; T. Aaltonen *et al.* (CDF and D0 Collaborations), arXiv:1207.2757.

[69] S. Chatrchyan *et al.* (CMS Collaboration), Phys. Lett. B **713**, 68 (2012).

[70] M. Carena, S. Heinemeyer, C. Wagner, and G. Weiglein, Eur. Phys. J. C **26**, 601 (2003).

[71] K. Nakamura (Particle Data Group), J. Phys. G **37**, 075021 (2010).

[72] H. Dreiner, S. Heinemeyer, O. Kittel, U. Langenfeld, A. Weber, and G. Weiglein, Eur. Phys. J. C **62**, 547 (2009).

[73] C. Baker *et al.*, Phys. Rev. Lett. **97**, 131801 (2006).

[74] B. C. Regan, E. D. Commins, C. J. Schmidt, and D. DeMille, Phys. Rev. Lett. **88**, 071805 (2002).

[75] W. C. Griffith, M. D. Swallows, T. H. Loftus, M. V. Romalis, B. R. Heckel, and E. N. Fortson, Phys. Rev. Lett. **102**, 101601 (2009).

[76] W. Hollik, J. Illana, S. Rigolin, and D. Stöckinger, Phys. Lett. B **416**, 345 (1998); **425**, 322 (1998).

[77] D. Demir, O. Lebedev, K. Olive, M. Pospelov, and A. Ritz, Nucl. Phys. **B680**, 339 (2004).

[78] D. Chang, W. Y. Keung, and A. Pilaftsis, Phys. Rev. Lett. **82**, 900 (1999); **83**, 3972(E) (1999); A. Pilaftsis, Phys. Lett. B **471**, 174 (1999).

[79] O. Lebedev, K. A. Olive, M. Pospelov, and A. Ritz, Phys. Rev. D **70**, 016003 (2004).

[80] J. Lee, A. Pilaftsis, M. Carena, S. Choi, M. Drees, J. Ellis, and C. Wagner, Comput. Phys. Commun. **156**, 283 (2004).

[81] W. Oeller, H. Eberl, and W. Majerotto, Phys. Rev. D **71**, 115002 (2005).

[82] The couplings can be found in the files MSSM.ps.gz, MSSMQCD.ps.gz, and HMix.ps.gz as part of the FeynArts package [61].